

Modelling and simulation of complex and compliant contacts of gear transmissions, in consideration of nominal and real geometries and kinematics.

by


Maksat T.S.

Submitted in partial fulfilment
of the requirements for the degree of
Doctor of Philosophy in Mechanical
Engineering

2023

Declaration

I declare that the research contained in this thesis, unless otherwise formally indicated within the text, is the author's original work. The thesis has not been previously submitted to this or any other university for a degree and does not incorporate any material already submitted for a degree.

Signed 
Dated 19.10.2023

MODELLING AND SIMULATION OF COMPLEX AND COMPLIANT CONTACTS OF
GEAR TRANSMISSIONS, IN CONSIDERATION OF NOMINAL AND REAL
GEOMETRIES AND KINEMATICS.

MAKSAT
TEMIRKHAN

Submitted in partial fulfillment of the requirements for the degree of
Doctor of Philosophy in Mechanical Engineering

School of Engineering and Digital Sciences
Nazarbayev University

Supervised by
Prof. Christos Spitas , PhD
Prof. Dongming Wei , PhD
Konstantinos Kaloudis , PhD, University of the Aegean.

May 2023

Abstract

An important aspect of gear design is the computer-aided modeling of gear tooth contact. It enables to evaluate the design of gears and the process of tooth contact, transmission errors (TE), tooth wear, alignment errors, vibration and noise. Contemporary gear tooth contact analysis models are multiple equation systems which rely on numerical solution techniques. Tooth contact analysis (TCA) is a crucial tool for designing and evaluating the efficiency of the gears in transmission systems. It stands for a significant approach to analyze contact locations, contact ratios, and kinematic errors in gear teeth. Gear manufacturers in various fields can greatly enhance the technology and quality of gears by simulating meshing and bearing contact on a computer. Additionally, TCA is a helpful method for forecasting a transmission's key characteristics, including the path of contact on the tooth surfaces and the motion graph.

The necessity to analyze non-conjugate meshing and surface contact led to the development of numerous tooth contact analysis approaches, such as parametric mathematical model or finite element simulation. These methods handle the contact problem by applying the surface tangency condition, which leads to a set of nonlinear equations that must typically be solved numerically. The original suggestion of the most well-known solution was presented by Litvin F. L. and his team, where they suggested the set of generalized five nonlinear contact equations with five unknown parameters, which forms the foundation of conventional TCA algorithm. Since these equations are nonlinear, an iterative process is used to calculate certain values. However, the main problem with this method is that each simulation requires careful selection of the initial or "guess" values for the convergence of parameters in an iterative process. Later, Litvin F. L. and his colleagues proposed the "local synthesis method" to eventually determine appropriate "guess values" and obtain convergence to lessen the systemic lack of stability in this solution. Although, this resulted in a computationally expensive and impractical implementation.

In this dissertation, by analytically transforming the same contact conditions as in the conventional model, a novel TCA method was presented to resolve convergence issue. As a result, a mathematical model of five conventional nonlinear tooth contact equations with five free parameters was reduced to a system of two nonlinear equations with only two unknown parameters in order to achieve more stable, accurate and fast converging algorithm. The proposed model was compared with the well-established conventional Tooth Contact Analysis (TCA) method in terms of accuracy, computational efficiency, and convergence probability,

thereby showing its superiority in terms of computationally efficient of the numerical solution. By using new TCA model the impact of tooth surface to various misalignments and modifications on different types of gears is examined, in order to determine the most suitable design approach and establish acceptable values for tooth modifications. Additionally, the present study investigated the effects of three types of longitudinal crowning and tip/root profile relief on gear meshing.

Table of Contents

List of Abbreviations and symbols	9
List of Tables	10
List of Figures	10
Chapter 1. Introduction	16
1.1 Gear geometry	16
1.2. The vital role of TCA in gear design.....	18
1.3. Thesis hypothesis	19
1.4. Published and Submitted articles.....	20
Chapter 2. Literature review	22
2.1 Types of gears used for simulations.....	22
2.2. Misalignments in the gearbox.....	26
2.3. Gear tooth surface modification	28
2.4. Parametric equations of tooth surface modification	32
2.5. Transmission error.....	31
2.6. Gear tooth contact analysis methods	32
2.7. Hertzian stress contact analysis	34
Chapter 3. Mathematical models of gear TCA method.....	38

3.1 Conventional TCA method	38
3.2 Novel TCA method.....	40
3.3 New TCA model in spherical coordinate system.....	42
Chapter 4. Cylindrical gears contact analysis using the proposed TCA	
method.....	44
4.1 Spur gears contact analysis.....	44
4.2 Helical gears contact analysis	50
Chapter 5. Bevel gears contact simulation through the new TCA method ..	60
5.1 Straight bevel gear	60
5.2 Spiral bevel gear.....	65
Chapter 6. Computational assessment of conventional TCA method.....	79
6.1 Testing the conventional TCA model	79
6.2 Comparison of conventional and new TCA method for spur gears	89
6.3 Comparison of conventional and novel TCA methods for straight bevel gear ..	93
6.4 Comparison of two TCA methods for spiral bevel gear	95
Chapter 6. Conclusions	100
6.1 In the end.....	100
6.2 Further research	102

References 104

List of Abbreviations and symbols

- $C^{1,2}$ continuous
- $S_{1,2}$ coordinate system of surfaces fixed in space
- S_f fixed coordinate system
- $\Sigma_{1,2}$ rotating tooth surfaces
- \vec{n}_i normal vector of tooth surface function
- a_{12} distance between S_1 and S_2
- R_i rotation matrix
- \vec{r}_i position vector function
- v_i projection of \vec{r}_i on the centerline
- u_i radius from origin to the point of contact ($i = 1, 2$)
- θ involute angle
- $w_{1,2}$ axis of rotation
- ϕ_i rotation angle around axis
- f_i vector function of parametric surface
- m gear module
- $R_{max}^{(1,2)}$ largest radius of curvatures
- $R_{min}^{(1,2)}$ smallest radius of curvatures
- $E_{1,2}$ modulus of elasticity
- $\nu_{1,2}$ Poisson's ratio
- p_o maximum pressures of cylindrical line contact
- p maximum pressures of elliptical point contact
- ε tooth surface modification function in (u_i, v_i) space
- $\Delta\delta$ out-of-plane angular misalignment
- $\Delta\gamma$ in-plane angular misalignment
- ΔE in-plane axial offset
- ΔH out-of-plane axial offset
- $\Delta\varphi$ transmission error (TE)
- σ stress ratio (SR)
- b gear face width

List of Tables

Table 1. Calculation of involute gear tooth profile size.....	17
Table 2. Parameters of helical gears.	50
Table 3. Amount of modifications for various in-plane angular misalignment errors for helical gears.	51
Table 4. Amount of adjustments in relation to angular misalignment out of plane for helical gear engagement.	54
Table 5. Simulation parameters of standard straight bevel gear pair.....	60
Table 6. Simulation parameters of alignment errors.....	61
Table 7. Crowning design for various alignment error.....	68
Table 8. Spur gears parameters.....	79
Table 9. Helical gears parameters.....	85
Table 10. Convergence outcomes of two algorithms	91
Table 11. Comparison of convergence result of two models.	95
Table 12. Computational results of two methods	96

List of Figures

Figure 1. The pitch diameter and pressure angle illustration	16
Figure 2. Involute gear profile parametrization.	17
Figure 3. 3D model of involute spur gear provided by SolidWorks program	21
Figure 4. 3D model of involute helical gear.....	22
Figure 5. Straight bevel gear model.....	23
Figure 6. Spiral bevel gear model.....	24
Figure 7. Misalignment errors' types	26
Figure 8. The coordinate systems for (a) out-of-plane, (b) in-plane angular misalignment, (c) in-plane off-set, and (d) out-of-plane off-set.....	27
Figure 9. Curves of profile modifications, where an unmodified tooth flank with a straightforward edge fillet is shown by the black line	30
Figure 10. The function of TE at the present of angular misalignment in gear system.....	31
Figure 11. Path of contact of spur gear with in-plane angular misalignment	32
Figure 12. This figure depicts a diagrammatic representation of the contact between the teeth	

of a helical gear pair.....	39
Figure 13. The diagrams demonstrate the interaction between the surfaces of the first and second teeth as they revolve around their respective fixed axes, w_1 and w_2	41
Figure 14. The interaction between involute bevel teeth is shown schematically.	43
Figure 15. The transmission function is discontinuous due to insufficient parabolic modification.....	45
Figure 16. With enough parabolic adjustment, the continuous transmission function can be obtained.	465
Figure 17. Path of contact with contact ellipses for (a) In-plane and (b) Out-of-plane angular misalignment; (c) Axial off-set	46
Figure 18. The contact path of the tooth surface with tip-root relief and crowning with in-plane (a) and out-of-plane (b) angular misalignments.	47
Figure 19. Transmission with tooth surface modification with angular misalignment.	48
Figure 20. Path contact with combined out and in-plane angular misalignments.....	48
Figure 21. SR vs u_1 regarding in-plane angular alignment error with longitudinal crowing..	49
Figure 22. SR vs u_1 with in-plane angular misalignment with longitudinal crowing and tip-root relief.	49
Figure 23. The TE functions (a) circular, (b) parabolic, and (c) logarithmic have varying degrees of crowning.....	52
Figure 24. TE of a helical gear with three different modifications and an angular misalignment of 0.2 (3.5 mrad)	52
Figure 25. Path of contact of longitude circular, parabolic, and logarithmic crowned helical gear with in-plane misalignment: 0.05 (0.87), 0.1 (1.7), and 0.2 (0.2 mrad) (3.5 mrad). The center of the tooth surface across the breadth of the gear is indicated by the dashed line.....	53
Figure 26. TE of a helical gear with three different modifications and an angular misalignment of 0.2 (3.5 mrad).	55
Figure 27. Path of contact of longitude circular, parabolic, and logarithmic crowned helical gear with out-of-plane misalignment: a) 0.05 (0.87), b) 0.1 (1.7), and c) 0.2 (0.2 mrad) (3.5 mrad). The center of the tooth surface across the breadth of the gear is indicated by the dashed line. At the 0.2° misalignment angle, the scaled contact ellipses at the pitch point are displayed.....	56
Figure 28. An illustration of a helical gear assembly model in space with (a) unaltered profiles, (b) circular crowning, and (c) logarithmic crowning	56

Figure 29. Helical gears with three different methods of profile modification were compared in terms of their stress ratio (Σ) and the degree of out-of-plane misalignment.....	57
Figure 30. The SR of crowned helical gears, where the blue outlines show the location of the contact ellipse at the contact point, with the least amount of circular profile alteration along the path of contact for an out-of-plane misalignment of 0.2° (3.5 mrad).	58
Figure 31. The following are examples of coordinate systems for misalignments: (a) angle change (in-plane misalignment), (b) center distance shift along y-axis, (c) pinion axial displacement along x-axis, and (d) gear axial displacement along z-axis.	60
Figure 32. Straight bevel gear pair illustration provided by Kisssoft program.	61
Figure 33. With a slight modification, transmission error function is used when the pinion is displaced axially.	62
Figure 34. Bevel gear surface with contact ellipses and contact paths.	62
Figure 35. Transmission error with parabolic crowning, tip relief, and center distance change.	63
Figure 36. Path of contact, maximum contact pressure, and contact ellipses with equal amounts of tip relief and parabolic crowning are all affected by the following: (a) change in center distance, ΔE ; (b) axial displacement of gear, ΔG	64
Figure 37. Maximum contact pressure, contact ellipses, and contact paths with significant lead modification.	64
Figure 38. For the case of shaft angle misalignment, transmission error function with three forms of longitude crowning.	65
Figure 39. Maximum contact pressure for three types of longitude crowning at various shaft angle misalignments.....	65
Figure 40. An involute bevel gear tooth surface generated graph.....	67
Figure 41. Coordinate system diagram for spiral bevel gear alignment issues.	69
Figure 42. Path contact results from the engagement of a spiral gear pair with various angular misalignments.	70
Figure 43. The tooth contact ellipses and the stress ratio at angular misalignment $\Delta\gamma = 0.2^\circ$ and longitudinal parabolic crowning.	70
Figure 44. Comparison of the path of contact with different linear misalignments and double crowning.....	71
Figure 45. Transmission results for spiral gear meshing at linear misalignment (ΔE).....	71
Figure 46. The stress ratio and contact ellipses in the condition of linear misalignment.	72
Figure 47. Path contact results in different linear misalignments ΔH	73

Figure 48. Transmission error in case of linear misalignment ΔH	74
Figure 49. Stresses and contact ellipses for a spiral bevel gear system with a linear misalignment of $\Delta H = 0.08$	75
Figure 50. The contact path with various combined linear misalignments with (a) $c1 = 0.005$ and (b) increased amount of longitudinal parabolic crowing $c1 = 0.02$	76
Figure 51. TE results of various combined linear misalignments.	76
Figure 52. Stress ratio and contact ellipses for linear misalignments at $\Delta E = \Delta H = 0.08$ and (a) $c1 = 0.005$,.....	77
Figure 53. An illustration of the results of stress ratio (σ) and pitch point deviation (δ) based on different and combined values of linear misalignments (ΔE and ΔH).	78
Figure 54. Inconsistencies in contact path of spur gear tooth surface due to unconverged point.	80
Figure 55. The simulation results for 1000 random points on the tooth surface are displayed, with (a) showing the starting guess values for the iterative process, and (b) displaying the outcomes of Litvin's solution, where hardly any point converged.	81
Figure 56. Converged and non-converged values on the initial value guess cloud for Litvin's model with different starting values for φ_{20} are demonstrated, where the starting values for φ_{20} close to the correct solution for (a) 0.5 rad; (b) 0.45 rad; (c) 0.4 rad.	82
Figure 57. The results of Litvin's solution are shown in (b) for 1000 random points generated for the simulation, where (a) displays the starting guess values for the iterative process. It was found that almost no single point converged during the simulation.	82
Figure 58. The results of the conventional TCA model for 1000 randomly generated starting points are shown in (a) and (b), where (a) displays the initial guess values and (b) presents the solution outcomes. 81.8% of the 1000 points converged to a single correct solution, which is represented as a blue dot.	83
Figure 59. The contact path along the tooth surface of the in-plane misaligned spur gear is depicted, and despite careful guess value selection, some points were not able to converge. ...	84
Figure 60. The outcomes of 1000 simulations using random starting points are depicted, where (a) displays the initial guess values and (b) exhibits the consequences of the conventional TCA model. In the image, a blue dot represents the accurate answer to which 800 points out of the 1000 converged.....	84
Figure 61. Path contact demonstration using arbitrarily selected starting values for the u_{20} and v_{20} parameters, but with a near approximation to the right solution for 0.05 rad. (a)	

Path contact solution that is aligned; (b) misaligned result with an in-plane deviation of $\Delta\lambda = -3 \text{ arcmin}$	86
Figure 62. The path contact of helical gears where the initial value close to actual contact for $u_{20} - u_2^{sol} = 4.89 \text{ mm}$ and $v_{20} - v_2^{sol} = 1.44 \text{ mm}$ and ϕ_2^0 close to right solution for 0.05 rad . (a) The contact trace is aligned; (b) the contact is misaligned with an in-plane deviation of $\Delta\lambda = -3 \text{ arcmin}$	87
Figure 63. The simulation results were obtained by analyzing 1000 random points on the surface of helical gear teeth. The starting guess values are depicted in (a), while the results of Litvin's solution, in which almost no single point converged, are shown in (b).	87
Figure 64. The results of simulating 1000 random points on the surface of an aligned helical gear tooth contact are presented below: (a) initial guess values; (b) Litvin's solution, where the correct answer (blue dot) was only converged to by 13.5% of the 1000 points.....	88
Figure 65. The simulation results were obtained by analyzing 1000 random points on the surface of misaligned helical gear teeth. The starting guess values are depicted in (a), while the results of Litvin's solution, where only 14.2% of the 1000 points converged to the correct solution (blue dot), are shown in (b).	89
Figure 66. The path of contacts on the spur gear tooth surface, where (a) some locations failed to converge due to inappropriate guess values for the parameter ϕ_2 , despite the fact that the selected guess values were within 0.2 rad of the correct response for the real pitch point contact solution.	90
Figure 67. The schematic representation of a spur gear pair.	91
Figure 68. Converged and non-converged values are shown on the guess cloud on the uv-plane with 1000 randomly selected points, where (a) the imposed initial guess values (domain), (b) the results of the traditional TCA solution (range) with some correct contact solution, and (c) the proposed new solution (range) with fully converged results. The blue dots denote converged points, while the red crosses denote non-converged points or points that converged erroneously.	92
Figure 69. Convergence outcomes of conventional TCA model, where (a) random variables (domain), and (b) its result of Litvin's non-linear equations (range).	93
Figure 70. Convergence outcomes of novel TCA model, where (a) random variables (domain), and (b) its result of Litvin's non-linear equations (range).	93
Figure 71. Even though the chosen guess value was within 92% of the correct answer, the route of contacts on the straight bevel gear tooth surface where one point failed to converge	

due to an inappropriate guess value of the parameter 2..... 94

Figure 72. Results of convergence of a cloud of 1000 randomly chosen guesses, where (a) the applied initial guess values (domain), (b) the results of Litvin's solution (range) with some concentration around the correct contact point, and (c) the proposed new solution (range) with fully converged results at the single correct point. 95

Figure 73. Convergence result of new TCA model where: (a) generated two dimensional 1000 random variables; (b) solution with 36% of convergence in five dimensional parametric space..... 97

Figure 74. Convergence result of new TCA model where: (a) generated two dimensional 1000 random variables; (b) solution with 100% of convergence in five dimensional parametric space..... 98

Figure 75. Path contact solution of two methods, where (a) conventional and (b) proposed model..... 99

Figure 77. The path contact solution for (a) conventional and (b) proposed model in space. 100

Figure 78. The 8-axis Rotary Test Bed with a CNC router machin. 103

Chapter 1. Introduction

The process of modeling and simulating tooth contacts within gear transmissions plays a crucial role in the design and manufacture of gears. By accurately representing the interactions between gear teeth under different loads, speeds, and operational conditions, this approach allows engineers to predict potential issues such as transmission errors, noise, and even tooth failure [1-5]. The consideration of both nominal and real geometries, as well as kinematic factors, ensures that the simulation results closely mirror real-world behavior. This aids in optimizing gear designs, selecting appropriate geometrical parameters, refining manufacturing processes, and enhancing the overall efficiency and reliability of gear systems. Ultimately, such simulations empower engineers to make informed decisions, leading to the creation of more durable, efficient, and effective gear transmissions.

1.1 Gear geometry

The manufacturing design process of gears begins with the definition of their dimensions, which are essential for both modeling and the selection of machine cutting tools [4]. Gear design typically involve key parameters like the number of teeth ($N_{1,2}$), module m (the ratio of pitch diameter ($d_{p1,2}$) to the number of teeth), and pressure angle (α). The pitch diameter and pressure angle are illustrated in Figure (1). The number of teeth plays a vital role in determining the gear's size and function. Meanwhile, the module helps establish the gear's dimensions and tooth size relative to the pitch diameter. The pressure angle influences the tooth profile's shape and the gear's load-bearing capacity. By manipulating these variables in gear design equations, engineers can tailor gears to meet specific performance requirements, ensuring smooth and reliable mechanical power transmission in a wide range of applications, from automotive transmissions to industrial machinery [6-9].

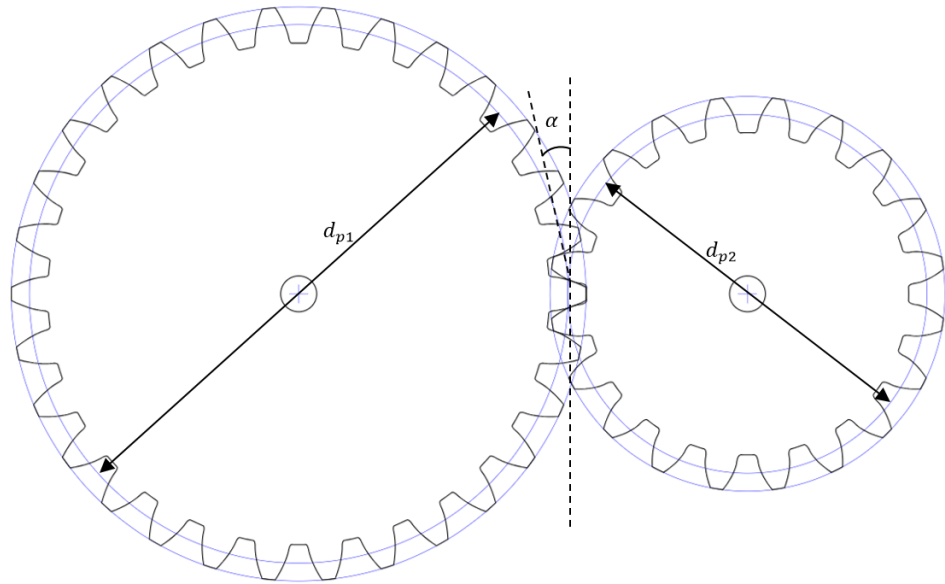


Figure 1. The pitch diameter and pressure angle illustration.

The aforementioned parameters are essential for establishing the range of minimum and maximum values for the corresponding radius of involute, denoted as u_i . These values, in turn, play a critical role in defining the tooth size. The procedure for establishing the minimum and maximum values of the radius for the corresponding involute curves is outlined in Table 1.

Table 1. Calculation of involute gear tooth profile size.

Terms	Symbols	Formula
Module	m	-
Pressure angle	α	
Number of teeth	$N_{1,2}$	
Pitch diameter	$d_{p1,2}$	$N_{1,2} \cdot m$
Base diameter	$d_{1,2}$	$d_{p1,2} \cdot \cos \alpha$
Tip diameter	$d_{a1,2}$	$d_{1,2} + 2m$
Involution minimum	u_{min}	$d_{1,2}/2$
Involution maximum	u_{max}	$d_{a1,2}/2$

In this study, we will examine the gear tooth profile exclusively as the involute type. The involute gear profile represented a crucial breakthrough in the field of machine design. Unlike alternative gear systems, an involute gear's tooth configuration relies solely on factors such as the gear's tooth number, pressure angle, and pitch. The contact between involute gear teeth occurs at a single instantaneous point. To determine positions along the tooth profile, we will employ the parameter u_i signifying the radius from the origin to the point of contact, as shown in Figure (2). The parametric expression for the involute gear profile in cylindrical coordinate system can be defined as follows:

$$\begin{cases} x = r (\cos \theta + \theta \sin \theta) \\ y = r (\cos \theta - \theta \sin \theta) \end{cases} \quad (1)$$

where r is a base radius and θ is the involute angle that was defined in [10]:

$$\theta = \sqrt{\frac{u_i^2}{r^2} - 1} \quad (2)$$

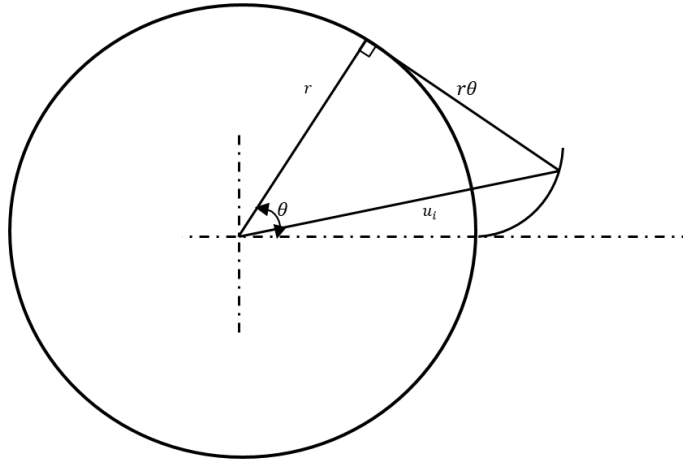


Figure 2. Involute gear profile parametrization.

1.2. The vital role of TCA in gear design

Tooth contact analysis (TCA) is an indispensable tool in the design and evaluation of gear efficiency within transmission systems. It enables the examination of contact points, contact ratios, and kinematic discrepancies in gear teeth. TCA empowers gear manufacturers across various industries to advance gear technology and quality by simulating meshing and bearing contact on a computer. Furthermore, TCA serves as a valuable method for predicting

critical characteristics of a transmission, such as the tooth surfaces' contact path and motion graph [1-3,7,10-15]. Despite its classical nature, this field has experienced renewed interest from numerous researchers with the objectives of (a) enhancing the robustness of TCA algorithms through automatic tuning of initial conditions to ensure the convergence of numerical root-finding procedures; (b) accelerating numerical computations by explicitly solving for the rotation angles based on equations that dictate surface normal collinearity; and (c) advancing gear drives and improving meshing characteristics to reduce sensitivity to misalignment, transmission errors, noise, and vibration. TCA technology finds widespread application in evaluating meshing quality, driven by the growing demand for improving the durability and mechanical efficiency of gears in diverse industrial sectors such as aviation, automotive, and civil engineering. Research in this field allows for the prediction of various meshing effects during the design stage, including the primary causes of transmission errors and misalignment, as well as strategies for avoiding edge contact and premature failure. Consequently, the simulation of gear meshing has led to the development of gears with involute profiles, enabling the maintenance of a constant velocity ratio in transmission.

1.3. Thesis hypothesis

Theoretical models for gears don't always align with real-world applications due to intentional modifications or manufacturing mistakes. If these discrepancies are not taken into account, traditional gear theories may produce incorrect results. Therefore, the analysis of non-conjugate gears is important to address the non-uniform motion transmission and altered contact direction.

In this study, we replicate the gear tooth contact analysis (TCA) model introduced by Litvin and his team [1]. We show that the model is fundamentally unstable and its numerical solutions are overly sensitive to the starting values chosen. Thus, the question arises on how to improve the stability of the TCA algorithm by adjusting the initial conditions to ensure the convergence of numerical techniques. To address these challenges, we propose a new approach for the general problem of contact between two rotating surfaces with fixed axes. Our goal is to simplify the model by reducing the number of unknown parameters from five to two, making it more explicit, stable, and straightforward. We analyze the sensitivity of misalignments on transmission error, contact paths, and stresses using various gears with tooth surface modifications. We compare the impact of three types of longitudinal crowning on transmission

error, maximum pressure, contact ellipse, and contact path. Our results demonstrate the effectiveness of the proposed method in obtaining convergent, accurate, and stable results, which can be used to optimize designs.

Hypothesis:

I. The conventional TCA model often encounters convergence challenges due to the intricate nature of the non-linear equations involved and the presence of multiple roots. A practical solution to mitigate these convergence issues lies in the reduction of unknown parameters within the gear system. This approach yields a more stable, expedited, and precise solution, independent of the initial guess values.

II. The reduction of unknown parameters in the gear system can be achieved by adopting a novel parameterization method for tooth surfaces. In this methodology, the parameters of the pinion can be deduced from fundamental mathematical principles and the parameters of the gear.

1.4. Published and Submitted articles

1. Temirkhan, M., Tariq, H. B., Kaloudis, K., Kalligeros, C., Spitas, V., & Spitas, C. (2022). Parametric quasi-static study of the effect of misalignments on the path of contact, transmission error, and contact pressure of crowned spur and helical gear teeth using a novel rapidly convergent method. *Applied Sciences*, 12(19), 10067.

<https://doi.org/10.3390/app121910067>

Journal Rank: Q2. **Impact Factor:** 2.921

2. Temirkhan M, Amrin A, Spitas V, Spitas C. Convergence and accuracy problems of the conventional TCA model – Critical analysis and novel solution for crowned spur gears. *Proceedings of the Institution of Mechanical Engineers, Part C: Journal of Mechanical Engineering Science*. 2023;0(0). doi:[10.1177/09544062231181834](https://doi.org/10.1177/09544062231181834)

Journal Rank: Q2. **Impact Factor:** 2.0

3. Temirkhan, M., Tariq, H.B., Spitas, V. *et al.* Parametric design of straight bevel gears based on a new tooth contact analysis model. *Arch Appl Mech* (2023).

<https://doi.org/10.1007/s00419-023-02488-z>

Journal Rank: Q2. **Impact Factor:** 2.467

4. Temirkhan, M., Spitas, V., & Spitas, C. (2023). Critical assessment of the stability and convergence of modern TCA: the reference case for modified aligned and misaligned spur and helical gears. *Acta Mechanica (Under Review)*

Journal Rank: Q1. **Impact Factor:** 2.645

5. Temirkhan, M., Amrin, A., & Spitas, C. (2023). Computerized analysis of a non-conjugate spiral bevel gears under advanced and fast convergent tooth contact model *Mechanism and Machine Theory (Under Review)*

Journal Rank: Q1. **Impact Factor:** 5.2

6. Temirkhan, M., Spitas, C., & Wei, D. (2023). A computationally robust solution to the contact problem of two rotating gear surfaces in space. *Meccanica (Under Review)*

Journal Rank: Q2. **Impact Factor:** 2.7

Chapter 2. Literature review

2.1 Types of gears used for simulations

In this chapter, we will explore the various types of gears employed for simulation and assessing conventional and proposed TCA methods. Spur gears are the simplest form of gears and are characterized by cylindrical shapes which are widely used in transmissions and machines with parallel shafts and are known for their low cost and ease of manufacture [16-18], Figure (3). The equation for general involute surfaces was developed by introducing the necessary parameters, denoted as u_i and v_i , tailored to a specific machine tool configuration. This formulation aims to establish a mathematical representation of the tooth surface in spur gears. The parametric equations describing the involute surface can be articulated as follows:

$$\begin{aligned}x_i &= u_i \cos(\alpha_i) \\y_i &= u_i \sin(\alpha_i)\end{aligned}\quad (3)$$

$$z_i = v_i$$

where α_i describes the angle of initial involution:

$$\alpha_i = \cos^{-1} \left(\frac{r_b}{u_i} (\cos(\theta_i) + \theta_i \sin(\theta_i)) \right) \quad (4)$$

where r_b is a base radius and θ_i is angle of involute shown in Equation 2.

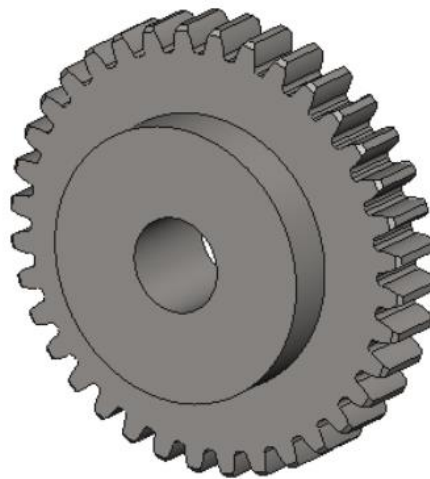


Figure 3. 3D model of involute spur gear provided by SolidWorks program.

Helical gears possess teeth with a helix shape, as shown in Figure (4), causing them to engage at an angle relative to the rotation axis. This unique design characteristic grants helical gears superior load-bearing capabilities and extended operational lifespans compared to spur gears [19-22]. In the context of a specific machine tool configuration, the parametrization of helical involute surfaces was computed and derived from a universal equation using the provided parameters u_i and v_i . The resulting parametric equations governing the involute shape are as follows:

$$\begin{aligned}
 x_i &= u_i \cos \left(\alpha_i \pm \sin^{-1} \left(\frac{v_i}{r_b} \sin \beta \right) \right) \\
 y_i &= u_i \sin \left(\alpha_i \pm \sin^{-1} \left(\frac{v_i}{r_b} \sin \beta \right) \right) \\
 z_i &= v_i
 \end{aligned} \tag{5}$$

In Equation (5), the symbol β represents the helix angle, while z_0 and z_f correspond to the initial and final positions of the parameter v_i . Within this equation, α_i signifies the angle characterizing the initial involute.



Figure 4. 3D model of involute helical gear.

Bevel gears are specialized conical gears with teeth that engage along axes that are neither parallel nor intersecting. They find widespread use in industrial drivetrains and automobiles for transmitting power between shafts positioned at right angles to each other [23].

The geometric characteristics of the tooth surfaces of bevel gears have been extensively studied in numerous research works [23-28]. In most practical cases, the geometry of bevel gear tooth surfaces is not readily available and must be determined through either implicit solution involving a set of nonlinear equations or cutting simulations, as standard spherical involute geometries are not commonly used without modifications. The parametric description of the spherical involute profile in terms of (u_i, v_i) within the plane can be defined as follows:

$$\beta_i = \frac{1}{\sin(\alpha_i)} \cos^{-1} \left(\frac{\cos(u_i)}{\cos(\alpha_i)} \right) \text{ and } R_i = v_i. \quad (6)$$

where β_i is the involute generating angle and α_i is the base cone angle. In the industrial sector, it is crucial to design straight bevel gears with the smallest feasible volume, Figure (5). This approach helps minimize the use of space and materials during the manufacturing process [29]. The position vector of the contact point on a straight bevel gear surface is defined in [30]:

$$\begin{aligned} x(u_i, v_i) &= R_i (\cos(\beta_i \sin(\alpha_i)) \sin(\alpha_i) \cos(\beta_i) + \sin(\beta_i \sin(\alpha_i)) \sin(\beta_i), \\ y(u_i, v_i) &= R_i (\cos(\beta_i \sin(\alpha_i)) \sin(\alpha_i) \sin(\beta_i) - \sin(\beta_i \sin(\alpha_i)) \cos(\beta_i), \\ z(u_i, v_i) &= R_i \cos(\beta_i \sin(\alpha_i)) \cos(\alpha_i), \end{aligned} \quad (7)$$

where R_i is a radius vector varied from inner to outer cone distance, and the position of the point of contact on the bevel tooth profile can be computed by varying parameter u_i from inner to outer cone angle.

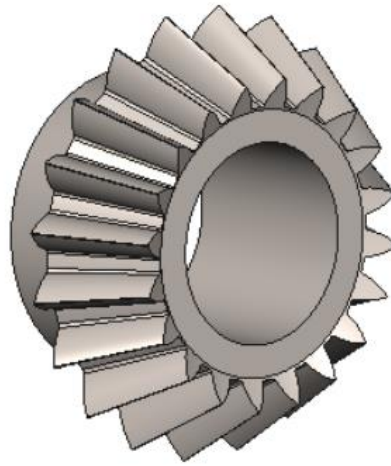


Figure 5. Straight bevel gear model.

For quite some time, researchers have explored spiral bevel gears using the principles of conjugate surfaces or conjugate curves, which rely on geometric elements (Figure (6)). However, with the growing demand for high-performance gear mechanisms, engineers face conflicting design objectives. They must simultaneously enhance power transmission efficiency and durability while also addressing factors like noise, vibration, and hardness, as discussed in references [31-33]. Consequently, numerical tools that can simulate the behavior of gearbox components and predict the overall system performance have become crucial in the production process. These tools empower engineers to experiment with various designs without the need for costly prototypes. The parametric definition of the involute spiral bevel gear is provided in terms of (u_i, v_i) within the plane.

$$\begin{aligned}
 x(u_i, v_i) &= R_i (\cos(\beta_i \sin(\alpha_i)) \sin(\alpha_i) \cos(\beta_i \pm \vartheta_i) + \sin(\beta_i \sin(\alpha_i)) \sin(\beta_i \pm \vartheta_i), \\
 y(u_i, v_i) &= R_i (\cos(\beta_i \sin(\alpha_i)) \sin(\alpha_i) \sin(\beta_i \pm \vartheta_i) - \sin(\beta_i \sin(\alpha_i)) \cos(\beta_i \pm \vartheta_i), \\
 z(u_i, v_i) &= R_i \cos(\beta_i \sin(\alpha_i)) \cos(\alpha_i),
 \end{aligned}
 \tag{8}$$

where R_i is a radius vector specified in (u_i, v_i) as follows, and α_i is the base cone angle, β_i is the involute generating angle. θ_i is logarithmic function with a spiral angle denoted as Φ and R_m is mean cone distance and described as:

$$\theta_i = \frac{1}{\sin(\alpha_i) \cot \Phi} \log \frac{R_m}{R_i}.
 \tag{9}$$

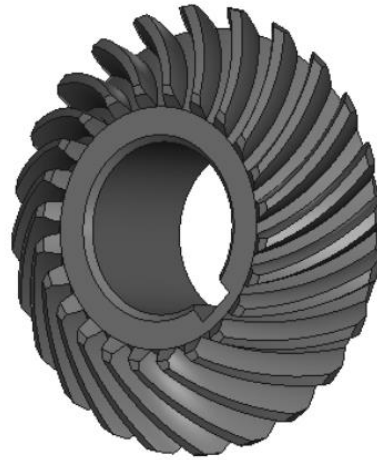


Figure 6. Spiral bevel gear model.

2.2. Misalignments in the gearbox

Gear misalignments, also known as gear alignment problems, are a significant issue in the power transmission industry. Issues such as manufacturing imperfections, misaligned assembly, and other elements can lead to noise and vibration during operation. Gear alignment issues have been a cause of concern for engineers for a long time. As a result, researchers have been investigating the effects of gear misalignments on the performance of gear systems. Misalignments of gear pairs can influence the physical and geometric properties of the tooth flanks. Establishing the contact performance of loaded teeth with misalignments is essential for furthering strength and stabilizing the gear transmission system.

Gear misalignments can be classified into two categories: angular and linear, both of which have a negative impact on gear contact and engagement. Hu and Mao [34] offered a more thorough division of gear misalignments, discerning them into four types: angular pitch and yaw misalignments and linear radial and axial misalignments, as illustrated in Figure (7-8). In-plane axial, radial and yaw misalignments, and out-of-plane pitch misalignments [35] have significant effect on gear tooth contact and transmission. Studies of spur gears have revealed that the gear tooth surface contact is more vulnerable to angular misalignments than to linear ones, and that the contact area between two gears is notably reduced in the case of angular misalignment compared to linear misalignments [36]. Ye and Tsai [37] found that under angular misalignment high-contact-ratio gears produce higher stress compared to linear ones.

One study by Simon [38] focused on the load distribution calculations in gear systems with misalignments. The author proposed that loaded tooth contact analysis (LTCA) can provide a more realistic contact pattern and pressure distribution compared to other methods. Another study by Ding et al. [39] utilized LTCA to determine the effects of misalignments on the tooth contact pattern and load distribution in gear systems. The authors concluded that LTCA is an effective tool for analyzing the performance of gear systems with misalignments.

A more recent study by Li, Cui, and Chen [40] investigated the dynamic behavior of planetary gear systems with misalignments. The authors proposed a method for improving the stability and performance of these systems by considering the effects of misalignments on the gear teeth. Another study by Zhang, Xiao, and Chen [41] focused on optimizing the load-

carrying capacity of planetary gears with misalignments. The authors utilized numerical simulations and experimental measurements to investigate the effects of misalignments on the gear system's performance.

These studies underscore the significance of factoring in misalignments at the stage of evaluating the efficiency and effectiveness of gear systems. Researchers have found that misalignments can significantly impact the geometric and physical performance of gear teeth, and thus, LTCA is an effective tool for determining the effects of misalignments on gear system performance.

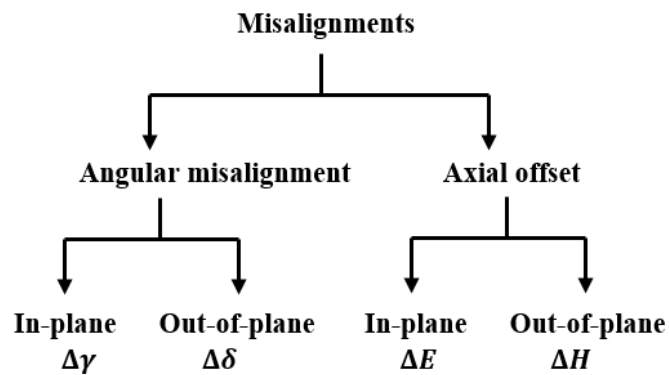
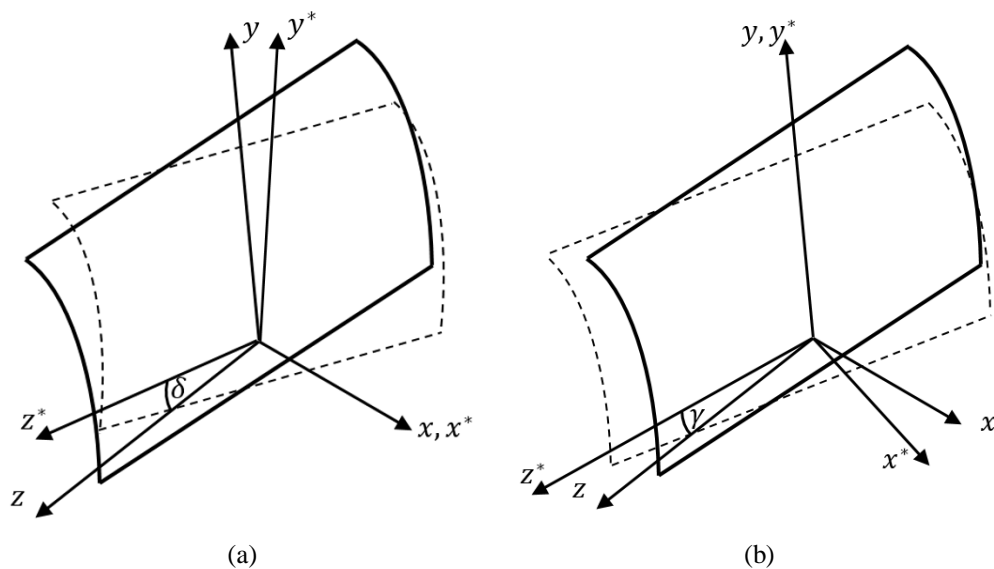


Figure 7. Misalignment errors' types



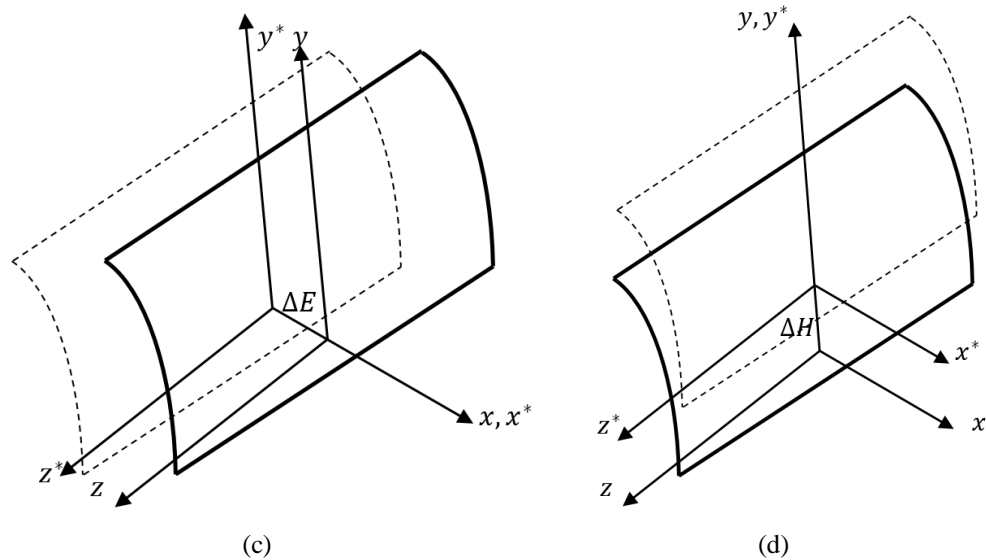


Figure 8. The coordinate systems for (a) out-of-plane, (b) in-plane angular misalignment, (c) in-plane off-set, and (d) out-of-plane off-set.

2.3. Gear tooth surface modification

Different researchers have explored various solutions to address the issue of gear misalignment in order to enhance the performance and longevity of gear systems. One such solution involves the use of gear tooth modifications, which aim to optimize the functioning of gears by reducing noise levels, improving performance, and increasing durability. Some of the most commonly used modifications include addendum modification, profile modification, lead modification, and crowning modification. Each of these modifications addresses specific problems and conditions, and choosing the right modification for a specific application is crucial for ensuring optimal results. Mao [42] suggested tooth modification, such as crowning, as a way to significantly reduce the stress concentration caused by misalignments. This approach, also known as "corrections," has been described in different guidelines [43,44]. The goal is to eliminate the risk of edge contact and related failure during tooth contact. However, it's important to note that these modifications are themselves errors, and excessive modifications can lead to increased transmission error (TE), overloads, and vibration [45]. The tooth modification focuses on crowning along the tooth flanks and profile modification along the tooth height, resulting in a smoother pressure distribution and preventing edge contact, making it an effective solution for misalignments. Li [46] also discussed misalignment in gears and recommended tooth flank modification as an appropriate solution. He emphasized the importance of finding the optimal criteria for crowning based on static loads and the extent of

misalignment, as proper tooth surface adjustment can reduce the risk of micro-pitting. Excessive modification of the tooth can cause micro-cracks and micro-pitting, which can shorten the life of the gear and worsen the dynamic response, while too little crowning can cause issues with contact localization [47].

Conventional gears' modification is shown as a parabolic curve. Concept of the pre-designed parabolic function was introduced by Litvin et al. [48], where they demonstrated that double-crowned gears can reduce the noise and vibration of gearbox and ensure continuous parabolic function of the transmission error (TE) by absorbing the linear function of TE caused by gear misalignment. Lin et al. [49] found that gear tooth parabolic modification is less sensitive to the change of load compared to linear relief. Afterwards, Gurumani and Shanmugam [50] demonstrated a more convenient approach to generate circular arc crowning. Litvin et al. [51] and Zhen et al. [52] discussed the benefits of double circular-arc helical gears, which lower the contact stress level and increase resistance to tooth bending, making this type of gear a common choice for handling higher torque. Bergesth and Bjorklund [53] recommended logarithmic crowning, which shifts the load peak from the edges to the middle of the tooth surface. The logarithmic crowning that originally created for roller bearings with the aim of enhancing the dispersion of stress, has not been extensively studied for its use in modifying the gear tooth surface. Lundberg's theory [54] was used to develop the logarithmic crowning, which was discovered to be more effective than conventional modification, resulting in considerably lower contact pressures when subjected to minor misalignments. Yangyang and colleagues [55] explored the development of the logarithmic equation, noting that several researchers have made enhancements and adjustments to the theoretical logarithmic convex equation [56-59]. Harianto and Houser [60] explain that longitudinal crowning is employed to counteract misalignments, and their selection is determined by the company's requirements, manufacturing precision, or load distribution analysis, which considers known peak misalignments.

Modifying the gear tooth surface can refine the contact properties of various gears and diminish the susceptibility to misalignments, but finding the appropriate amount of modification is essential to ensure smooth gear system transmission. Currently, different studies are focused on finding the optimal tooth modification, including crowning with various profiles, to minimize TE in the quest for higher transmission quality.

2.4 Parametric equations of tooth surface modification

In practical applications, misalignments of gears can have a significant impact on transmission quality and meshing performance. This can result in transmission errors, a high distribution of stress, and tooth edge contact, which can significantly increase vibration and noise in gear drives. In this study, the tooth contact performance of modified gear drives with alignment errors was investigated to evaluate the effect of tooth crowning. Accurate modifications are necessary in gear drives to avoid discontinuous transmission and edge contact when there is misalignment during transmission. However, excessive crowning can cause increased transmission error, while insufficient crowning can lead to gear teeth edge contact. Thus, the amount of crowning applied must be adjusted to provide engagement contact at a specific distance from the tooth surface edges, as well as an appropriate transmission error function.

Figure (9) displays the curves of modified longitudinal profiles of gear teeth, which exhibit similar flattening near the middle of the tooth flank. Nevertheless, the logarithmic profile has more bending compared to the parabolic or circular profile towards the edges of the tooth face. Consequently, meshing teeth with logarithmic crowning at regions close to the edges may result in unexpected outcomes in contrast to conventional profile modifications like circular or parabolic. Equations (10-12) present the function of the curves of the modified tooth flank.

$$\delta_p = c_1(v_i - v_o)^2 + c_2(v_i - v_o) + c_3, \quad (10)$$

$$\delta_c = R - \sqrt{R^2 - (v_i - v_o)^2}, \text{ where } R = \frac{4c_c^2 + b^2}{8c_c} \quad (11)$$

$$\delta_l = a_1 \text{Log} \left(\frac{1}{1 - a_2 \left(\frac{v_i - v_o}{v_o} \right)^2} \right), \quad (12)$$

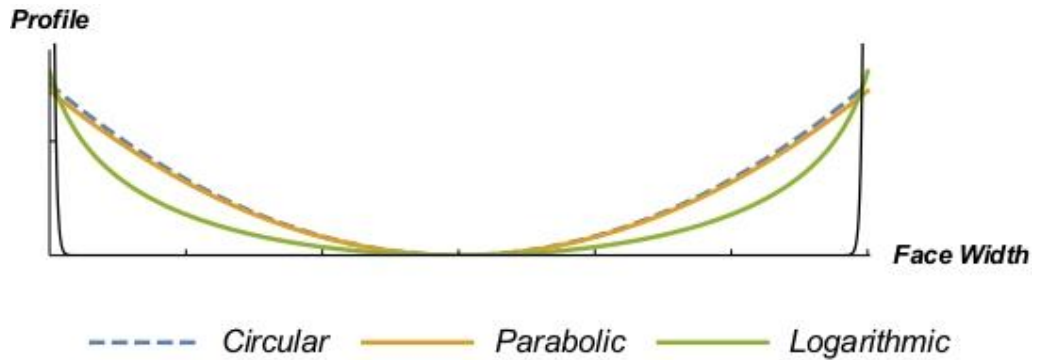


Figure 9. Curves of profile modifications, where an unmodified tooth flank with a straightforward edge fillet is shown by the black line.

Tip relief modification is another popular method for improving the contact and transmission performance of gears. It is typically used to prevent contact shocks that occur when a single-tooth contact transitions to double-tooth contact and vice versa. The tip relief function is shown in Equation (13), which involves surface parameterization using (u_i, v_i) and utilizes the Heaviside function to modify only a specific section of the profile.

$$\delta_t = H(u - u_0)c_m \left(\frac{u-u_0}{L}\right)^2. \quad (13)$$

In this equation, the variable u_0 represents the starting point of the correction, while c_m indicates the extent of modification. L refers to the length of the relief.

2.5 Transmission error

Transmission error (TE) is a primary source of noise and vibration in gear sets. It can be defined as the "discrepancy between the real position of the output gear and where it would be positioned if the gear drive were perfectly matched." This type of gear transmission error is commonly encountered in real gear systems due to factors such as irregular tool geometry, imperfect mounting, misalignment between the two gears, and other similar issues. The TE vary from zero due to surface mismatch or misalignment and can be calculated using the equation below:

$$\Delta\varphi = (\varphi_2 - \varphi_{20}) - \frac{N_1}{N_2}(\varphi_1 - \varphi_{10}), \quad (14)$$

where φ_{10} and φ_{20} are the rotational angles of the pinion and the gear when tooth surfaces are in contact at an initial contact point. Here, φ_2 is the gear rotational angle corresponding to the pinion rotational angle φ_1 , which is an independent variable. The function of transmission error $\Delta\varphi$ is a periodic function with the period $T = 2\pi/N_1$. $\Delta\varphi$ has different shapes depending on conditions such as the angle of misalignment or applied crowning. Figure (10) displays example of the result of TE ($\Delta\varphi$) caused by gear misalignment without applying any modification.

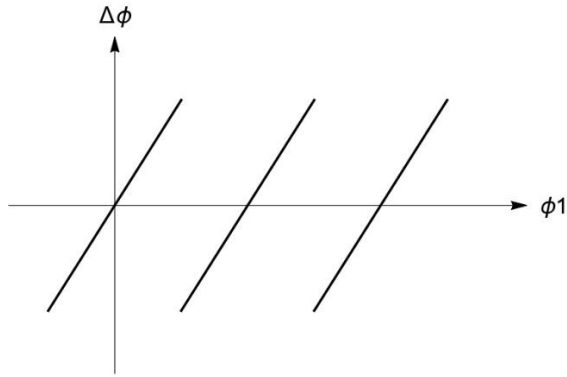


Figure 10. The function of TE at the present of angular misalignment in gear system.

In the case where meshing gears without crowning are misaligned, their axes are crossed or intersected. In that case, the edge of the pinion tooth surface will be in tangency with the gear tooth surface, which will lead to the path of contact located at the edge of the tooth flank as in Figure (11), accompanied by the discontinuous function of TE as shown in Figure (10). In this circumstance, gear transmission at the end of the meshing cycle is inevitably accompanied by a jump in the angular velocity, vibration, and noise.

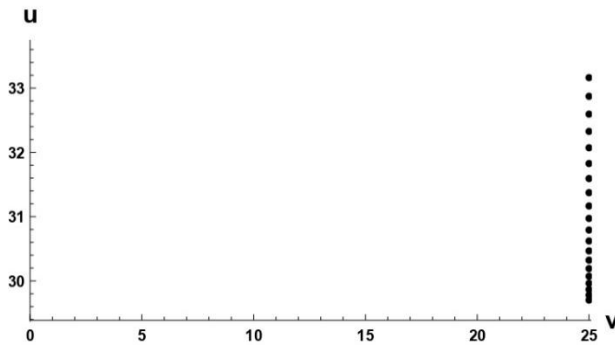


Figure 11. Path of contact of spur gear with in-plane angular misalignment.

2.6 Gear tooth contact analysis methods

The study of gear tooth contact analysis (TCA) is critical in the design and performance evaluation of gear systems. TCA involves the determination of the contact conditions between meshing gears, including the contact pattern, contact pressure distribution, and tooth surface strains. Computer simulation of gear tooth interaction allows to evaluate all gear-related processes during the design phase, which can encompass misalignment, transmission errors, tooth damage, noise, and vibration.

Litvin [1] is a well-known expert in this field and has developed essential methods for tooth contact analysis (TCA) and local synthesis, determining the interaction between two gear teeth in machine tool settings. To minimize noise and vibration in a meshing spur and helical gear pair, Litvin and his team [61-63] proposed a five degree of freedom equation system to modify their geometry and reduce transmission errors while avoiding tooth edge contact. They later applied this method to examine the interaction of misaligned spur and helical gear pairs by using double crowning of tooth surfaces with a parabolic transmission error function. In addition, Litvin and his team [64,65] utilized this tooth surface topology to pinpoint the bearing interaction. The primary limitation of the model is that determining the location of the surface contact is essential for obtaining an accurate solution, but this demands a substantial amount of computational power. If this computational power is not available, the numerical computation process experiences convergence issues. To address this and other related problems, different studies have proposed alternative models for tooth contact analysis.

Bracci [66] proposed a geometric approach that does not require considering the curvature of the surface to estimate the contact pattern. This method employs a surface intersection procedure that simulates the removal of marking compound during meshing, ultimately estimating the instantaneous contact area.

Lin and Fong [67] suggested an alternative approach that eliminates the need for using normal vectors to determine the coordinates of contacting points based on surface position. They introduced a numerical approach vector exclusively for this purpose.

Spitas and colleagues [68] introduced a novel set of basic two-dimensional contact equations for the two-dimensional issue, specifically for spur parallel-axis gearing, which reduced Litvin's model of five nonlinear equations with five unknowns and one independent parameter to a system of only two equations with two unknowns and one independent parameter.

Wang et al. [69] introduced optimization methods that involve the discretization of unknown parameters. In contrast, this study introduces a simplified model for the conventional TCA method of gear analysis, incorporating new perspectives on geometry and kinematics.

While these methods are indeed more advanced TCA approaches, it's important to note that they still primarily serve as optimizations of conventional TCA methods or describe only two-dimensional contact cases. In contrast, our work offers a more explicit solution, allowing for the definition of unknown free parameters through a straightforward geometric approach. This distinction underscores the unique contribution and innovation in our research compared to the refinement of existing approaches by other authors.

One traditional TCA method is the use of the elliptical contact theory, which assumes a uniform contact pressure distribution over the entire tooth surface. However, this theory has been shown to provide unrealistic results, particularly in cases where the load distribution is not uniform. To address this issue, studies on loaded tooth contact analysis (LTCA) have been carried out to assess contact properties that avoid edge contact, concentrated stresses, low vibration, and acceptable transmission error [70].

2.7 Hertzian stress contact analysis

Hertzian stress is a term used to describe the stress that arises at the point of contact between two bodies in mechanical systems. This stress is proportional to the pressure applied at the point of contact and is described by the Hertz theory, which was developed by the German physicist Heinrich Hertz in the late 19th century. Hertzian stress is a critical factor in many engineering applications, such as in the design of bearings, gears, and other mechanical components. Contact analysis is a crucial tool in the determination of Hertzian stress and its effects on mechanical systems. This analysis involves the use of mathematical models and simulations to understand the behavior of stress at the point of contact and to predict the behavior of mechanical components under different loads and conditions [71,72]. There have been numerous studies conducted on Hertzian stress and contact analysis, and this research has contributed to a better understanding of the relationship between contact stress and the behavior of mechanical components. Some of the key findings from this research include the importance of considering surface roughness and material properties in contact analysis, the role of geometry and load distribution in determining Hertzian stress, and the importance of taking into account the dynamic behavior of mechanical components in contact analysis [73,74]. In recent years, advances in computer-aided design (CAD) and simulation software have allowed for more accurate and efficient analysis of Hertzian stress in mechanical systems. This has led to improvements in the design of mechanical components and has opened up new possibilities for the optimization of existing systems [75-78]. The Hertzian stress is also an important concept

in gear tooth contact analysis. In gear systems, the Hertzian stress can play a critical role in determining the durability and efficiency of the gears, as well as the overall performance of the system. When gear teeth come into contact, the Hertzian stress is generated at the point of contact. This stress is a result of the indentation force that is generated by the meshing of the gear teeth. The Hertzian stress can have a significant impact on the life of the gear teeth and the gear system as a whole. For example, if the Hertzian stress is too high, it can cause deformation, pitting, or fatigue failure in the gear teeth. Gear tooth contact analysis is used to evaluate the Hertzian stress and predict its effects on the gear system. This analysis can be used to optimize the design of the gear teeth [79-81]. Additionally, gear tooth contact analysis can be used to identify potential failure modes and to develop maintenance schedules for gear systems.

This study proposes an analytical method for assessing stress in misaligned gear drives with localized bearing contact. The method, based on Hertz theory, determines the area of contact and maximum contact stress for various gear drives by using crowned tooth surfaces to avoid edge contact. The contact pressure is transmitted along an elliptical area during engagement of the crowned teeth, which is influenced by the contact geometry and tooth modifications. The dimensions of the contact ellipse can be determined by using the principal curvatures of the gear teeth surfaces at the point of contact [82,83], as follows:

The first fundamental forms of the tooth surface are calculated using the surface parametric equation $\vec{f}_i(u_1, v_1)$, to determine the maximum and minimum principal curvatures at the point of contact on the tooth surface,

$$E = \frac{\partial \vec{f}_i(u_1, v_1)}{\partial u} \cdot \frac{\partial \vec{f}_i(u_1, v_1)}{\partial u} \quad G = \frac{\partial \vec{f}_i(u_1, v_1)}{\partial v} \cdot \frac{\partial \vec{f}_i(u_1, v_1)}{\partial v} \quad F = \frac{\partial \vec{f}_i(u_1, v_1)}{\partial u} \cdot \frac{\partial \vec{f}_i(u_1, v_1)}{\partial v} \quad (15)$$

and second fundamental forms as:

$$L = \hat{n} \cdot \frac{\partial^2 \vec{f}_i(u_1, v_1)}{\partial u^2} \quad N = \hat{n} \cdot \frac{\partial^2 \vec{f}_i(u_1, v_1)}{\partial v^2} \quad M = \hat{n} \cdot \frac{\partial^2 \vec{f}_i(u_1, v_1)}{\partial u \partial v} \quad (16)$$

After determining the maximum and minimum principal curvatures of the point of contact on the tooth surface using the normal vector at contact point, the first fundamental forms of the tooth surface are calculated using the surface parametric equation $\vec{f}_i(u_1, v_1)$. From these fundamental forms, the Gaussian and mean curvatures of the surface $\vec{f}_i(u_1, v_1)$ can be calculated.

$$K = \frac{LN-M^2}{EG-F^2} \quad \text{and} \quad H = \frac{EN+GL-2FM}{2(EG-F^2)}, \quad (17)$$

Here, K represents the intrinsic property of curvature, and H represents the extrinsic property of curvature, which are not dependent on the coordinate system. The maximum and minimum principal curvatures at the contact point on the tooth surface (u_1, v_1) can be determined using the following equation:

$$\kappa_{max}^{(i)} = \frac{1}{R_{max}^{(i)}} = H + \sqrt{H^2 - K} \quad \kappa_{min}^{(i)} = \frac{1}{R_{min}^{(i)}} = H - \sqrt{H^2 - K}, \quad (18)$$

The maximum and minimum radii of curvatures, denoted as $R_{max}^{(i)}$ and $R_{min}^{(i)}$, respectively, are used to determine the shape of the contact area for crowned canonical involute profiles of gears, which results in an elliptical shape even when there is a misalignment during transmission. To calculate the eccentricity of the contact ellipse, the composite radii are defined as:

$$\frac{1}{R_x} = 2A = \frac{1}{R_{max}^{(1)}} + \frac{1}{R_{max}^{(2)}} \quad \text{and} \quad \frac{1}{R_y} = 2B = \frac{1}{R_{min}^{(1)}} + \frac{1}{R_{min}^{(2)}}, \quad (19)$$

The numerical estimation of the eccentricity of the contact area is obtained by equating:

$$\frac{1}{[K(e)-E(e)]} \left[\frac{E[e]}{(1-e^2)} - K(e) \right] = \frac{B}{A}, \quad (20)$$

The eccentricity of the contact area is estimated numerically using Newton's method. The first and second kind complete elliptic integrals, $K(e)$ and $E(e)$, respectively, are involved in the estimation process. These integrals can be expressed in terms of a function.

$$K(e) = \int_0^{\pi/2} \frac{d\theta}{\sqrt{1-e^2\theta}} \quad \text{and} \quad E(e) = \int_0^{\pi/2} \sqrt{1-e^2\theta} d\theta. \quad (21)$$

The major axes a and minor axes b of the contact ellipse can then be obtained after determining the eccentricity (e) :

$$a = \left(\frac{3PC_E[K(e)-E(e)]}{2\pi e^2 A} \right)^{1/3} \quad \text{and} \quad b = a\sqrt{1-e^2}, \quad (22)$$

where the material modulus C_E is:

$$C_E = \frac{1-\nu_1^2}{E_1} + \frac{1-\nu_2^2}{E_2}, \quad (23)$$

The equation for the maximum contact pressure can be found after specifying the load P and using the Young's modulus E_1 and E_2 , and the Poisson's ratios ν_1 and ν_2 of the pinion and gear. The equation is:

$$p = \frac{3P}{2\pi ab}. \quad (24)$$

Calculating a dimensionless pressure value can help evaluate the impact of tooth profile or alignment changes on stress distribution and streamline simulation. This involves dividing the maximum contact pressure obtained from Equation (24) by the maximum pressure for an aligned and unmodified tooth contact, which is denoted as p_o . The resulting dimensionless pressure value can then be used to compare the effects of profile modification or misalignment on stress distribution, and to make the simulation process more convenient. The stress ratio SR (or σ) can be expressed as:

$$SR = \frac{p}{p_o}. \quad (25)$$

Chapter 3. Mathematical models of gear TCA method

3.1 Conventional TCA method

Litvin et al. [1] presented a solution for the problem of the geometrical contact of two rotating surfaces in the context of gear tooth contact analysis, as shown in Figure (12). Their approach involved assuming the presence and smoothness of surface gradients and using a surface tangency condition to represent the gear tooth contact. Specifically, the tooth surfaces S_1 and S_2 were considered to be in point tangency, and vector equations in the coordinate system S_f were used to describe the instantaneous tangency of the surfaces.

$$\vec{r}_f^{(1)} - \vec{r}_f^{(2)} = 0, \quad (26)$$

$$\vec{n}_f^{(1)} - \vec{n}_f^{(2)} = 0. \quad (27)$$

The unit vector of surface normal is represented by $\vec{n}_f^{(1,2)}$, and the position vectors are illustrated by $\vec{r}_f^{(1,2)}$. Equation (26) generates three independent scalar equations, while Equation (27) generates only two, as

$$|\vec{n}_f^{(1)}| = |\vec{n}_f^{(2)}| = 1, \quad (28)$$

If needed, the collinearity of the surface normals can be determined in the following manner:

$$N_1 = \lambda N_2 \quad (\lambda \neq 0), \quad (29)$$

Assuming that gear 1 is the reference gear, Equations (26-27) provide a set of six non-linear equations, where five are independent, with five unknowns and one applied parameter (ϕ_1), denoted by

$$f_i(u_1, v_1, \phi_1, u_2, v_2, \phi_2) = 0, \quad f_i \in C^1, \quad (i = 1, \dots, 5). \quad (30)$$

where f_i belongs to the set of continuously differentiable functions C^1 (Equation (30)). The local frame of reference bound to each gear is used to describe the corresponding surfaces

with two parameters (u_1, v_1) and (u_2, v_2) which rotate together with their respective gears by angles ϕ_1 and ϕ_2 . The equations can be solved for a contact point using the Theorem of Implicit Function System Existence, with the condition that the Jacobian is non-zero, as shown in Equation (31).

$$0 \neq \frac{D(f_1, f_2, f_3, f_4, f_5)}{D(u_1, v_1, u_2, v_2, \phi_2)}, \quad (31)$$

$$\{u_1(\phi_1), v_1(\phi_1), u_2(\phi_1), v_2(\phi_1), \phi_2(\phi_1)\} \in C^1. \quad (32)$$

The aim is to obtain the unknown parameters of the reference gear (u_1, v_1) and its mating gear (u_2, v_2, ϕ_2) , where these parameters are continuously differentiable functions according to Equation (32). This method is generally applicable to any gear tooth surface geometry and to gear tooth surfaces that are not aligned, as demonstrated by Figure (12), which shows the helical gear tooth surface contact in the case of in-plane misalignment.

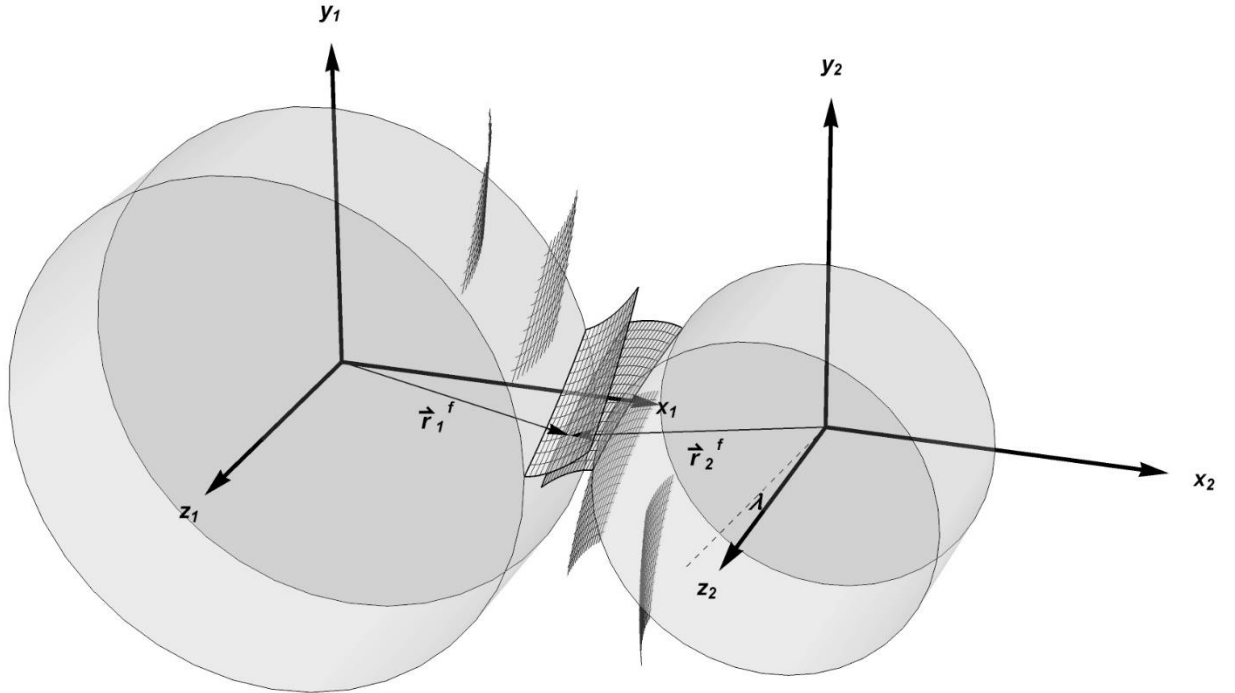


Figure 12. This figure depicts a diagrammatic representation of the contact between the teeth of a helical gear pair.

The simulation process involves analytical expression of gear tooth misalignment through the rotation matrix $R(\lambda)$. The system's solution relies on the application of subroutines

with an iterative process. However, numerical solutions are sensitive to the selection of initial "guess values," and therefore heavily rely on it. Inaccurate results may be generated by the numerical algorithm, such as convergent solutions that are not accurate compared to the actual ones, or the algorithm may fail to converge if the guess values are not carefully selected.

3.2 Novel TCA method

In order to overcome convergence issues that appear in conventional passive models, we have presented a novel set of nonlinear equation to describe tooth contact condition. It is assumed that the surfaces of the contacting teeth are continuous C^1 and revolve about axes w_i in a fixed coordinate system, as shown in Figure (13). The surface meshing is achieved by fulfilling the surface tangency conditions.

$$\vec{n}_1(u_1, v_1, \phi_1) \times \vec{n}_2(u_2, v_2, \phi_2) = 0, \quad (33)$$

$$\vec{n}_i = \frac{\partial \vec{r}_i}{\partial u} \times \frac{\partial \vec{r}_i}{\partial v} \quad \text{and} \quad \vec{r}_i = R_i(\phi_i) \vec{f}_i(u_i, v_i) \quad i = 1, 2, \quad (34)$$

The tooth meshing equation is formed based on this parameterization of the surfaces, which is represented by the radial distance u_i of a contact point from the surface rotation axis w_i and the algebraic projection v_i of the position vector \vec{r}_i onto the same axis.

$$v_i = \vec{w}_i \cdot \text{proj}_{\vec{w}_i} \vec{r}_i, \quad (35)$$

$$u_i = \|\vec{r}_i - \text{proj}_{\vec{w}_i} \vec{r}_i\|. \quad (36)$$

The position vector $\vec{r}_i(u_i, v_i)$ is assumed to be a C^1 continuous function. The parameters u_i and v_i describe the lengths of a right triangle with the hypotenuse as the position vector \vec{r}_i of the contact point on the tooth surface. A rotation matrix $R_i(\phi_i)$, which represents the rotation of the tooth by an angle ϕ_i , is used in combination with the surface equations (\vec{f}_i) to define the vector $\vec{r}_i(u_i, v_i)$.

$$\vec{r}_i = R_i(\phi_i) \vec{f}_i(u_i, v_i) \quad i = 1, 2. \quad (37)$$

In addition, the common point of contact is obtained by summing the free vectors:

$$\vec{r}_1 - \vec{a}_{12} - \vec{r}_2 = \vec{0}. \quad (38)$$

The vector distance between the coordinate systems of each surface is represented by \vec{a}_{12} . With specific geometric relationships, the parameters u_2, v_2 and ϕ_2 can be directly calculated in terms of u_1, v_1, ϕ_1 .

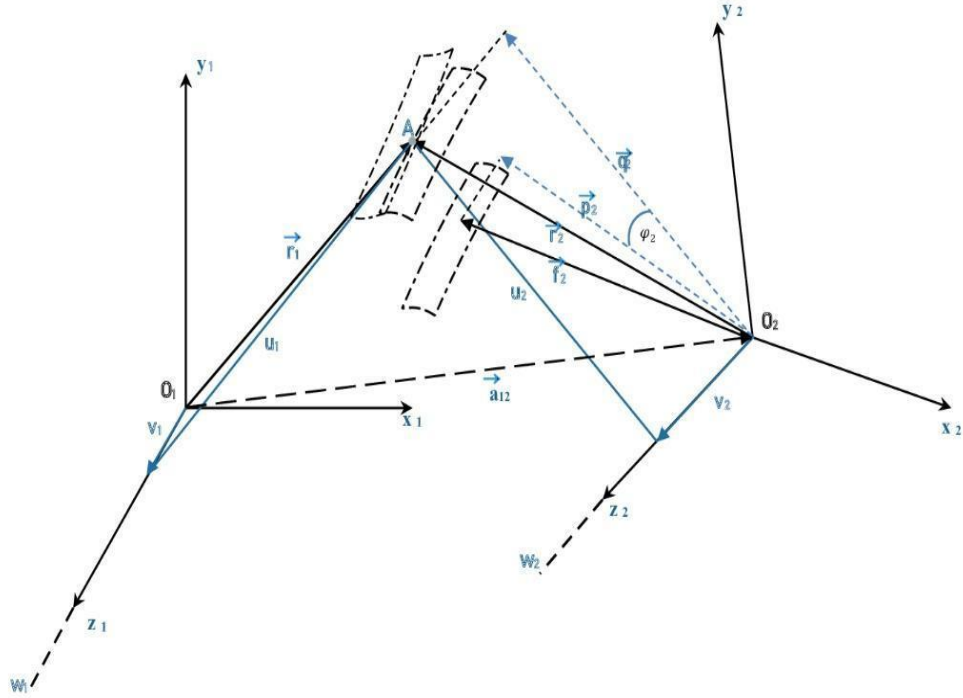


Figure 13. The diagrams demonstrate the interaction between the surfaces of the first and second teeth as they revolve around their respective fixed axes, w_1 and w_2 .

$$v_2 = \text{proj}_{\vec{w}_2} \vec{r}_2 = \vec{w}_2 \cdot (R_1(\phi_1) f_1 - \vec{a}_{12}), \quad (39)$$

where the applied parameter angle ϕ_1 describes the rotation of the first surface. The Pythagorean theorem states:

$$u_2 = \sqrt{\vec{r}_2(u_2, v_2)^2 - v_2^2} = \sqrt{(R_1(\phi_1) f_1(u_1, v_1) - \vec{a}_{12})^2 - v_2^2}, \quad (40)$$

The projection of vectors \vec{f}_2 and \vec{r}_2 onto a \hat{z}_2 -plane is used to calculate the rotation angle

ϕ_2 around fixed axis \vec{w}_2 , where $\vec{f}_2(u_2, v_2)$ and $\vec{r}_2(u_2, v_2)$ describe the surface and position vector of a meshing teeth, respectively.

$$\vec{p}_2(u_2, v_2) = \text{proj}_{\hat{z}_2\text{-plane}} \vec{f}_2(u_2(u_1, v_1), v_2(u_1, v_1)) , \quad (41)$$

$$\vec{q}_2(u_2, v_2) = \text{proj}_{\hat{z}_2\text{-plane}} \vec{r}_2(u_2(u_1, v_1), v_2(u_1, v_1)) , \quad (42)$$

where $\vec{q}_2(u_2, v_2)$ is a projection of $\vec{r}_2(u_2, v_2)$ on the \hat{z}_2 -plane and $\vec{p}_2(u_2, v_2)$ is a projection of $\vec{f}_2(u_2, v_2)$. With the dot product concept, the following problems can be resolved:

$$\phi_2 = \pm \cos^{-1} \frac{\vec{p}_2(u_2, v_2) \cdot \vec{q}_2(u_2, v_2)}{\|\vec{q}_2\|^2} . \quad (43)$$

$$\frac{\vec{p}_2(u_2, v_2) \times \vec{q}_2(u_2, v_2)}{\|\vec{p}_2(u_2, v_2) \times \vec{q}_2(u_2, v_2)\|} \cdot \vec{w}_2 = \pm 1 , \quad (44)$$

where the direction will be positive for a clockwise rotation and negative for an anticlockwise rotation. Equations (34-44) can be substituted into Equation (33) to obtain scalar equations that only depend on two independent parameters (u_1, v_1) and one applied parameter ϕ_1 . A numerical method can be used to calculate the surface contact point for the first tooth, and the remaining unknowns can be explicitly defined through back substitution. This allows the contact point on the meshing surface and its position in space to be determined. In the proposed method, a parametric quasi-static study is carried out on the contact between gear teeth by introducing innovative kinematic and geometric perspectives to enhance the understanding of the meshing process. As a result, it should be noted that the research primarily focuses on these aspects and does not explicitly involve rotational speed as a variable in the study.

3.3 New TCA model in spherical coordinate system

The tooth contact analysis (TCA) model for spur and helical gears is typically described using the cylindrical coordinate system. However, when analyzing other types of gears, such as bevel gears, it is necessary to switch to a spherical coordinate system for TCA. The proposed

solution for the bevel gear tooth contact problem is represented using surface tangency conditions as in previous section. These conditions involve two surfaces, S_1 and S_2 , which revolve around a fixed axis \vec{w}_i and are C^1 continuous. The conditions are illustrated in Figure (14). To perform TCA in the spherical coordinate system, we will define $u_{1,2}$ as the angle between the $w_{1,2}$ axis and the contact point, and $v_{1,2}$ as the radial distance from the origin $O_{1,2}$ to the contact point. The process for calculating the contact position is the same as in the previous section, with the exception that u_2 is defined differently as follows:

$$u_2 = \cos^{-1}(\cos \Sigma_o \cos u_1 + \sin \Sigma_o \sin u_1 \cos (|\varphi_1| \pm \vartheta_1)), \quad (45)$$

$$\vartheta_1 = \frac{1}{\sin(\alpha_1)} \sin(\alpha_1) \tan\left(\frac{\tan(\alpha_1)}{\tan(u_1)}\right) - \frac{\tan(\alpha_1)}{\tan(u_1)}. \quad (46)$$

The variable ϑ_1 represents the involute polar angle of the meshing gear. When there is contact between the gear tooth surface and the addendum, ϑ_1 assumes a positive sign, whereas when there is contact with the dedendum, it assumes a negative sign. The angle of the shaft is denoted by Σ_o . By substituting Equations (34-44), two scalar equations with two independent parameters (u_1, v_1) can be defined.

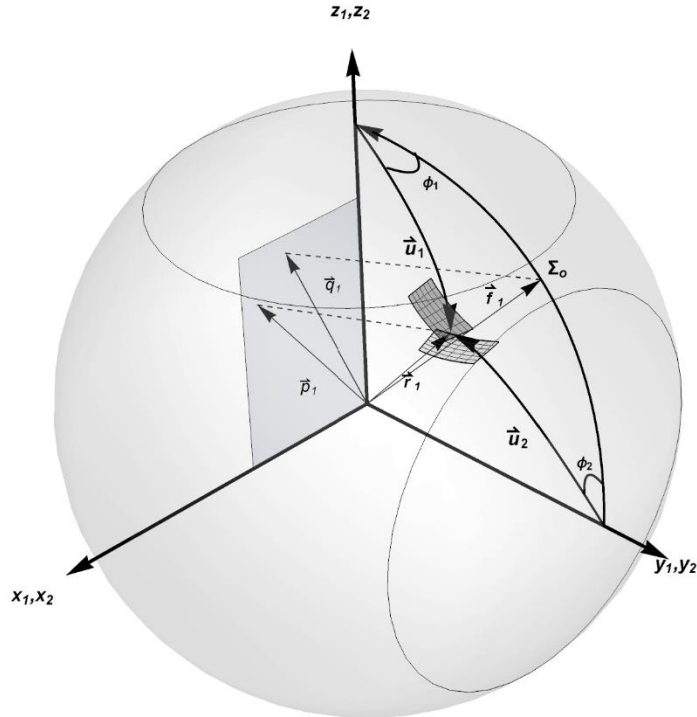


Figure 14. The interaction between involute bevel teeth is shown schematically.

Chapter 4. Cylindrical gears contact analysis using the proposed TCA method

4.1 Spur gears contact analysis

The Wolfram Mathematica software was utilized to simulate a proposed new set of equations for TCA, which involve two unknown parameters (u_i and v_i), for meshing two C^1 spur involute surfaces with alignment errors. Involute spur gears are susceptible to in-plane and out-of-plane angular misalignment, which can be prevented by crowning the mating tooth surface to localize bearing contacts while keeping the second gear unmodified. The modelling process considered both in-plane ($\Delta\gamma$) and out-of-plane ($\Delta\delta$) angular misalignment, as well as in-plane (ΔE) and out-of-plane (ΔH) axial off-set along the x and y-axis. The misalignment amounts used in the simulation were $\Delta\gamma=17.5$ mrad, $\Delta\delta=17.5$ mrad, $\Delta E=0.2$, and $\Delta H=0.2$. During the simulation, the gears' rotation axes were parallel ($\vec{w}_1 || \vec{w}_2$) and oriented along the z-axis. The simulation used the following gear parameters: number of teeth $N_1 = N_2 = 25$, module $m = 1$, pressure angle $\alpha = 20^\circ$, and tooth face width $b = 10$, where m and b were non-dimensionalized.

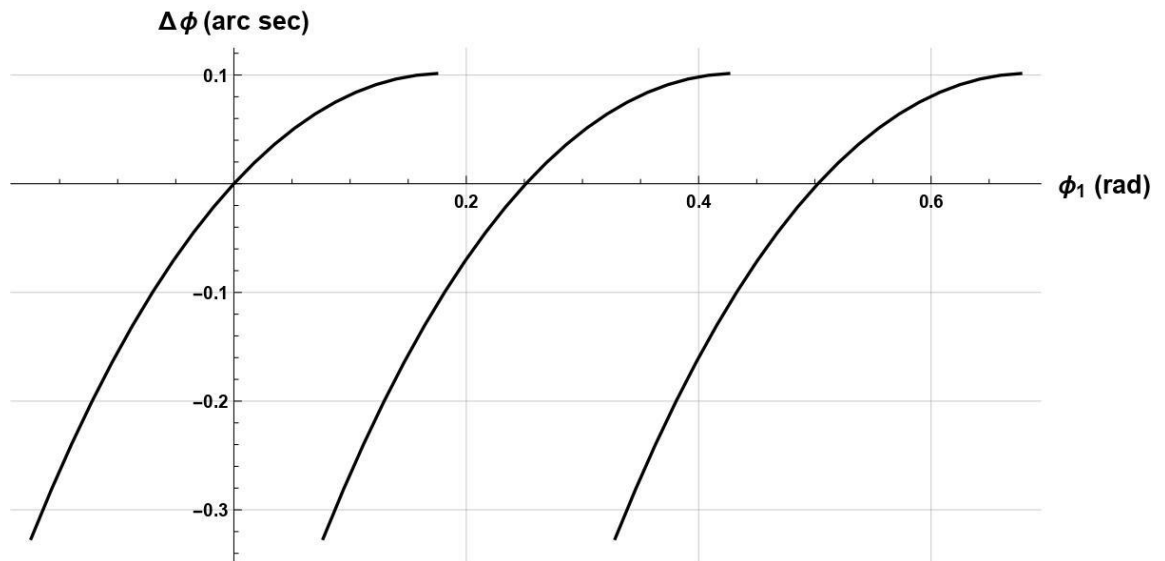


Figure 15. The transmission function is discontinuous due to insufficient parabolic modification.

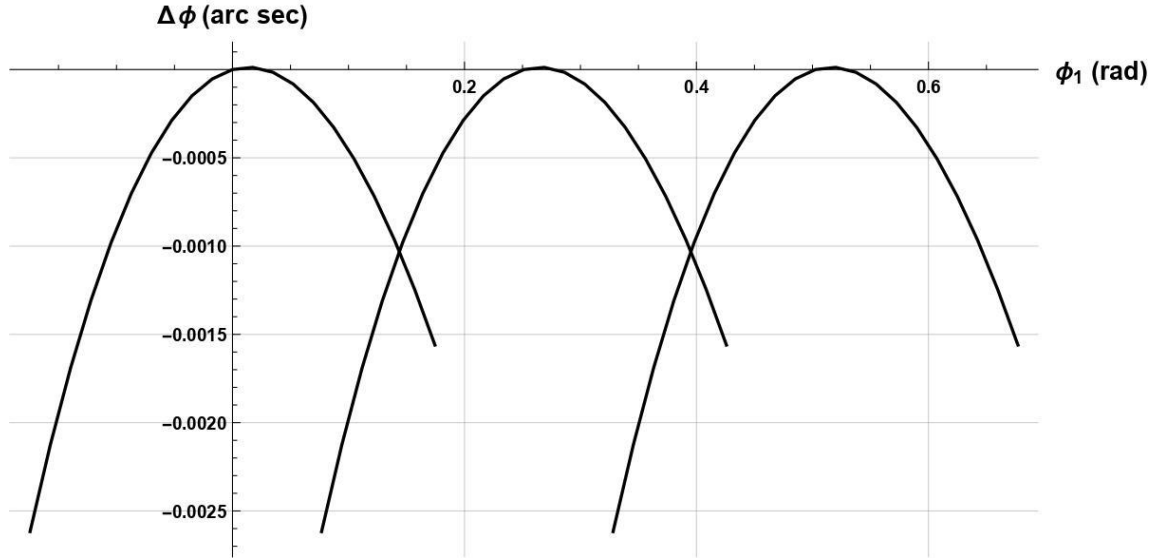
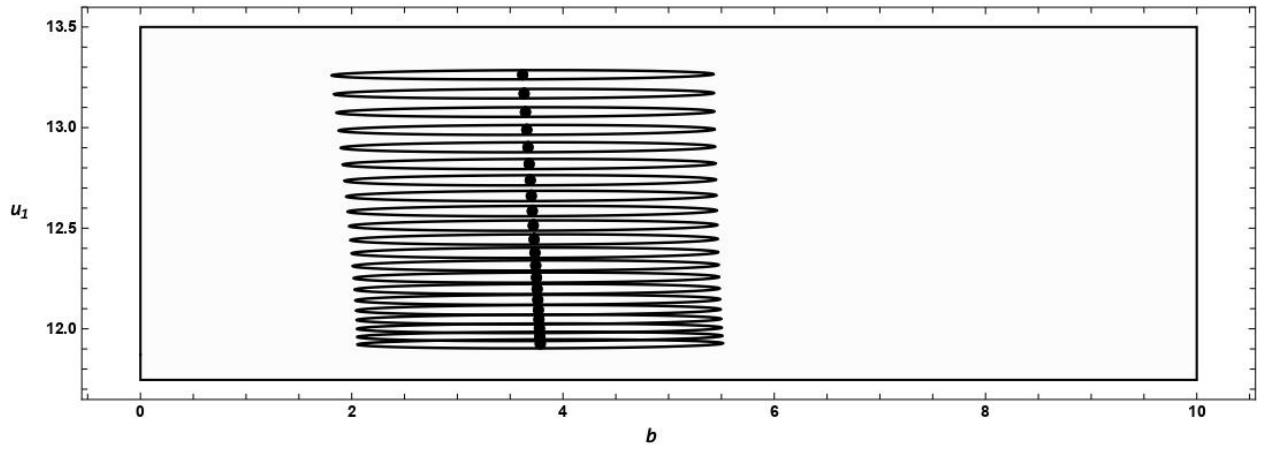


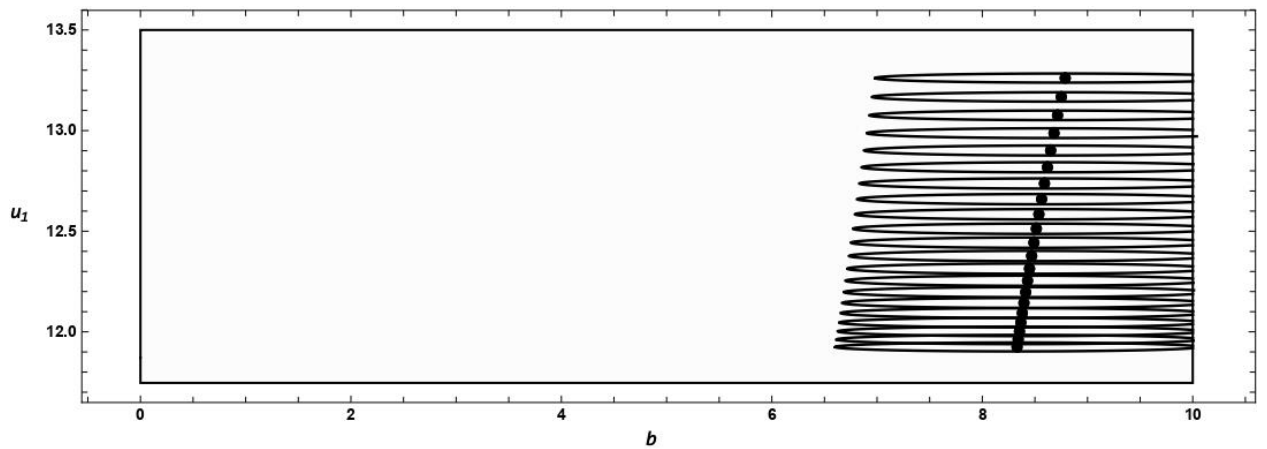
Figure 16. With enough parabolic adjustment, the continuous transmission function can be obtained.

Figures (15) and (16) illustrate the results of the analysis of the transmission function. In Figure (15), a parabolic crown with a value of $a_1 = 0.00125$ in inverse non-dimensional length units is utilized, causing a curved transmission error function due to in-plane misalignment. The intermittent function suggests that the modifications made were insufficient, which may result in gear tooth engagement noise and vibration. However, Figure (16) demonstrates that a satisfactory modification of $a_1 = 0.01675$ was made, leading to a continuous parabolic transmission function. For the stress simulation analysis, the Poisson's ratio of the gears was set to $\nu = 0.3$, the elasticity modulus to $E = 200$ GPa, and a total applied load of $F = 56 \times 10^{-6}$ was utilized to determine the contact trace and contact ellipses for various misalignments and surface modifications, as depicted in Figures (17) and (18). Figure (17) shows the contact path when longitudinal parabolic crowning of $a_1 = 0.0025$ is applied to prevent contact with the edges in the case of angular and linear alignment errors. However, this leads to discontinuous transmission. On the other hand, Figure (18) displays the contact path for in and out-of-plane misalignment with tip and root relief and longitudinal crowning, resulting in an unusual contact trace but an asymmetrically continuous transmission function with similar outcomes for both angular misalignments, as shown in Figure (15). The number of modification parameters for the crowning and the tip-root relief were selected as $a_1 = 0.0025$, $L_1 = 0.6$, $L_2 = 0.4$ and $c_m = 0.4$. Lastly, Figure (19) illustrates the contact path in the presence of both

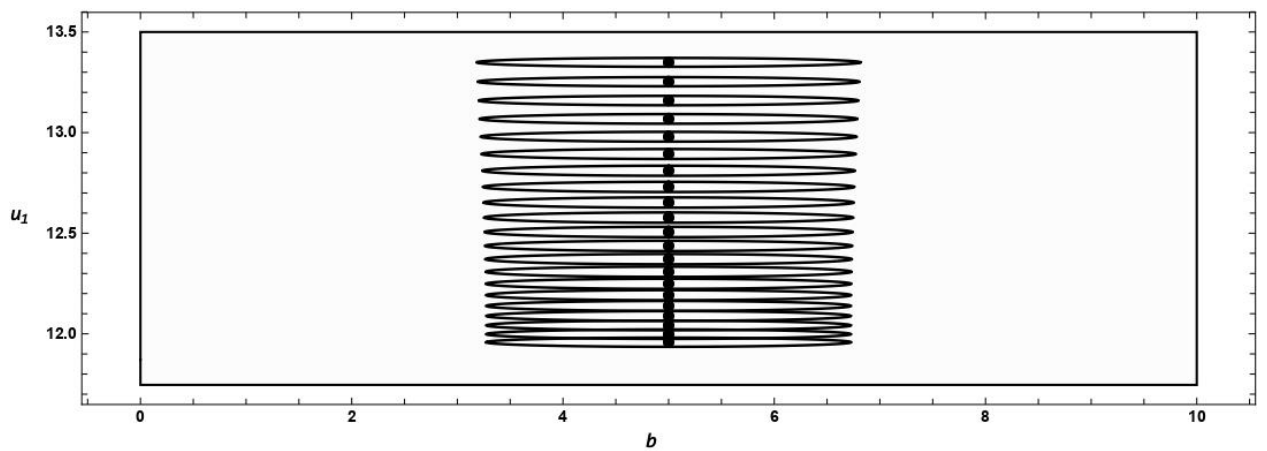
out and in-plane angular misalignments with the same modification parameters, and the result of the transmission function is not significantly different from Figure (20).



(a)

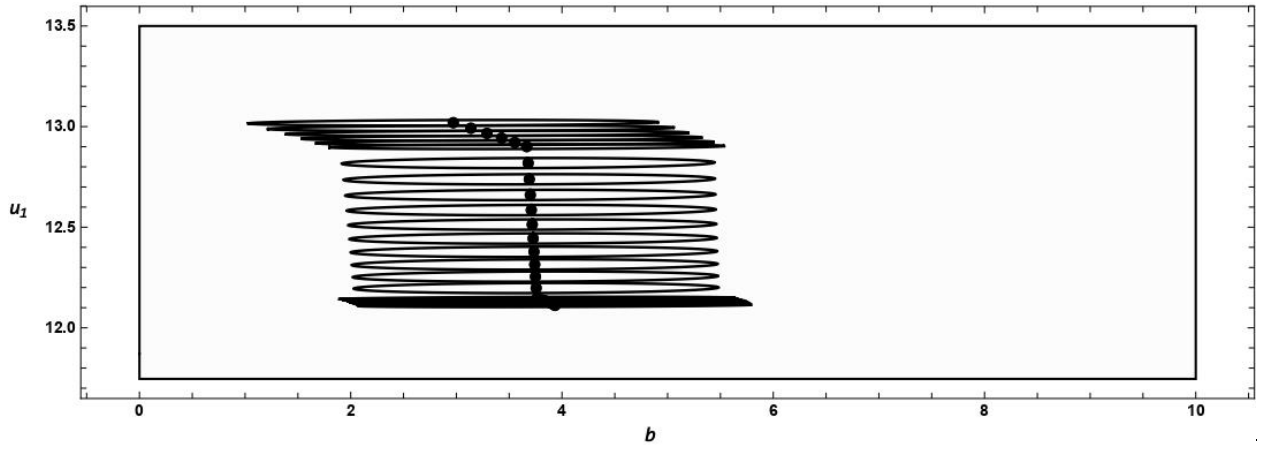


(b)

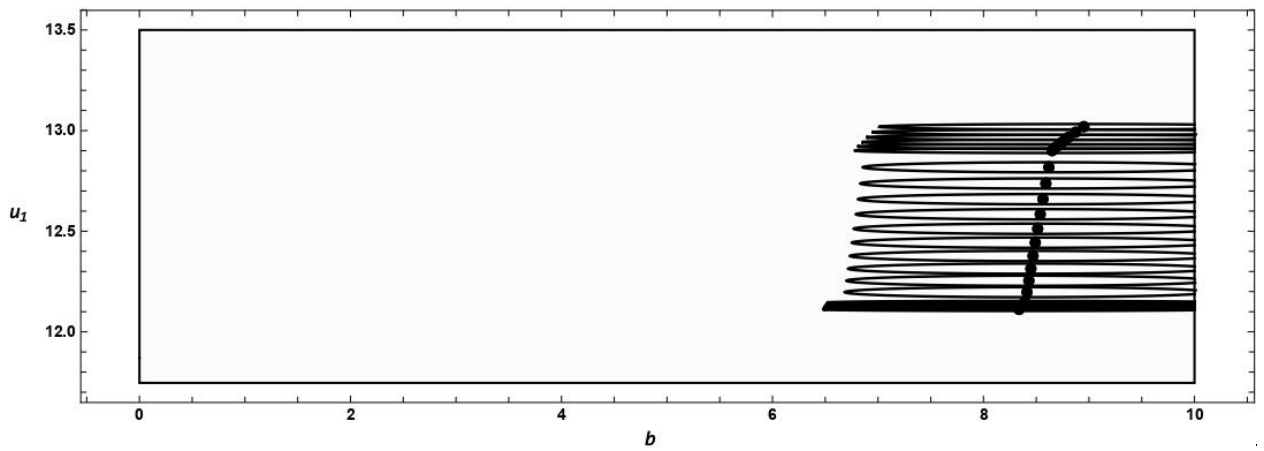


(c)

Figure 17. Path of contact with contact ellipses for (a) In-plane and (b) Out-of-plane angular misalignment; (c) Axial off-set



(a)



(b)

Figure 2. The contact path of the tooth surface with tip-root relief and crowning with in-plane (a) and out-of-plane (b) angular misalignments.

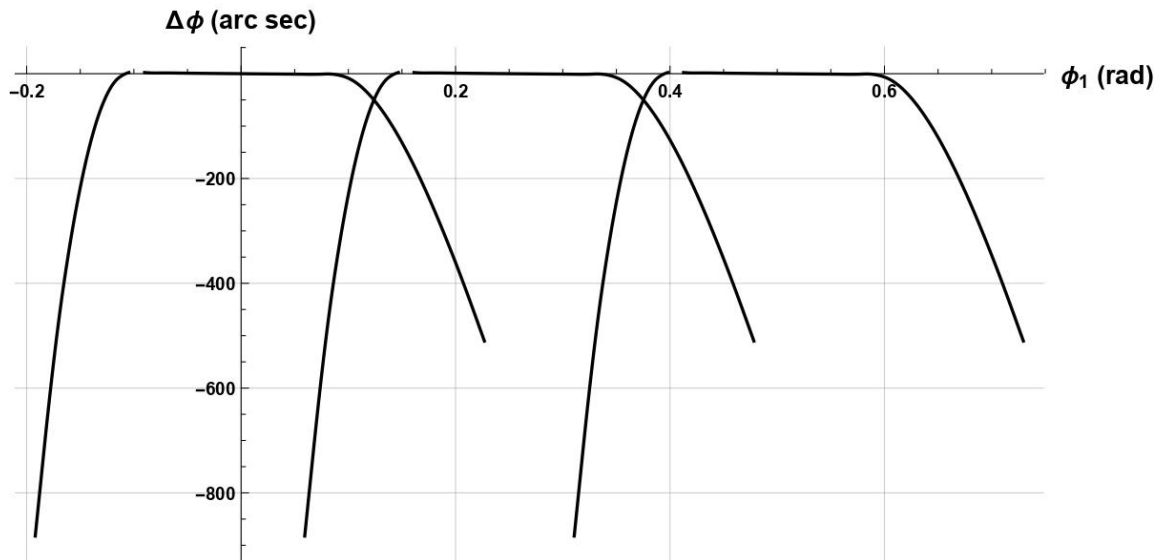


Figure 19. Transmission with tooth surface modification with angular misalignment.

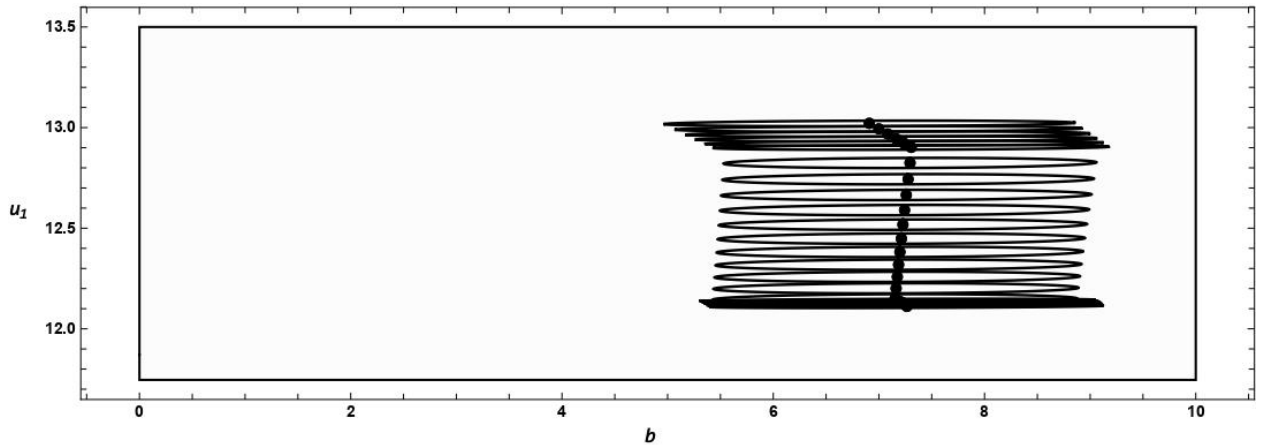


Figure 20. Path contact with combined out and in-plane angular misalignments.

Figures (21) and (22) were presented to visualize how contact stress changes at different stages of contact. The vertical axis represents a non-dimensionalized tooth profile, while the horizontal axis represents the stress ratio. Figure (21) shows the stress distribution for in-plane angular misalignment with longitudinal crowning of the tooth, whereas Figure (22) shows stress distribution for in-plane alignment error with both root tip relief and longitudinal crowning. Comparing the two figures, it is evident that the tip-root relief alters the contact trajectory in an unusual way and unevenly distributes pressure. In both cases, the highest pressure on the tooth surface is exerted at the top and bottom, which aligns well with previous studies conducted on this topic and supported by experimental or finite element methods validation [84-91].

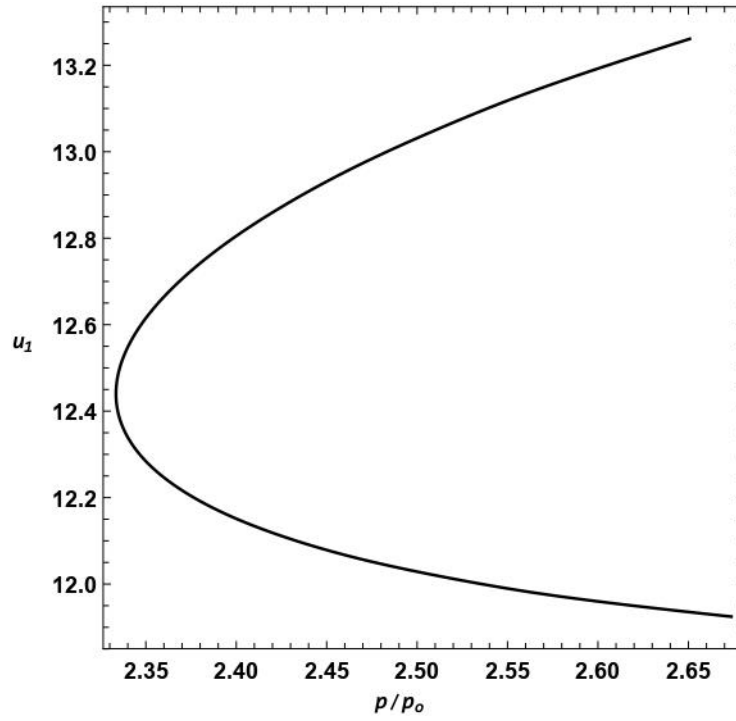


Figure 21. SR vs u_1 regarding in-plane angular alignment error with longitudinal crowing.

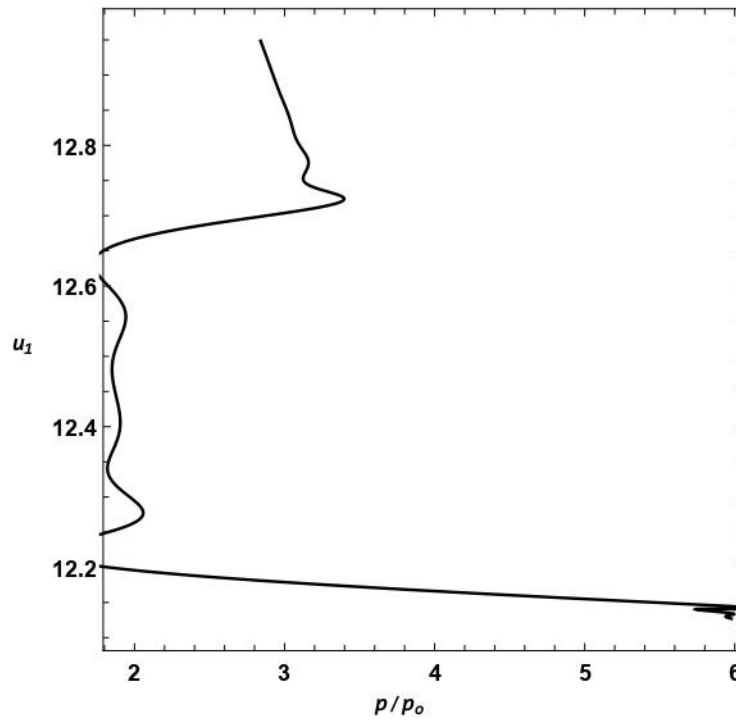


Figure 22. SR vs u_1 with in-plane angular misalignment with longitudinal crowing and tip-root relief.

4.2 Helical gears contact analysis

The need to modify involute helical gears is evident from the application of design principles and testing with TE and contact, particularly when there is angular misalignment. The involute gearing is sensitive to assembly errors, including changes in the shaft angle, which affects the contact between tooth surfaces. Although traditional designs ensure immediate contact along a line, angular misalignment can cause the contact line to change to a point at the tooth flank's edge, leading to inconsistent linear functions of TE, noise, and vibration. The angles of angular misalignment used in the study were chosen based on and consistent with previous research [1].

In this study, a new set of three-dimensional equations for contact between teeth surfaces was used to simulate the TCA (tooth contact analysis) of misaligned helical gears. This approach is similar to what was done for spur gears in earlier sections. The effects of different types of crowning, such as parabolic, circular and logarithmic, were assessed by analyzing the TE function, the path of contact, and the area of the TE function. Various parameters were also adjusted to meet specific criteria, as in the case of the spur gears. Table 1 lists the simulation parameters used for the helical gears, which were rotated on parallel axes during the simulation. The involute gear was not modified, and only the involute pinion was altered.

Table 2. Parameters of helical gears.

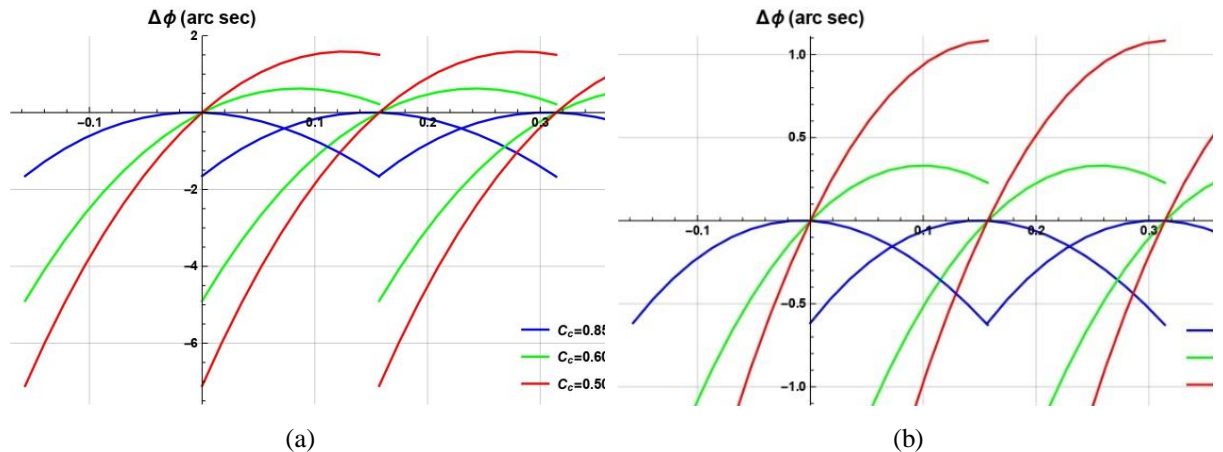
Parameters	Pinion	Gear
Number of teeth	40	37
Module, mm	1	
Pressure angle, degree	20	
Helix angle, degree	14	
Face width, mm	20	
Center distance, mm	39.67	
Poisson's ratio	0.3	
Modulus of Elasticity, GPa	206	
Total load, N	200	

Akin to the analysis done for spur gears, a study was conducted to determine the amount of crowning necessary for achieving a continuous TE function across all three crowning types, as illustrated in Figure (23). The study revealed that inadequate crowning leads to a

discontinuous TE function, and therefore optimization is crucial to attain a contact path near the center of tooth surfaces that results in a continuous TE function. Table (2) presents the findings that led to a continuous TE function for the modification parameter for all three types of crowning. The study showed that the level of crowning required for a continuous TE function decreases as the misalignment level increases. Additionally, the maximum TE ($\Delta\phi_{max}$) was determined for each modification. By comparing the values of $\Delta\phi_{max}$ for each modification and misalignment angle, the logarithmic modification resulted in the smallest value, followed by the circular and parabolic modifications.

Table 3. Amount of modifications for various in-plane angular misalignment errors for helical gears.

Angular misalignment γ (deg)	Circular		Parabolic		Logarithmic	
	C_c (mm)	$\Delta\phi_{max}$ (arcsec)	c_1 (mm^{-1})	$\Delta\phi_{max}$ (arcsec)	a_1 (mm)	$\Delta\phi_{max}$ (arcsec)
-0.05°	2.398	-0.15843	0.0227	-0.158389	2.515	-0.158352
	2.400	-0.15384	0.0233	-0.159286	2.600	-0.158858
	2.565	-0.153797	0.0240	-0.154701	2.669	-0.153776
-0.1°	1.104	-0.31696	0.0110	-0.316706	1.201	-0.316326
	1.150	-0.316498	0.0113	-0.317616	1.236	-0.31794
	1.173	-0.316498	0.0115	-0.31153	1.275	-0.30746
-0.2°	0.507	-0.633315	0.0051	-0.635564	0.537	-0.628879
	0.520	-0.637441	0.0052	-0.636932	0.553	-0.632365
	0.535	-0.618792	0.0053	-0.625768	0.572	-0.611297



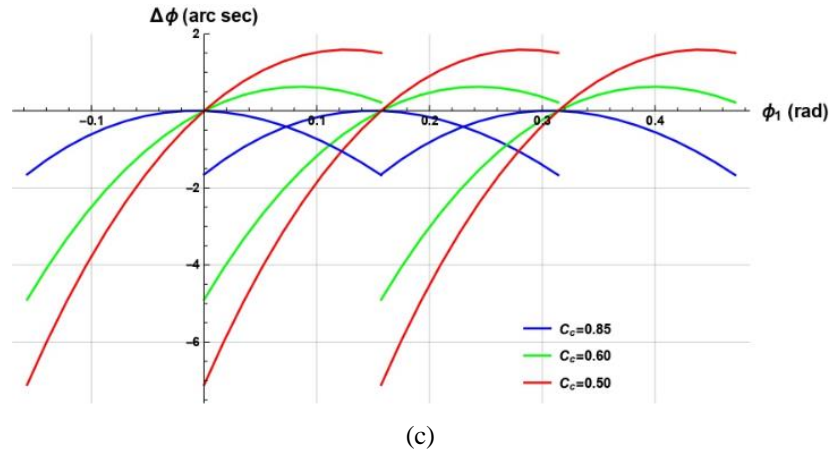


Figure 23. The TE functions (a) circular, (b) parabolic, and (c) logarithmic have varying degrees of crowning.

The helical gear with in-plane misalignment displays slight variations in the TE function among different surface modifications (as shown in Figure 24). To precisely quantify these differences, the area $S_{c,p,l}$ of the TE functions was computed, which yielded the following results:

$$S_c = -0.220082; S_p = -0.223297; S_l = -0.218083.$$

The computations reveal that the logarithmic modification produces superior outcomes compared to the other modifications. Specifically, the area of the TE function for the logarithmic modification is 2.33% and 0.9% less than that of the parabolic and circular modifications, respectively.

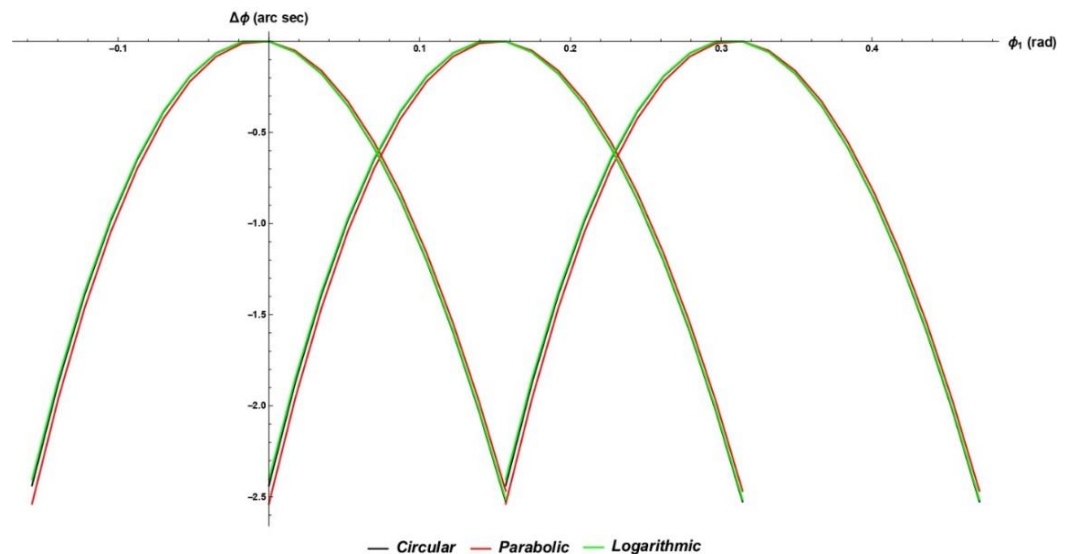


Figure 24. TE of a helical gear with three different modifications and an angular

misalignment of 0.2 (3.5 mrad)

Figure (25) illustrates the contact paths for various misalignment angles. As the misalignment angle increases, the contact path for each of the three modifications shifts away from the center. Although all three types of crowning yield a similar contact path, a closer analysis of the data reveals that the circular crown is closer to the center at misalignment angles of 0.1° (1.7 mrad) and 0.2° (3.5 mrad), while the logarithmic modification performs better at the smaller misalignment angle of 0.05° (0.87 mrad).

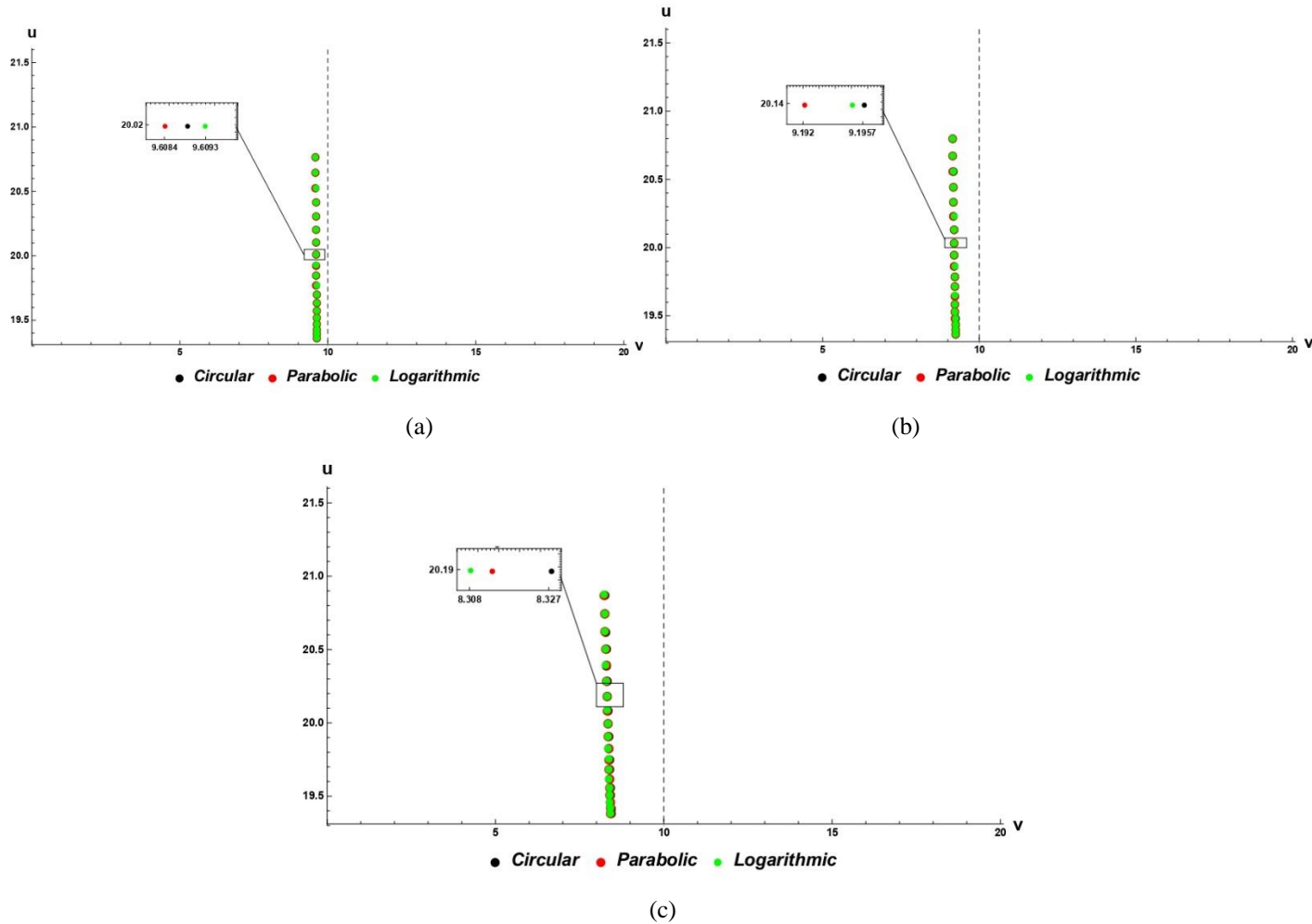


Figure 25. Path of contact of longitude circular, parabolic, and logarithmic crowned helical gear with in-plane misalignment: 0.05 (0.87 mrad), 0.1 (1.7 mrad), and 0.2 (3.5 mrad). The center of the tooth surface across the breadth of the gear is indicated by the dashed line.

Further we will investigate the effects of misalignment along the x-axis on helical gear systems. Specifically, the study looks at how different modifications to three crown types (C_c , c_1 and a_1) can ensure continuous TE function for misalignment angles ranging from 0.05 - 0.2° (0.87-3.5 mrad). The results are shown in Tab. (3), and $\Delta\varphi_{max}$ (maximum TE) is also calculated

for each crown type and misalignment angle. The study finds that as misalignment increases, the necessary modification for all three crown types decreases. Additionally, the logarithmic modification yields the smallest value for $\Delta\varphi_{max}$, followed by the circular and then the parabolic modifications.

Table 4. Amount of adjustments in relation to angular misalignment out of plane for helical gear engagement.

Angular misalignment δ (deg)	Circular		Parabolic		Logarithmic	
	C_c (mm)	$\Delta\varphi_{max}$ (arcsec)	c_1 (mm ⁻¹)	$\Delta\varphi_{max}$ (arcsec)	a_1 (mm)	$\Delta\varphi_{max}$ (arcsec)
0.05°	0.804	-0.4225422	0.00799	-0.42257	0.873	-0.42094
	0.830	-0.424252	0.00820	-0.424946	0.900	-0.423014
	0.853	-0.410921	0.00847	-0.410987	0.927	-0.409179
0.1°	0.360	-0.845263	0.00359	-0.845918	0.368	-0.831488
	0.370	-0.850059	0.00370	-0.849776	0.380	-0.836597
	0.381	-0.823004	0.00380	-0.825234	0.393	-0.809249
0.2°	0.143	-1.69059	0.00143	-1.69062	0.046	-1.4328
	0.146	-1.70474	0.00146	-1.7048	0.055	-1.49707
	0.150	-1.66515	0.00150	-1.66508	0.081	-1.48844

To gain a more comprehensive understanding of the variation between crown types, the area $S_{c,p,l}$ is computed for all of them under a misalignment angle of 0.2° (3.5 mrad), using their TE functions (Figure 26).

$$S_c = -0.645048; S_p = -0.642903; S_l = -0.509613$$

The results indicate that the logarithmic modification produces transmission function area that is approximately 21% smaller than that of the circular and parabolic modifications. Therefore, the logarithmic function is considerably more effective than the other two crown types.

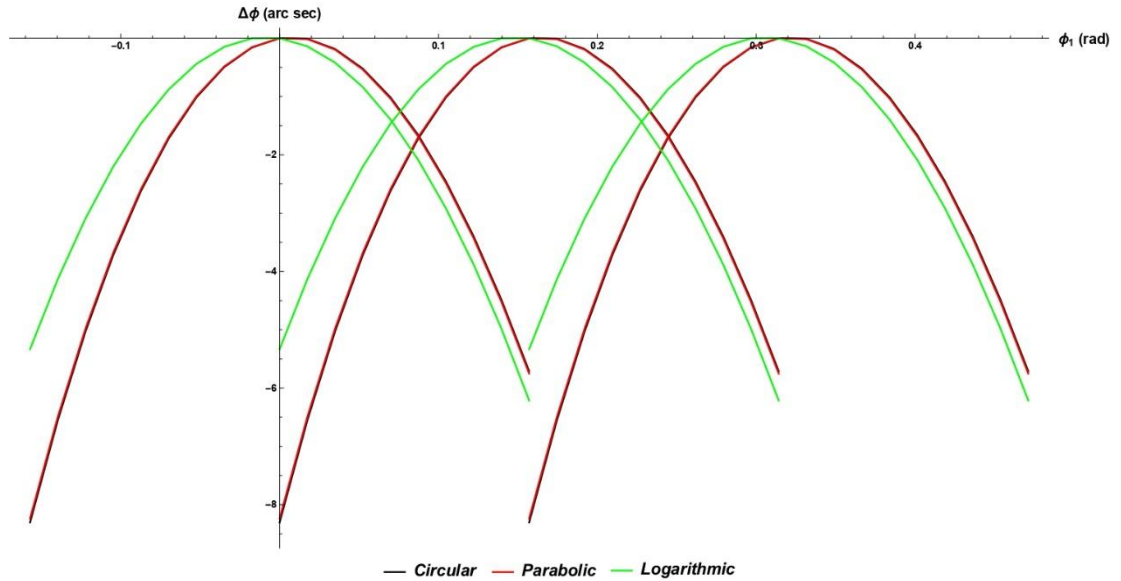
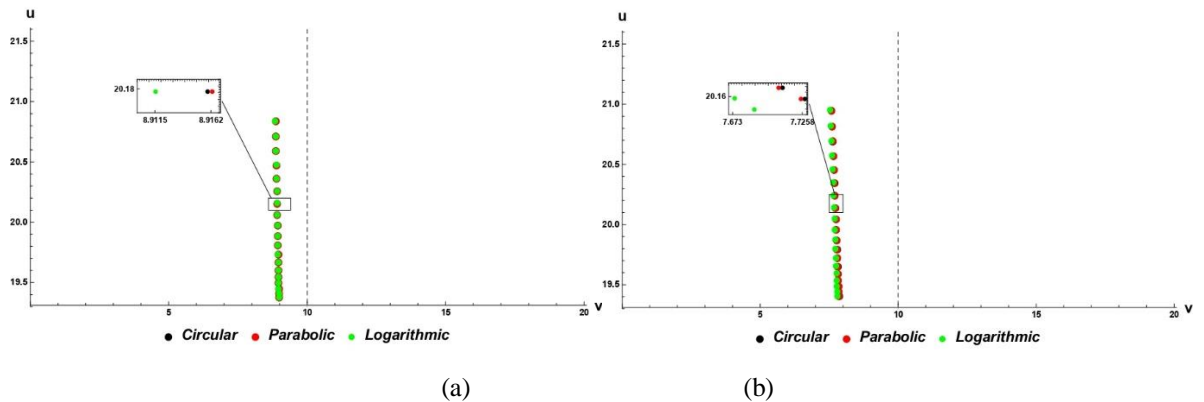
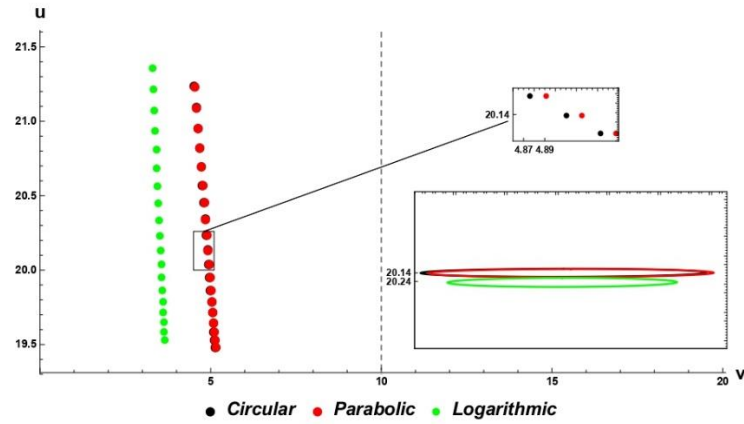


Figure 26. TE of a helical gear with three different modifications and an angular misalignment of 0.2 (3.5 mrad).

Figure (27) displays the contact path for each crown type and misalignment angle (0.05-0.2°). As the out-of-plane misalignment angle increases, the point of contact moves farther away from the center. The contact path for 0.05° and 0.1° misalignment is comparable, but at 0.2° misalignment, the contact path for the logarithmic crowning is noticeably farther from the center than the other two types. For a misalignment angle of just 0.2°, the shift is 1.3 mm for in-plane misalignment and 5.0-6.5 mm (depending on the crown type) for out-of-plane misalignment. Consequently, a significant finding of the simulation comparison between spur and helical gear meshing is that helical gears experience a much greater shift of the contact path from the center of the tooth in the presence of misalignments.





(c)

Figure 27. Path of contact of longitude circular, parabolic, and logarithmic crowned helical gear with out-of-plane misalignment: a) 0.05 (0.87), b) 0.1 (1.7), and c) 0.2 (0.2 mrad) (3.5 mrad). The center of the tooth surface across the breadth of the gear is indicated by the dashed line. At the 0.2° misalignment angle, the scaled contact ellipses at the pitch point are displayed.

Figure (28) displays the three-dimensional mesh contact of helical gears with circular and logarithmic modifications. The parabolic crown is not shown because its surface is almost indistinguishable from the circular crown. Examining the figure, it is evident that when there is a significant misalignment between the two gear teeth, the surface with circular crowning will encounter edge contact. However, for the same situation, a much more severe misalignment angle is required for the logarithmic crown to experience edge contact.

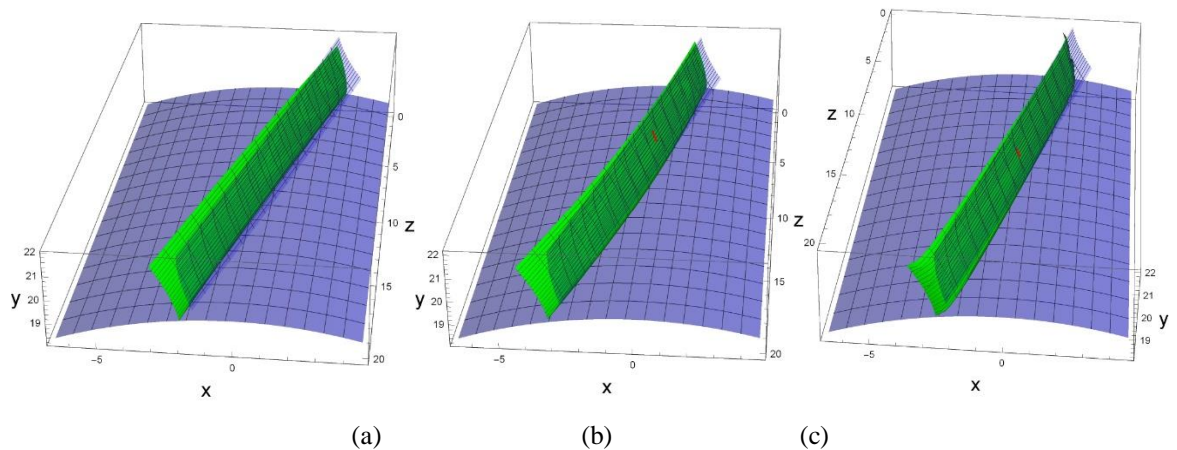


Figure 28. An illustration of a helical gear assembly model in space with (a) unaltered surface, (b) circular crowning, and (c) logarithmic crowning

The study utilized Hertz contact equations for an elliptical contact point to determine the stress ratio (SR) of two helical gear pairs at various angles of out-of-plane misalignment. Figure

(29) displays the SR values for all three crown types with respect to misalignment angle. At the smallest misalignment angle of 0.01° (0.17 mrad), the logarithmic crown has the highest ($SR = 15.1803$), while the circular and parabolic crowns have lower SR values (15.0962 and 15.1661, respectively). In contrast to spur gears, where the parabolic crowning yielded the lowest SR value for all misalignment angles, each crown type for helical gears produced the lowest SR value at a different misalignment angle. At 0.02° (0.35 mrad), the logarithmic crown had the lowest ($SR = 12.4127$), while the circular crown had the highest ($SR = 12.6628$). At 0.05° (0.87 mrad), the parabolic crown had the lowest value ($SR=10.0767$), whereas the logarithmic crown had the highest value ($SR = 10.1105$). The circular crown had the lowest SR value at 0.1° (1.7 mrad) of misalignment, and the parabolic crown had the lowest SR value again at 0.2° (3.5 mrad) of misalignment. The SR values for the various crown types at misalignment angles between 0.01 - 0.1° were similar, but at 0.2° of misalignment, the logarithmic crown had a significantly higher SR compared to the other traditional crowns, likely due to the unique curvature of its profile, which is more pronounced in helical gears.

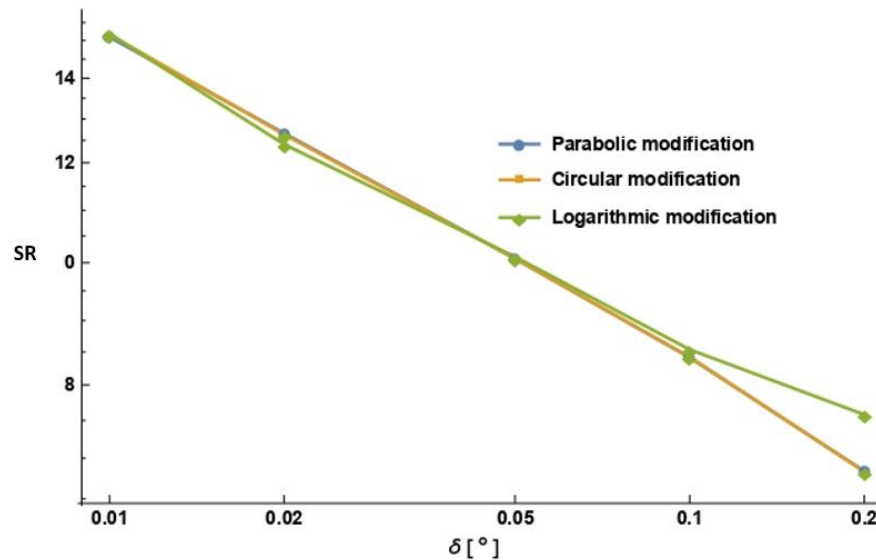


Figure 29. Helical gears with three different methods of profile modification were compared in terms of their stress ratio (Σ) and the degree of out-of-plane misalignment.

The pressure contact behavior of the circular profile at an out-of-plane misalignment of 0.2° is depicted in Figure (30) using contact ellipses. The SR at the upper portion of the gear tooth surface is higher than that of the lower portion, and it gradually decreases along the contact path, which is consistent with prior research [1-2, 88-91]. The pressure contact behavior for the other profiles is similar.

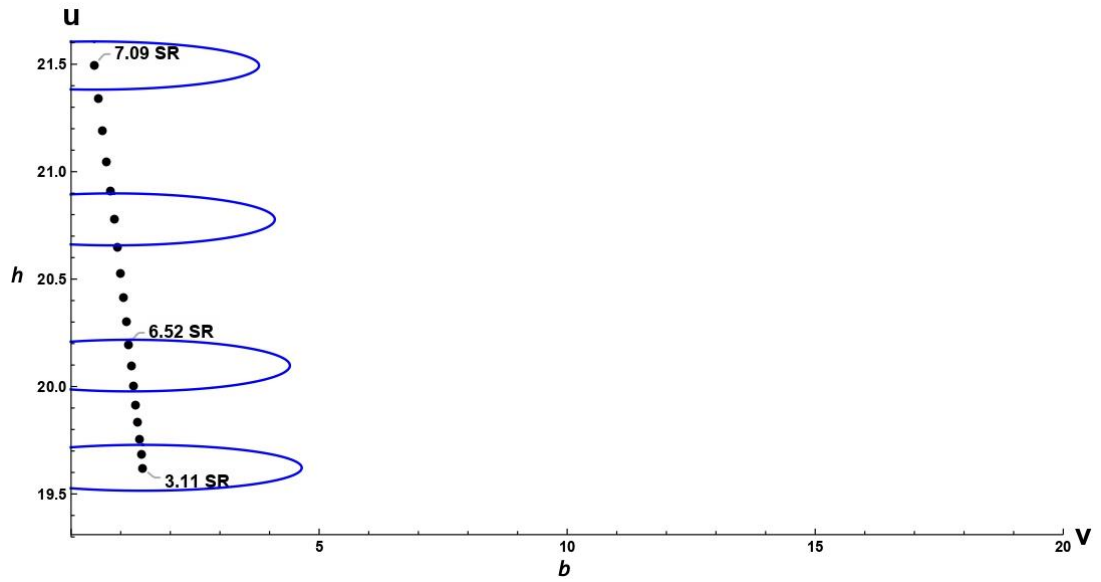


Figure 30. The SR of crowned helical gears, where the blue outlines show the location of the contact ellipse at the contact point, with the least amount of circular profile alteration along the path of contact for an out-of-plane misalignment of 0.2° (3.5 mrad).

Chapter 5. Bevel gears contact simulation through the new TCA method

5.1 Straight bevel gear

The logical extension of the involute plane profile that describes a cylindrical surface, such as a spur or helical gear tooth face, is a spherical involute profile. Its generation is based on spherical trigonometry and can be defined by the direct definition method by a point unwrapped from a base cone circle.

The surface contact parametric model described earlier was utilized to simulate the engagement of a straight bevel gear set with misalignment errors and assess their impact on transmission, stress, and contact trace. A specific straight bevel gear set with dimensions listed in Table (4), was used as a sample for numerical examples. Double crowning was employed as a design modification to improve the resilience of the contact pattern against misalignments. These modifications were a combination of tip relief and one of the longitudinal tooth face crowning, which were only applied to gear 1.

Table 5. Simulation parameters of standard straight bevel gear pair.

Parameters	Symbol	Gear 1	Gear 2
Number of teeth	N_1, N_2	39	32
Shaft angle, (deg)	Σ	90°	
Module, mm	m	2.5	
Pressure angle, (deg)	β	20°	
Base cone angle, (deg)	α_i	47.79°	36.53°
Outer cone angle, (deg)	δ_i	52.90°	41.64°
Face width, mm	b	14	
Poisson's ratio	$\nu_{1,2}$	0.3	
Modulus of Elasticity, GPa	E	206	
Maximum load capacity, kN	P	2.675	
Applied load, kN	P_o	1.5	

Figure (31) shows the coordinate system of a misaligned two-bevel gear system, where

misalignment is caused by three axial displacements (along the x, y, and z-directions) and one angular displacement (around the y-axis). Deviation around the x- and z-axes does not contribute to misalignment in bevel gears because of the canonical shape of bevel gears, which is considered in a spherical coordinate system.

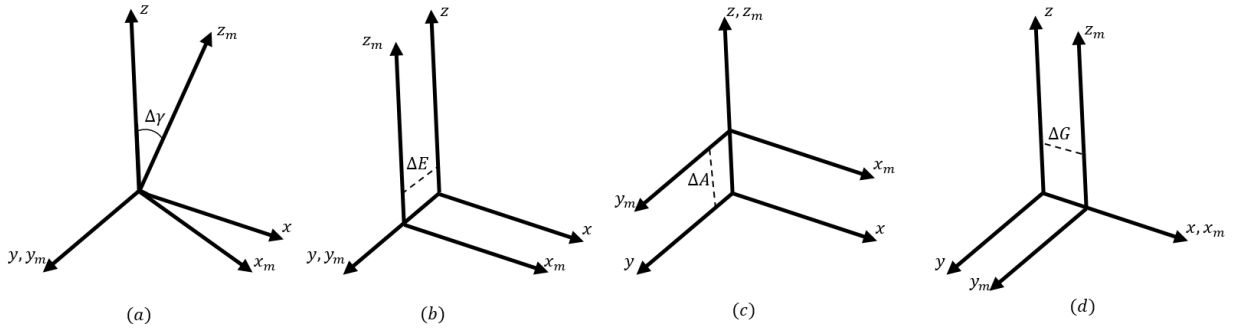


Figure 31. The following are examples of coordinate systems for misalignments: (a) angle change (in-plane misalignment), (b) center distance shift along y-axis, (c) pinion axial displacement along x-axis, and (d) gear axial displacement along z-axis.

Parametrically, the axial displacement can be represented as a shift along the axes, resulting in a non-zero value for the axial distance \vec{a}_{12} between the coordinate systems, as shown in Equation (47). On the other hand, angular displacement will cause in-plane deviation and a change in the shaft angle, as shown in Equation (48).

$$\vec{a}_{12} = \{ \Delta A, \Delta E, \Delta G \} \quad (47)$$

$$\Sigma_o = \Sigma - \Delta\gamma \quad (48)$$

Table (6) shows the values of misalignments used during the simulation of straight bevel gears meshing.

Table 6. Simulation parameters of alignment errors.

Misalignments	Value
Change of shaft angle, $\Delta\gamma$ (deg)	0.2°
Change of centre distance, ΔE (mm)	0.1
Axial displacement of pinion, ΔA (mm)	0.1
Axial displacement of gear, ΔG (mm)	0.1

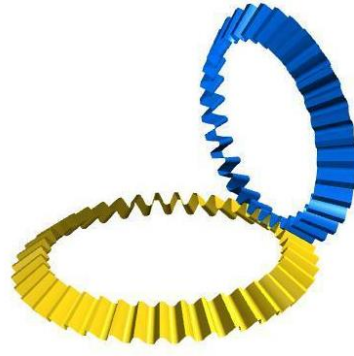


Figure 32. Straight bevel gear pair illustration provided by Kisssoft program.

Insufficient or excessive amount of crowning in the crossed surfaces of bevel gears can result in edge tooth contact and interrupted transmission, as illustrated in Figures (33) and (34). The transmission function in Figure (33) is a curved line that does not intersect, indicating that insufficient crowning has been applied in the presence of misalignment. This is further confirmed by the contact trace results shown in Figure (34), which display partial contact with the edge of the tooth surface.

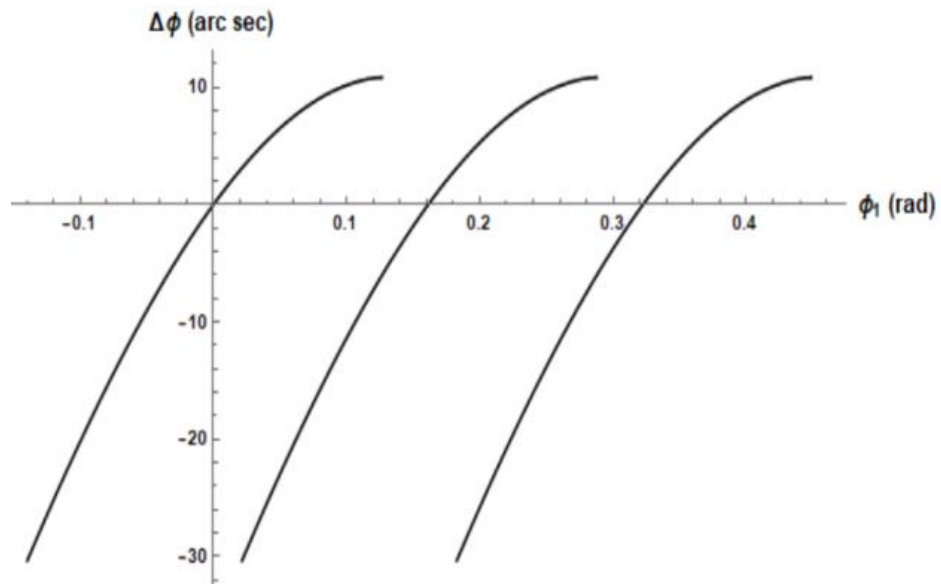


Figure 33. With a slight modification, transmission error function is used when the pinion is displaced axially.

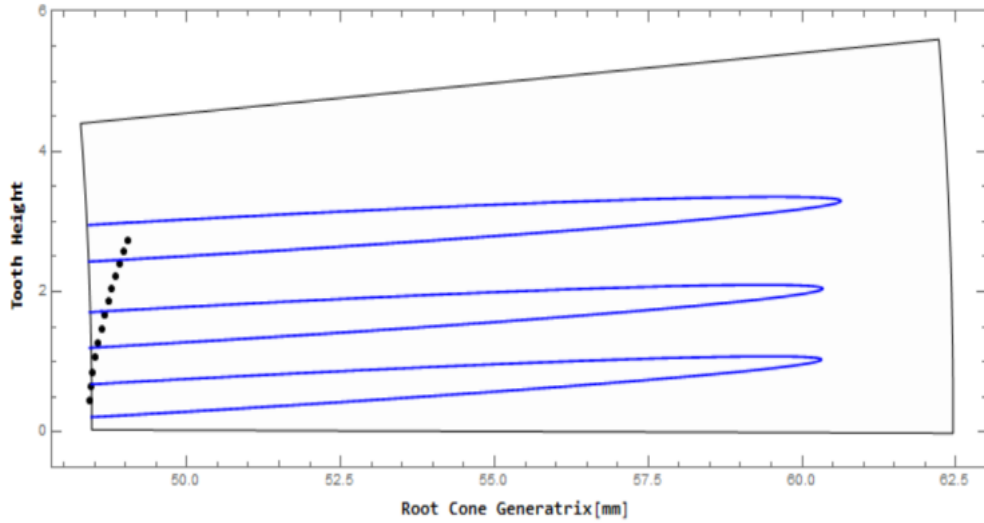


Figure 34. Bevel gear surface with contact ellipses and contact paths.

To prevent edge contact and achieve continuous transmission in the presence of different misalignments, double crowning was applied to the driven gear. The simulation results indicated that the most effective tooth surface modification for achieving smooth transmission is through tip relief crowning. On the other hand, applying longitudinal modifications without tip relief crowning led to an intermittent transmission error function. However, after incorporating an appropriate amount of tip relief modification, the transmission function became continuous, as shown in Figure (35).

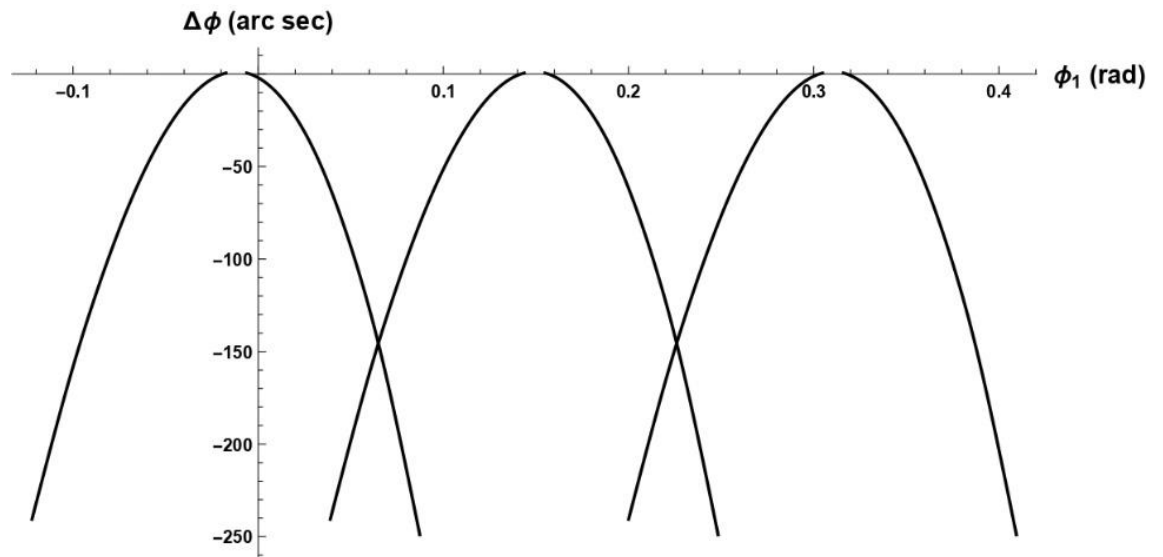
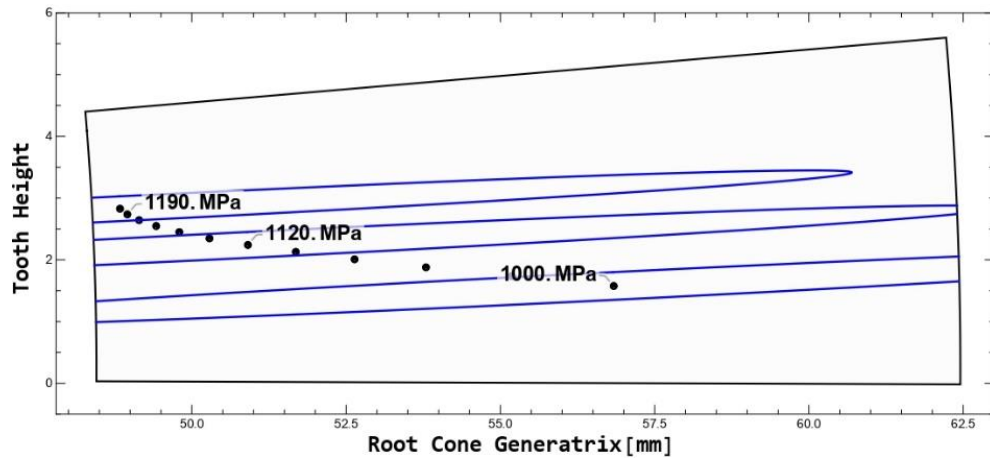


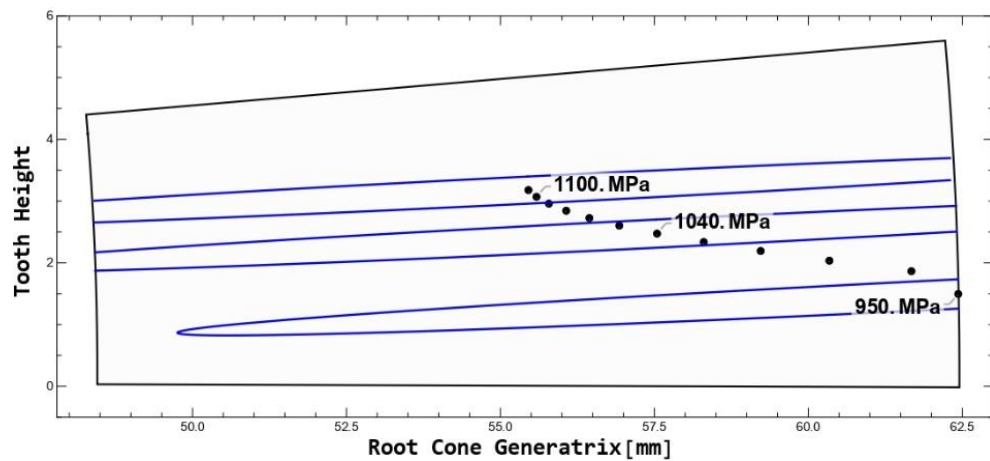
Figure 35. Transmission error with parabolic crowning, tip relief, and center distance change.

The simulation results show that changes in the longitudinal modification have a direct

impact on the location of the path contact. Additionally, different types of misalignment have varying effects on the location of the contact trace and transmission error. For example, in Figure (36), it is evident that a certain amount of longitudinal crowning can produce acceptable results for one type of misalignment error, such as a deviation in center distance (ΔE), but unacceptable results for another error, such as axial displacement of the gear (ΔG). Therefore, it is crucial to determine the appropriate amount of profile and lead modification that will yield satisfactory results for various types of alignment errors), which is consistent with earlier research [92,93].



(a)



(b)

Figure 36. Path of contact, maximum contact pressure, and contact ellipses with equal amounts of tip relief and parabolic crowning are all affected by the following: (a) change in center distance, ΔE ; (b) axial displacement of gear, ΔG .

Figure (37) demonstrates that an overabundance of lead modification alters the direction of the contact trace and focuses it nearer to the middle of the tooth surface compared to a minimal amount of crowning, as depicted in Figure (36a). Additionally, the major axis of the

elliptical contact becomes shorter, suggesting an increase in contact pressure. It can be observed from Figure (37) that an increase in the magnitude of the longitudinal modification results in nearly an 80% increase in contact pressure.

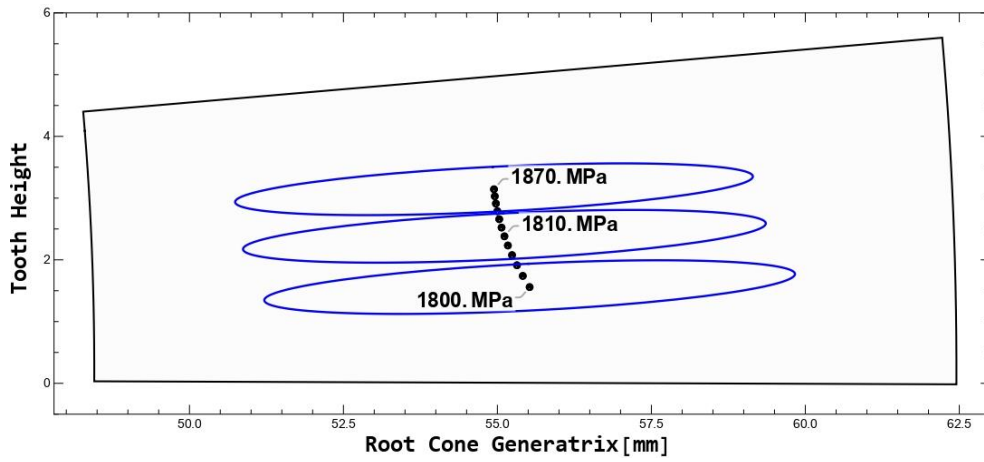


Figure 37. Maximum contact pressure, contact ellipses, and contact paths with significant lead modification.

As previously stated, lead profile crowning can be categorized into three types. The simulation results indicate that there is minimal disparity among them when meshing straight bevel gears, as demonstrated in Figure (38), where the transmission error function of each crowning differs by only one or two arc seconds. Similarly, the stress analysis outcomes do not display significant differences among the simulation results of distinct longitudinal modifications at various shaft angle misalignments, as depicted in Figure (39).

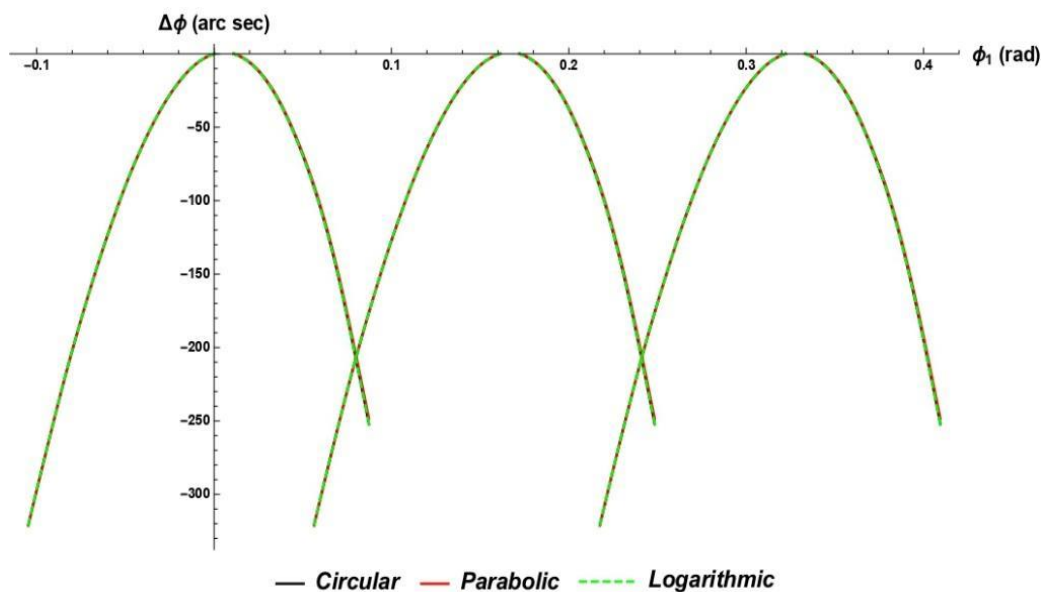


Figure 38. For the case of shaft angle misalignment, transmission error function with three

forms of longitude crowning.

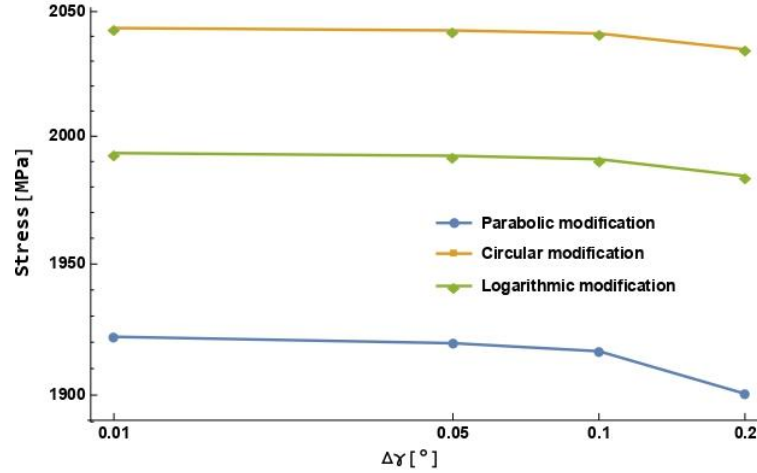


Figure 39. Maximum contact pressure for three types of longitude crowning at various shaft angle misalignments.

5.2 Spiral bevel gear

The spherical involute profile is an extension of the involute plane profile, which is used to represent the tooth face of cylindrical surfaces such as spur or helical gears. It can be defined using the direct definition approach, which utilizes spherical trigonometry and unwraps a point from a base cone circle. The parametric definition of the spherical involute profile is given in terms of (u_i, v_i) in the plane.

$$\vec{r}_i = \begin{bmatrix} R_i (\cos(\beta_i \sin(\alpha_i)) \sin(\alpha_i) \cos(\beta_i \pm \vartheta_i) + \sin(\beta_i \sin(\alpha_i)) \sin(\beta_i \pm \vartheta_i)) \\ R_i (\cos(\beta_i \sin(\alpha_i)) \sin(\alpha_i) \sin(\beta_i \pm \vartheta_i) - \sin(\beta_i \sin(\alpha_i)) \cos(\beta_i \pm \vartheta_i)) \\ R_i \cos(\beta_i \sin(\alpha_i)) \cos(\alpha_i) \end{bmatrix} \quad (48)$$

where R_i is a radius vector specified in (u_i, v_i) as follows, and α_i is the base cone angle, β_i is the involute generating angle

$$\beta_i = \frac{1}{\sin(\alpha_i)} \cos^{-1} \left(\frac{\cos(u_i)}{\cos(\alpha_i)} \right), \quad (49)$$

$$R_i = v_i. \quad (50)$$

The parameter v_i spans the distance from the inner to outer cone, while the parameter u_i spans the angle from the inner to outer cone. A formula can be derived for logarithmic tooth surfaces with a spherical involute profile.

$$\vartheta_i = \frac{1}{\sin(\alpha_i) \cot \Phi} \log \frac{R_m}{R_i}. \quad (51)$$

The logarithmic function ϑ_i is defined with a spiral angle Φ and mean cone distance R_m . Figure (40) shows that the involute tooth surface of a spiral bevel gear can be created using Equations (48-51) in a parametric way.

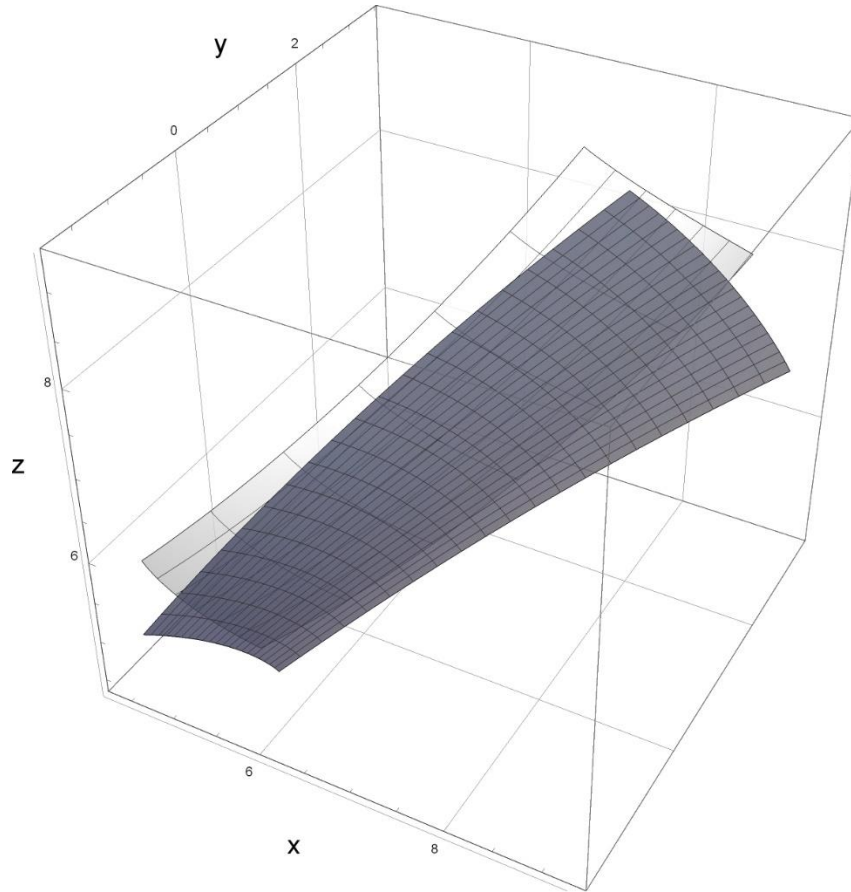


Figure 40. An involute spiral bevel gear tooth surface generated graph.

The process of measuring units can be made simpler and more organized by using non-dimensionalization techniques. We offer a non-dimensionalization method for measuring the strength and size of gears, which involves comparing them to certain properties of the gear material, such as the module m , Young's modulus E , and gear thickness \hat{b} . By doing so, any length \hat{l} and force magnitude \hat{F} can be standardized using the following equations:

$$l = \frac{\dot{l}}{m}, \quad (52)$$

$$F = \frac{\dot{F}}{Em\dot{b}} \quad (56)$$

The subsequent analysis considers all magnitudes as non-dimensional in accordance with the aforementioned rule.

The quality of transmission and contact performance of spiral bevel gears can be negatively affected by misalignments, leading to transmission errors, unbalanced load distribution, and tooth edge contact. This can cause a significant increase in the noise and vibration of gearboxes. To examine the tooth contact performance of modified spiral bevel gear drives with alignment problems and tooth crowning, a new parametric model of surface contact was utilized. This model simulated the engagement of spiral bevel gears with misalignments and assessed their impact on transmission, stress, and contact path. The simulation used a gear configuration with $N_1 = N_2 = 17$, the shaft angle $\Sigma = 90^\circ$, the module $m = 1$, the spiral angle $\Phi = 35^\circ$, and a face width of $b = 4.8$. Three types of misalignments were applied during the simulation, including two linear alignment errors and one angular alignment error represented by ΔE , ΔH , and $\Delta\gamma$, respectively. Figure (41) shows an illustration of the coordinates of a spiral bevel gear system in the presence of misalignment. The design modifications implemented double crowning, which combined tip/root relief with longitudinal parabolic tooth face crowning applied only to the meshing tooth, to improve the contact pattern's resistance to inevitable misalignments. This modification aimed to enhance the tooth contact performance and reduce noise and vibration in the gearbox.

Table 2, Crowning design for various alignment error

Types of Misalignments	Range of misalignments Value	Tip/Root relief Parameters	Parabolic Modification parameters
Angular misalignment, $\Delta\gamma$	$0^\circ - 0.2^\circ$	$c_t = 0 \quad L_t = 0$	$c_1 = 0.002 - 0.02$
Linear misalignment, ΔE	$0.02 - 0.1$	$c_t = 0.04 - 0.08$ $L_t = 0.16$	$c_1 = 0.002 - 0.02$
Linear misalignment, ΔH	$0.02 - 0.1$	$c_t = 0.04 - 0.08$ $L_t = 0.16$	$c_1 = 0.002 - 0.02$

Table (6) provides information on the magnitude of different types of misalignment and tooth surface modification used in the simulation. Figure (42) illustrates the contact path trajectory in the absence of misalignment and with various angular deviations. The contact path trajectory remains almost the same, with only minor movement towards the tooth tip despite a significant angular deviation. The simulation also indicates that the angular alignment error does not affect the transmission error, which is determined to be zero.

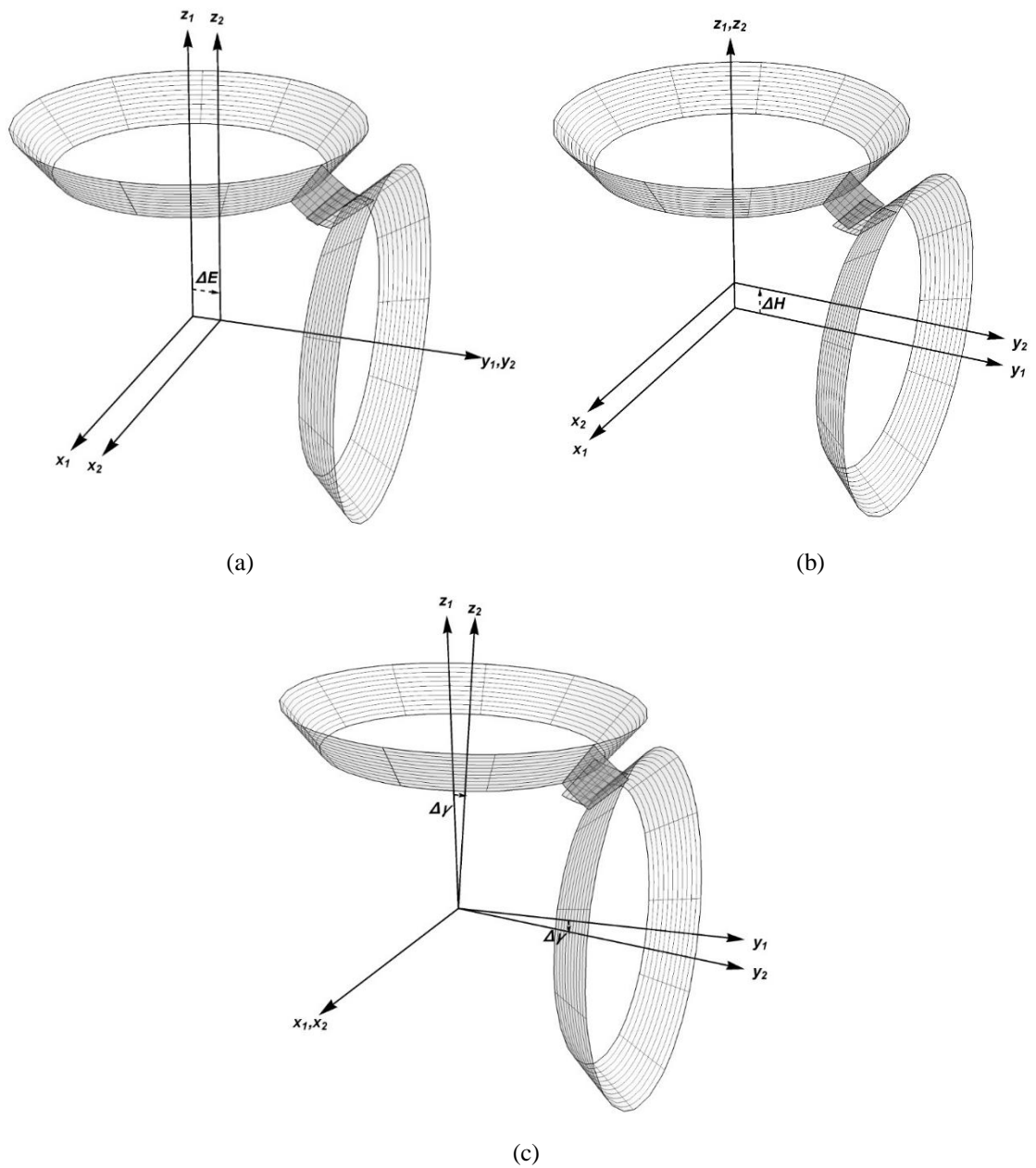


Figure 41. Coordinate systems diagram for spiral bevel gears with alignment issues.

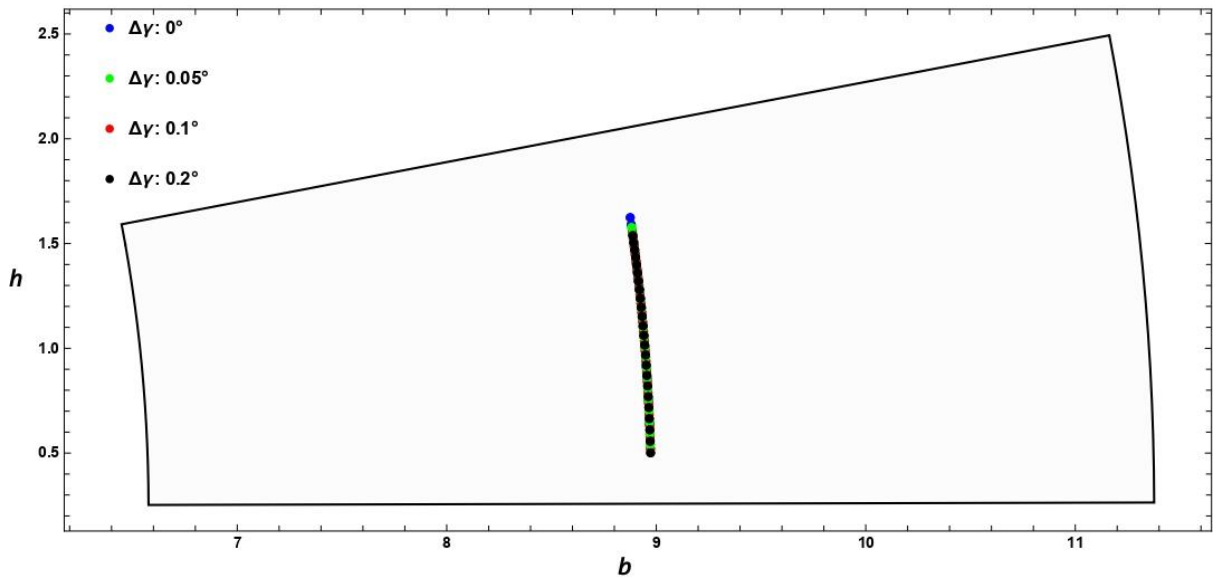


Figure 42. Path contact results from the engagement of a spiral gear pair with various angular misalignments.

In Figure (43), the path of contact with contact ellipses is displayed for a deviation in angle ($\Delta\gamma$) of 0.2° and the implementation of longitudinal parabolic crowning ($c_1 = 0.002$), but without profile modification like tip/root relief ($c_t = 0 ; L_t = 0$). The figure illustrates that the contact stress ratio remains relatively constant throughout the engagement. The contact ellipses and stress ratio of the engagement were determined using the following parameters: elastic modulus $E_1 = E_2 = 210 \times 10^3 \text{ N/mm}^2$, Poisson's ratio $\nu_1 = \nu_2 = 0.3$, and a non-dimensional normal load of $F = 55.5 \times 10^{-6}$.

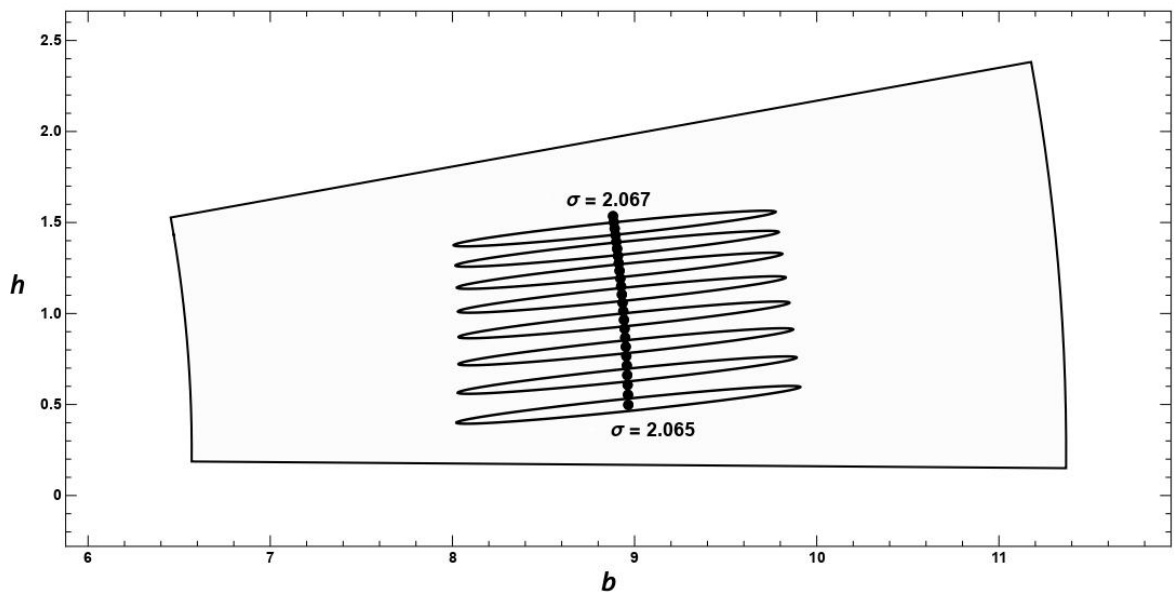


Figure 43. The tooth contact ellipses and the stress ratio at angular misalignment $\Delta\gamma = 0.2^\circ$ and with longitudinal parabolic crowning.

Figure (44) shows how the contact trajectory changes with linear displacement (ΔE) in a spiral bevel gear system, which is a marked difference from the contact path presented in Figure (42), which is consistent with earlier research [94,95]. A greater ΔE value causes a significant deviation in the contact trace. Tooth surface modification was implemented correctly to achieve continuous parabolic TE functions for $\Delta E=0.04$, Figure (45). This was accomplished by incorporating lead and profile crowning parameters of $c_1 = 0.02$, $c_t = 0.08$ and $L_t = 0.16$. However, when a higher ΔE is used, the modifications are insufficient, leading to a discontinuous but still parabolic transmission function.

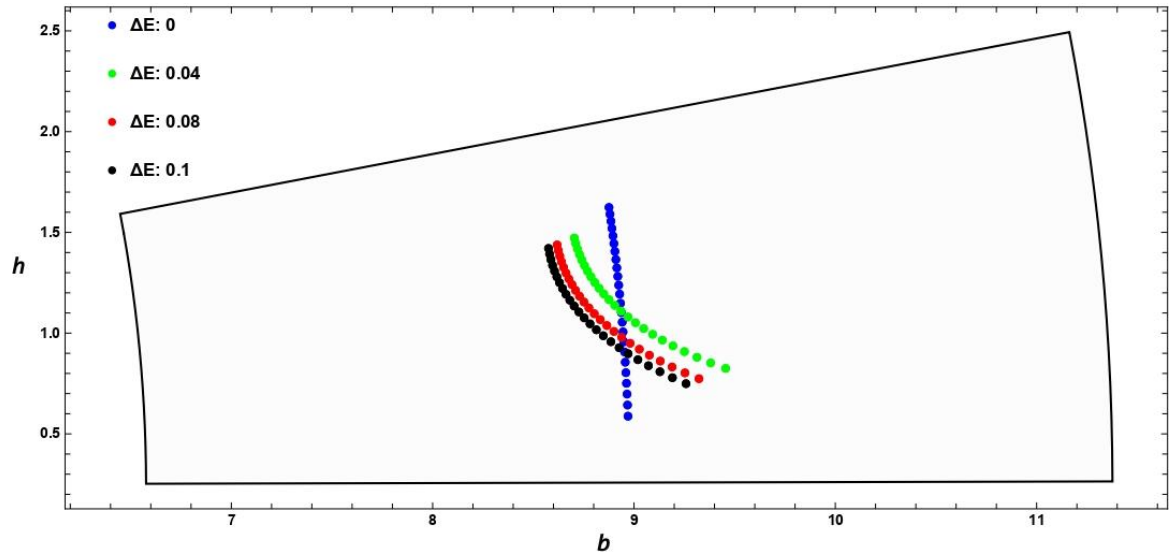


Figure 44. Comparison of the path of contact with different linear misalignments and double crowning.

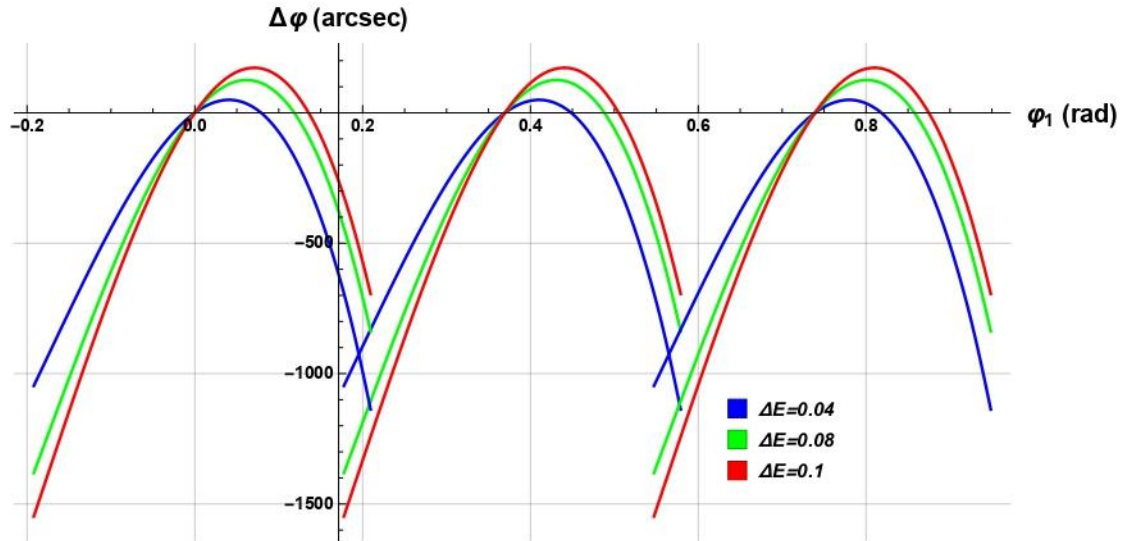


Figure 45. Transmission results for spiral gear meshing at linear misalignment (ΔE)

Figure (46) displays the stress ratio and contact ellipses for an alignment error of $\Delta E=0.08$, while using tooth surface modification parameters $c_1 = 0.005$, $c_t = 0.04$ and $L_t = 0.16$. The figure indicates that stress levels increase gradually from the tooth tip towards the middle, then decrease again towards the root.

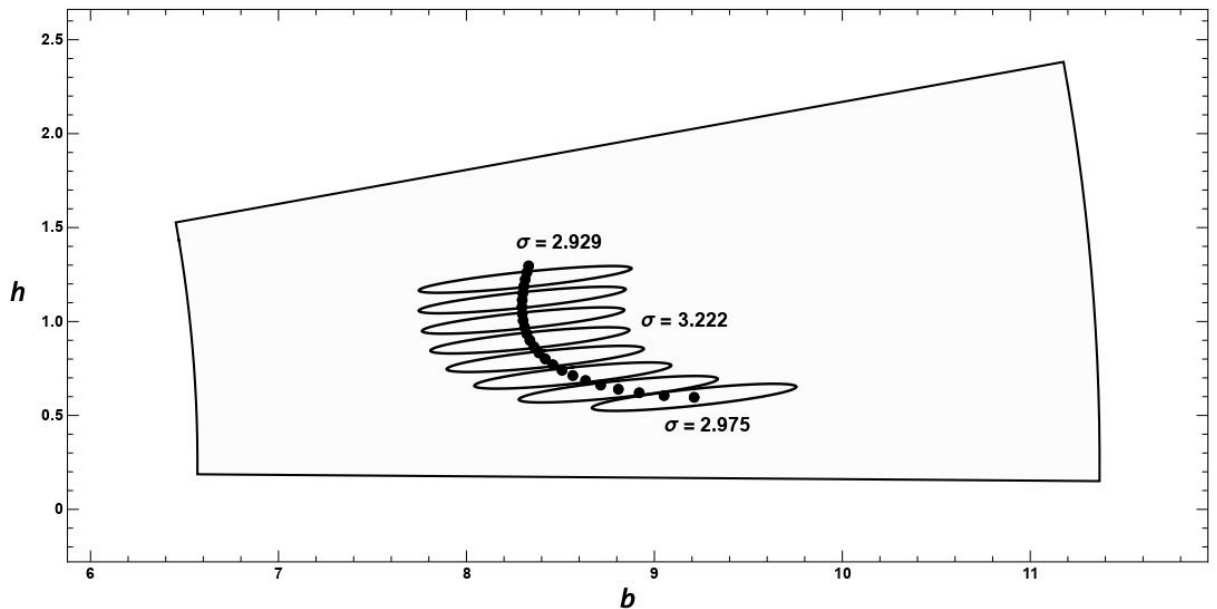


Figure 46. The stress ratio and contact ellipses in the condition of linear misalignment.

Figures (47-49) illustrate the results of spiral bevel tooth meshing under linear z-axis misalignment (ΔH). Compared to the case where tooth contact is aligned, the contact trajectory now deviates downwards towards the tooth root. Despite using the same amount of crowning

and profile modification as in the previous case ($c_1 = 0.02$, $c_t = 0.08$, $L_t = 0.16$), the maximum transmission error amplitude reached almost 820 arcsec when $\Delta H = 0.04$, which is less compared to the previous case where linear misalignment along the y-axis ($\Delta E = 0.04$), resulted in a transmission function amplitude of 920 arcsec. Moreover, the slight increase in the alignment error value shows that the deviations between the contact path are relatively small compared to Figure (46). Additionally, one noteworthy characteristic of the transmission function is its asymmetry, as seen in Figure (48). Previous research provided by Litvin et al. [1] had assumed that the transmission function would follow a parabolic function, but this is not always the case and does not accurately represent the transmission of spiral bevel gear teeth contact. Litvin et al. [1] posited that the transmission error (TE) resulting from gear misalignment, would follow a parabolic pattern, expressed as $\Delta\varphi = -a\varphi_1^2$. However, it is evident from prior research conducted by other researchers [96-98] and our simulations that, in certain instances, it may exhibit asymmetry or irregularity.

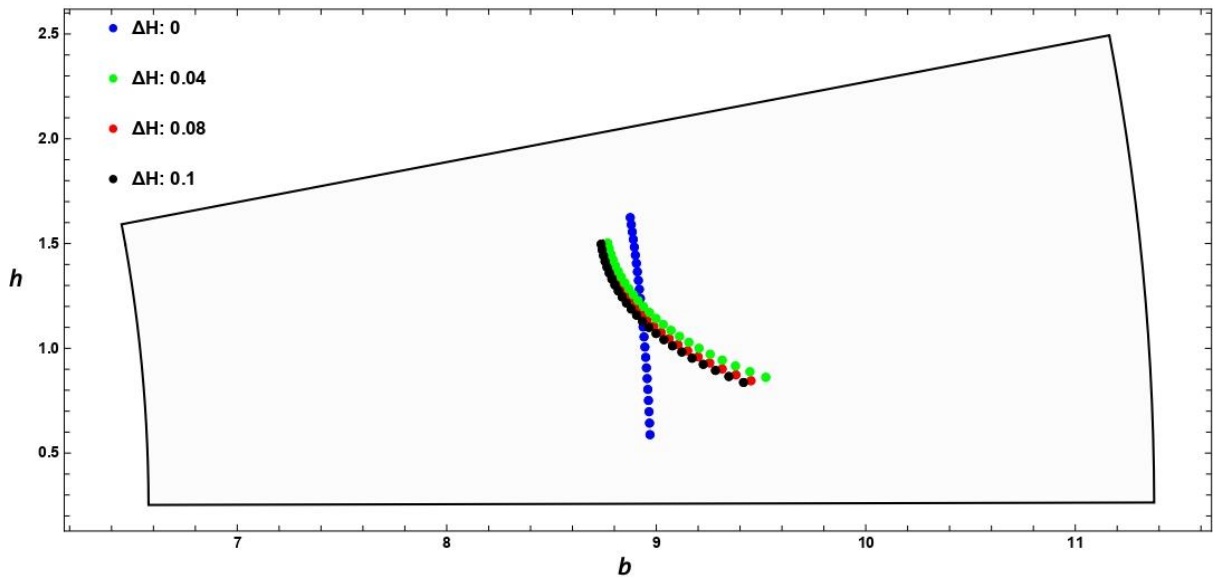


Figure 47. Path contact results in different linear misalignments ΔH .

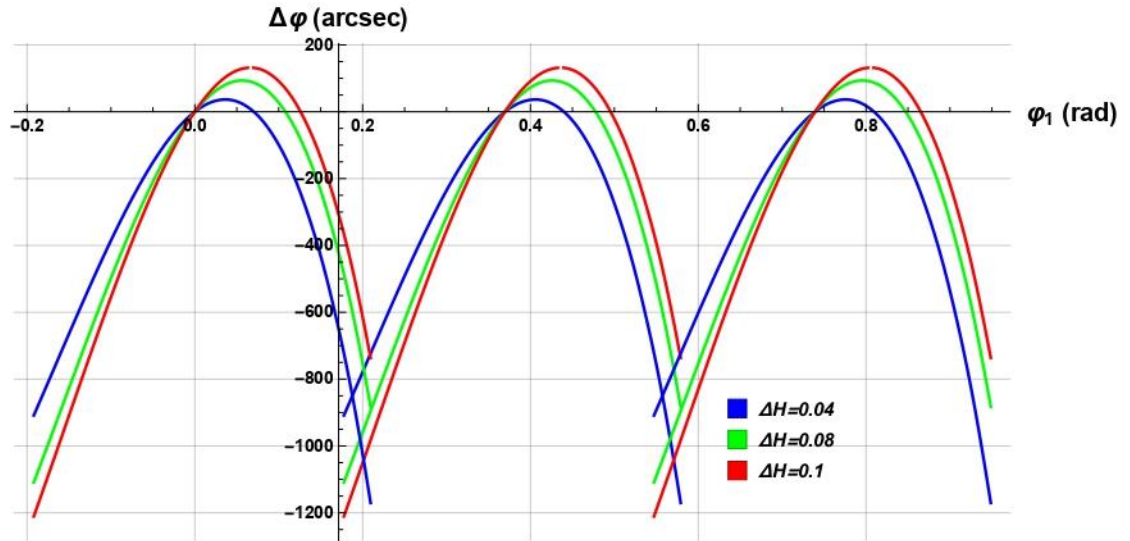


Figure 48. Transmission error in case of linear misalignment ΔH .

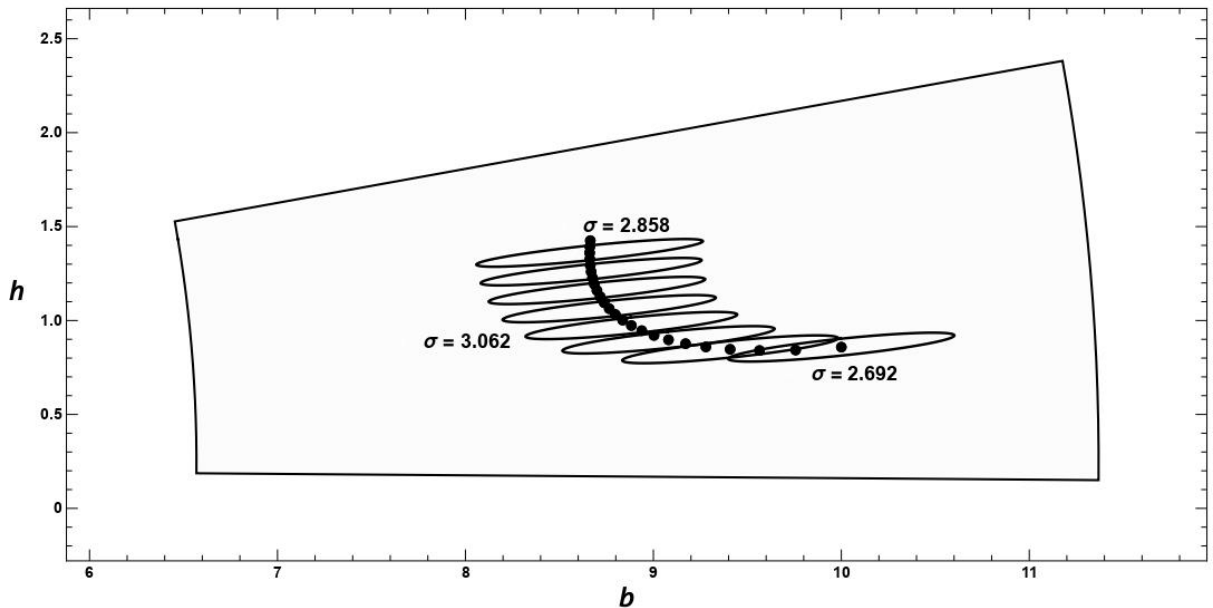
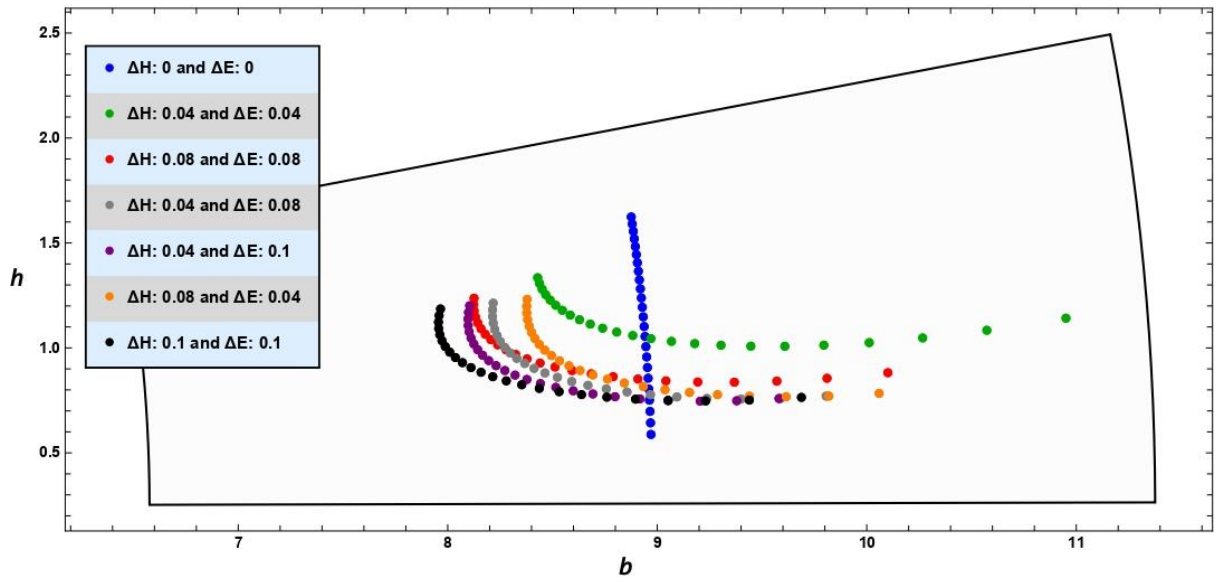


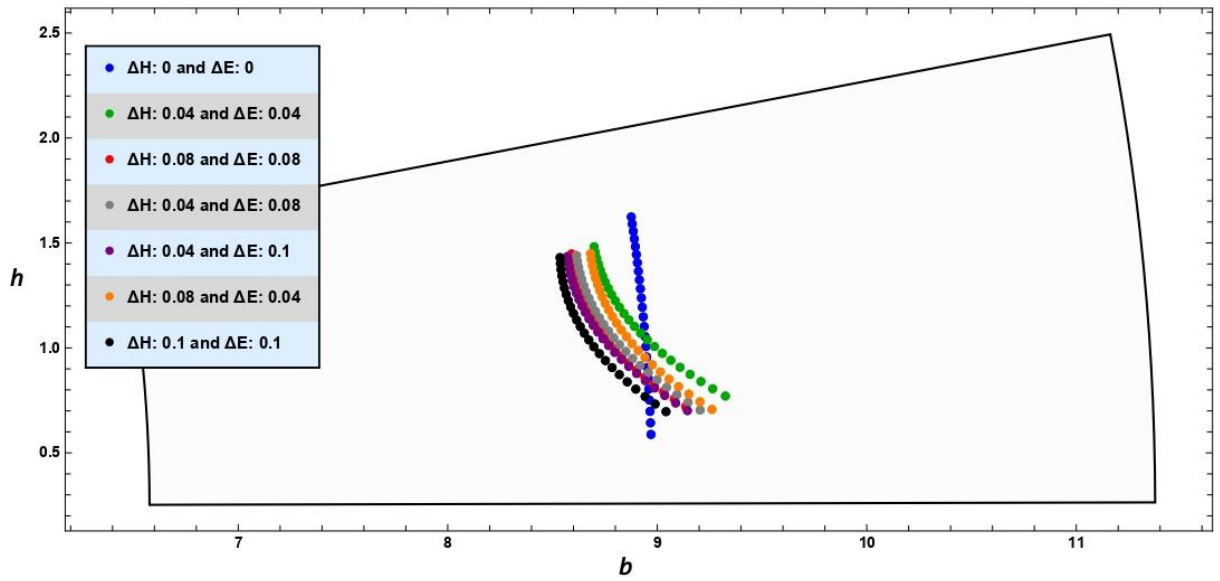
Figure 49. Stresses and contact ellipses for a spiral bevel gear system with a linear misalignment of $\Delta H = 0.08$.

Figure (49) displays the contact trace, contact ellipses, and stress ratio at the top, middle, and root of the tooth, where the misalignment value ΔH was chosen as 0.08, and the modification parameters were $c_1 = 0.005$, $c_t = 0.04$ and $L_t = 0.16$. The figure indicates that the stress reaches its peak at the middle of the tooth face. Next, we examine a combined misaligned case, as shown in Figure (50a), where modifications were applied with parameters $c_1 = 0.005$, $c_t = 0.08$ and $L_t = 0.16$. It is evident that the differences in the contact path for various misalignment values are more pronounced. Furthermore, Figure (51) demonstrates that the transmission

amplitude increases up to 1500 arcsec when combined misalignments were applied, $\Delta E = \Delta H = 0.04$. To focus the contact path more towards the center of the tooth face, we increased the modification parameters to $c_1 = 0.02$, $c_t = 0.08$ and $L_t = 0.16$, as seen in Figure (50b).



(a)



(b)

Figure 50. The contact path with various combined linear misalignments with (a) $c_1 = 0.005$ and (b) increased amount of longitudinal parabolic crowning $c_1 = 0.02$.

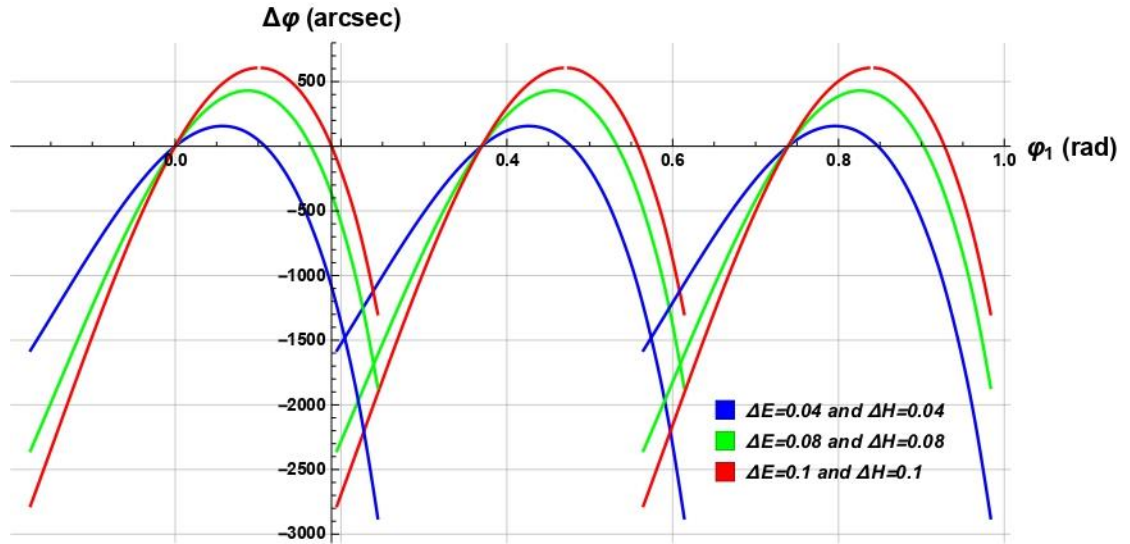
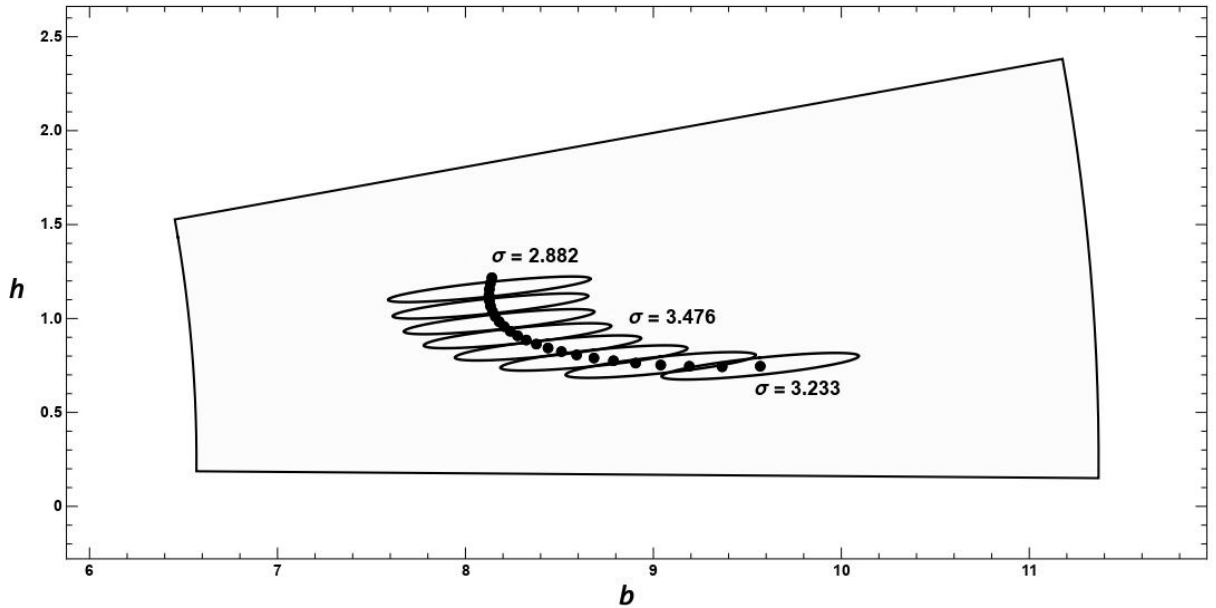


Figure 51. TE results of various combined linear misalignments.

The results indicate that adding more adjustments can regulate the contact trajectory, but it could also result in higher stress levels, which aligns well with previous studies [95-98]. This is apparent from the comparison of Figures (52a) and (52b), where the same amount of profile crowning was implemented ($c_t = 0.08$ and $L_t = 0.16$) but with different longitudinal parabolic crowning parameters $c_1 = 0.005$ and $c_1 = 0.02$ in Figure (52a) and Figure (52b), respectively. It is noticeable that the stress ratio increased by 1.2-1.4 times in Figure (52b) compared to Figure (52a).



(a)

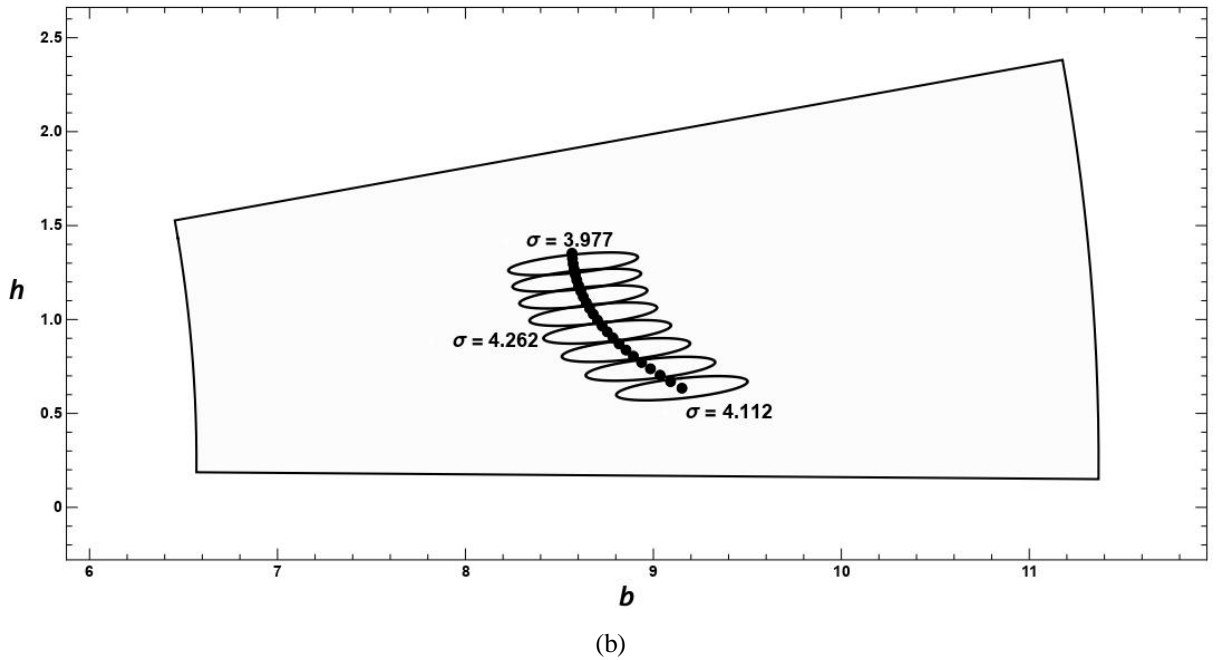


Figure 52. Stress ratio and contact ellipses for combined linear misalignments at $\Delta E = \Delta H = 0.08$ and (a) $c_1 = 0.005$, (b) $c_1 = 0.02$.

Figure (53) displays the outcomes of varying combinations of linear misalignment values of ΔE and ΔH on stress ratio (σ) and pitch point deviation (δ). Pitch point deviation refers to the difference between the location of the pitch point (v_o) and the central contact point (v_1) in a misaligned gear tooth, represented as $\delta = v_1 - v_o$. As previously demonstrated, the results from Figure (53) indicate that ΔE has a greater impact on stress and contact deviation compared to ΔH . Additionally, it is apparent that the stress ratio increases with increasing levels of misalignment, reaching its maximum at $\Delta E = \Delta H = 0.1$. In all simulation cases illustrated in Figure (53), the same value of modification parameters were implemented ($c_1 = 0.005$, $c_t = 0.08$ and $L_t = 0.16$).

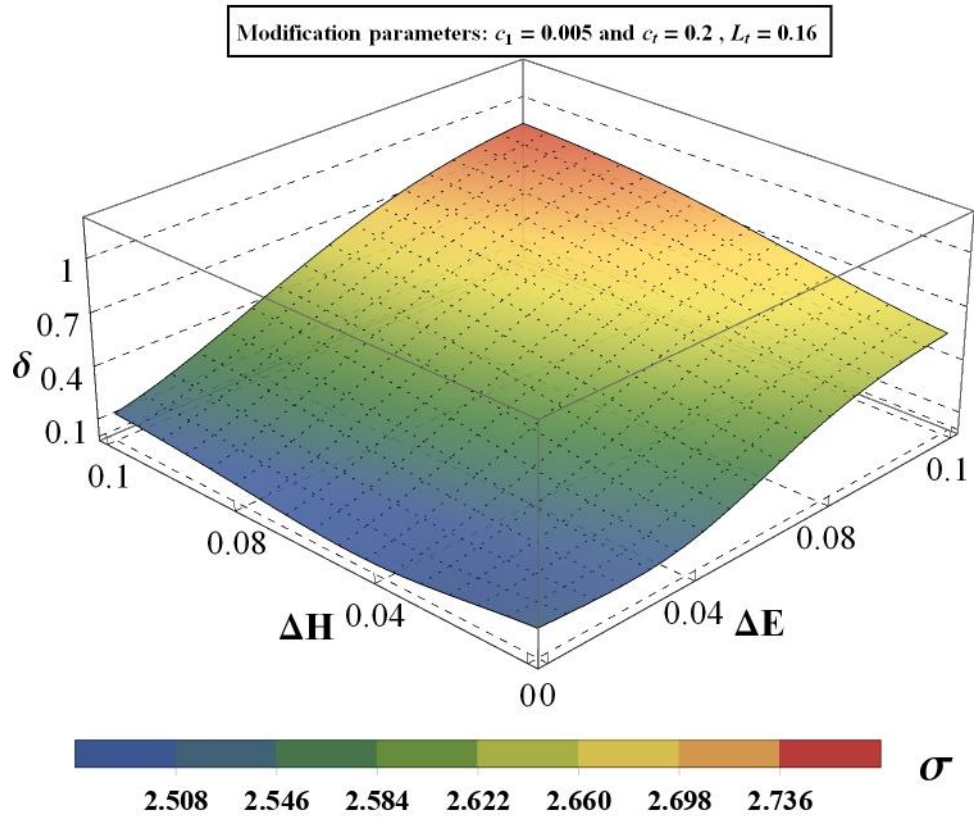


Figure 53. An illustration of the results of stress ratio (σ) and pitch point deviation (δ) based on different and combined values of linear misalignments (ΔE and ΔH).

Chapter 6. Computational assessment of conventional TCA method

6.1 Testing the conventional TCA model

The conventional gear tooth contact analysis (TCA) model originally proposed by Litvin et al. [1] is independently reproduced in this section. Based on the basic principles, it is shown that the fundamental parametrization of the conventional model, although mathematically correct, has computational drawbacks. To simulate the standard solution presented by Litvin et.al [1], the computational environment of Wolfram Mathematica was employed. The contact between two C^1 spur involute surfaces with similar properties was considered for a single meshing position. The parameters of the surfaces are shown in Table (8).

Table 8. Spur gears parameters

Parameters	Gear 1 and Gear 2
Number of teeth	25
Module, mm	2.5
Pressure angle, degree	20
Face width, mm	25

The surfaces in the contact problem were designed to have rotation axes parallel to each other, similar to standard spur gear designs ($w_1 || w_2$). The parametrization of the involute surfaces was carried out using a general equation based on specific parameters u_i and v_i , which were chosen according to the machine tool setup. To localize the surface contact, additional variables were included in the involute surface equation. This was done to ensure that the contact problem had a single point solution, which is consistent with manufacturing procedures for profile modification such as tip and root relief and crowning. The parametric equations for the involute are as follows:

$$\begin{aligned}
 x_i &= r_b(\cos(\theta_i) + \theta_i \sin(\theta_i)) + \delta_x , \\
 y_i &= r_b(\cos(\theta_i) - \theta_i \sin(\theta_i)) + \delta_y , \quad i = 1,2 \\
 z_i &= v_i ,
 \end{aligned}
 \tag{57}$$

the base radius of which is r_b , where θ_i is the involution angle described by Equation (2).

The modification applied to the tooth surface is denoted by δ_x and δ_y , with the latter being a longitudinal parabolic modification that is applied throughout the modeling process.

The current simulation assumes that there is no misalignment when the teeth are transferring. To achieve point contact, a small modification has been made to the gear tooth meshing by applying a parabolic shape with $a_p = 0.0001 \text{ mm}^{-1}$ and $\delta_x = 0$. This results in the contact being concentrated in the center of the tooth surfaces. Figure (54) shows the contact trajectory obtained using the TCA model proposed by Litvin. To determine the position of the contacts, an initial value needs to be chosen to start the iterative process of solving the nonlinear equations of gear coupling. In this case, the center of the surfaces is chosen as the starting values for the unknown parameters of the second gear tooth (u_2, v_2), while a value that is 0.03 rad close to the correct solution of the first contact and nearly 0.3 rad close to the last contact is selected for the unknown angle parameter (ϕ_2). The final result is obtained after numerous simulations that are repeated until the program stops issuing divergence-related warning messages. However, despite significant support in the initial value selection, the model provides an erroneous answer for some contact points. By "erroneous outcomes," we mean points where the iterations either move the approximation away from the required root or lead exactly to the starting point.

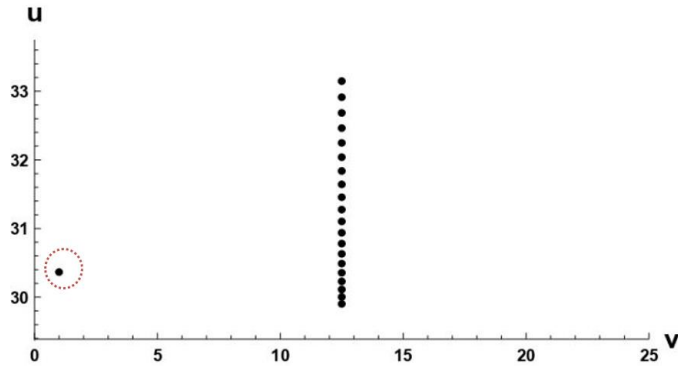


Figure 54. Inconsistencies in the contact path of the spur gear tooth surface are caused by unconverted points, as indicated by the red dashed circle.

Litvin et al. [2,3] found that the TCA algorithm is more sensitive to the angle position parameter ϕ_2 compared to other parameters such as u_1, v_1, u_2 and v_2 . They also noted that in order to achieve convergence, it is important to first determine the angular location of the mating

surface. To address this issue, a computationally intensive parametric sweep needs to be carried out before using the TCA model. To determine the pitch point contact position in space, 1000 randomly generated starting values on the (u_1, v_1) -plane (first surface, S_1) are applied to the TCA method, as shown in Figure (55a). The results of the solution (range) are presented in Figure (55b), where no single point converged. During the 1000 simulations, the midpoint of the second surface S_2 is selected as the initial value for the u_2^0 and v_2^0 parameters, and $\varphi_2^{(0)}$ is set to zero.

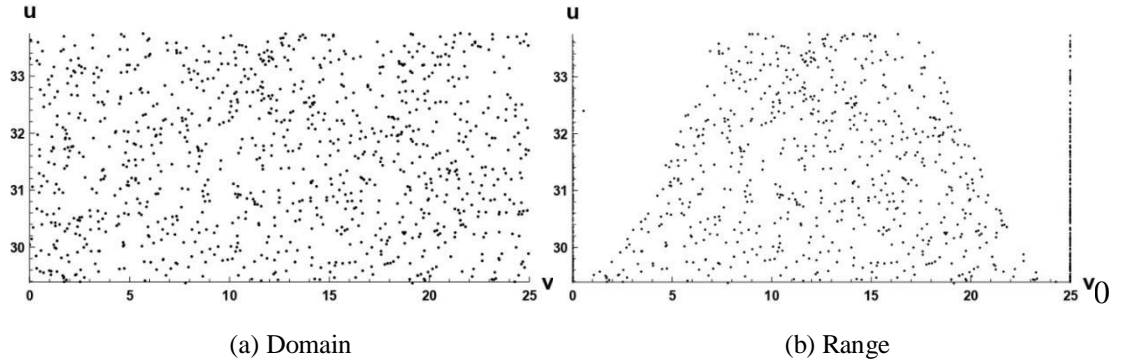


Figure 55. The simulation results for 1000 random points on the tooth surface are displayed, with (a) showing the starting guess values for the iterative process, and (b) displaying the outcomes of Litvin's solution, where hardly any point converged.

The data presented in Figure (56) demonstrates the effectiveness of the implicit TCA model in converging to various initial values of the angle parameter, $\varphi_2^{(0)}$. As previously stated, the algorithm is heavily reliant on the value of $\varphi_2^{(0)}$, with values close to the correct answer resulting in greater convergence. At an initial angle of $\varphi_2^{(0)} = -1.1$ rad, only 480 out of 1000 points converged, resulting in a convergence rate of 48%, while the number of converged points increased to 670 with an initial angle of $\varphi_2^{(0)} = -1.15$ rad. Finally, almost all points converged for $\varphi_2^{(0)} = -1.2$ rad, resulting in a pitch point contact position in space for both surfaces of: $u_1 = 31.103$ mm; $v_1 = 12.5$ mm; $u_2 = 31.402$ mm; $v_2 = 12.5$ mm; $\varphi_2 = -1.6$ rad at $\varphi_1 = 1.5707$ rad. All of the cases examined had the same conditions as the previous analysis, which used the midpoints of S_2 as the initial values for the parameters u_2^0 and v_2^0 , respectively. These results emphasize the need to perform either a parametric sweep or use a large number of random initial conditions to ensure convergence of the implicit Litvin's model and prevent incorrect results, which in both cases is time-consuming and computationally complex.

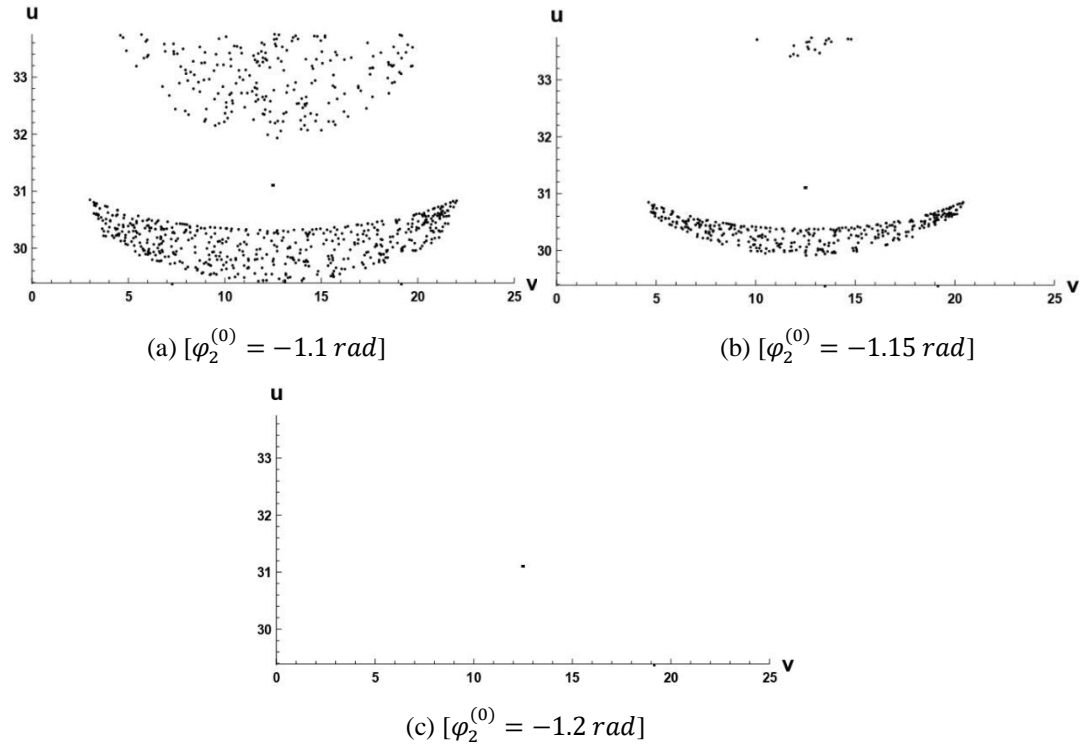


Figure 56. Converged and non-converged values on the initial value guess cloud for Litvin's model with different starting values for $\varphi_2^{(0)}$ are demonstrated, where the starting values for $\varphi_2^{(0)}$ close to the correct solution for (a) 0.5 rad; (b) 0.45 rad; (c) 0.4 rad.

The TCA method was applied to the domain of 1000 randomly generated starting values for $(u_1^{(0)}, v_1^{(0)}, \varphi_2^{(0)})$ -parameters to determine the pitch point contact position in space, as shown in Figure (57a). Figure (57b) displays the solution results (range), where all points failed to converge. The initial value for the $u_2^{(0)}$ and $v_2^{(0)}$ parameters during the 1000 simulations was selected as the midpoint of the second surface.

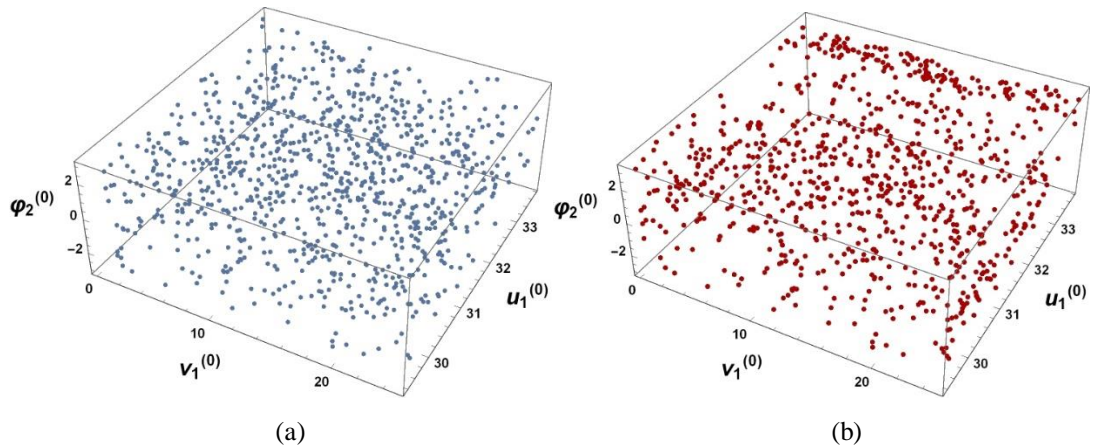


Figure 57. The results of Litvin's solution are shown in (b) for 1000 random points generated for the simulation, where (a) displays the starting guess values for the iterative process. It was found that almost no single point converged during the simulation.

To achieve a higher convergence rate than Figure (57) for 1000 initial random values in $(u_1^{(0)}, v_1^{(0)}, \varphi_2^{(0)})$ - space, the range of the randomly generated angular parameter $\varphi_2^{(0)}$ was restricted to $-1 \text{ rad} < \varphi_2^{(0)} < -1.7 \text{ rad}$, which was closer to the most converged solution $\varphi_2 = -1.6 \text{ rad}$ obtained in the previous simulation, as shown in Figure (56). As a result, the simulation yielded 818 converged points out of 1000, as seen in Figure (58).

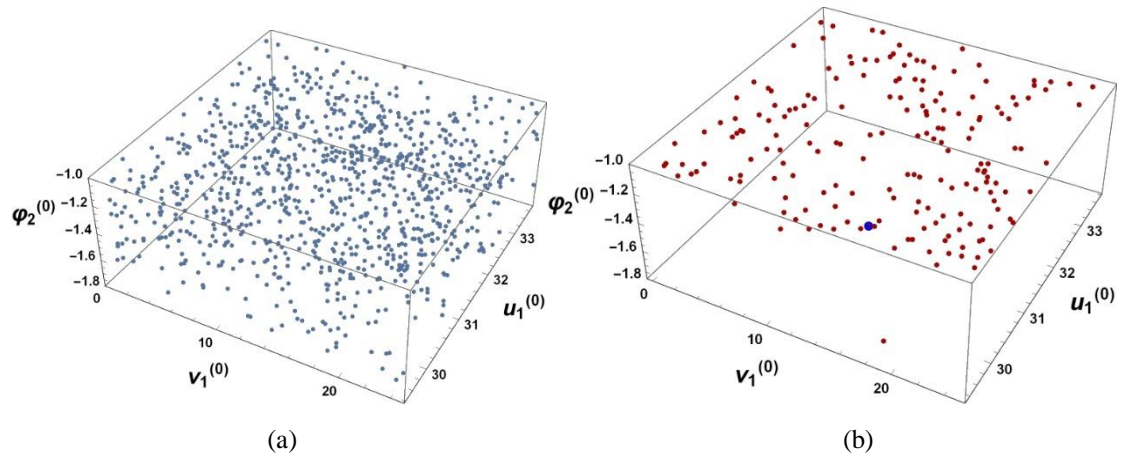


Figure 58. The results of the conventional TCA model for 1000 randomly generated starting points are shown in (a) and (b), where (a) displays the initial guess values and (b) presents the solution outcomes. 81.8% of the 1000 points converged to a single correct solution, which is represented as a blue dot.

It is important to note that we are examining the most basic contact model of a spur gear pair, assuming no misalignments. However, additional adjustments are required to determine the contact position, such as narrowing the range of initial starting values. Additionally, it is sometimes necessary to visually inspect the results to confirm that the correct contact has been identified, since the model can produce inaccurate or divergent outcomes. As with iterative methods such as Newton Raphson, unsuccessful convergence may be due to the initial guess being too far from the root or the function not being continuous in the region being searched for the root.

Further, the same simulation process is performed for the spur gear, but with a presence of 0.1° in-plane misalignment. Figure (59) illustrates the computed contact path. We used the centers of the surfaces as the starting values for the 2nd gear tooth's unknown parameters (u_2, v_2) , as we did in the previous case. However, for the unknown angle parameter, ϕ_2 , we chose a value that is 0.03 rad close to the right answer for the first contact and almost 0.3 rad close to the last contact. The results demonstrate that, despite strong initial value selection support, the model produces incorrect answers at several contact points.

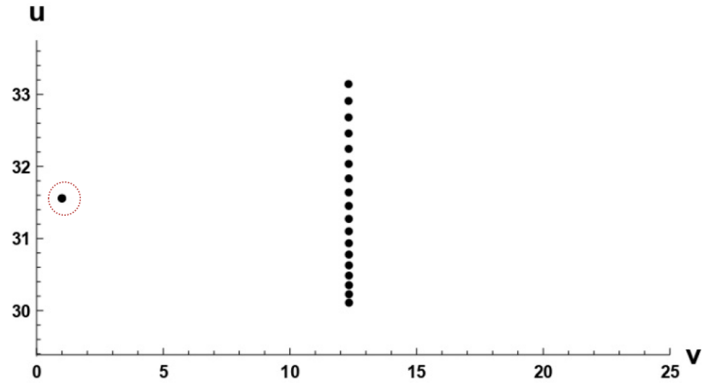


Figure 59. The contact path along the tooth surface of the in-plane misaligned spur gear is depicted, and despite careful guess value selection, some points were not able to converge, as indicated by the red dashed circle.

The conventional TCA method was used to determine the pitch point contact position in space for misaligned spur gear by employing 1000 randomly generated starting values, as depicted in Figure (60a). In order to increase the rate of convergence, we restricted the range of the selected random angular parameter $\varphi_2^{(0)}$ to be within $-1 \text{ rad} < \varphi_2^{(0)} < -1.7 \text{ rad}$. As shown in Figure (60b), the simulation yielded an 80% convergence rate out of the 1000 points.

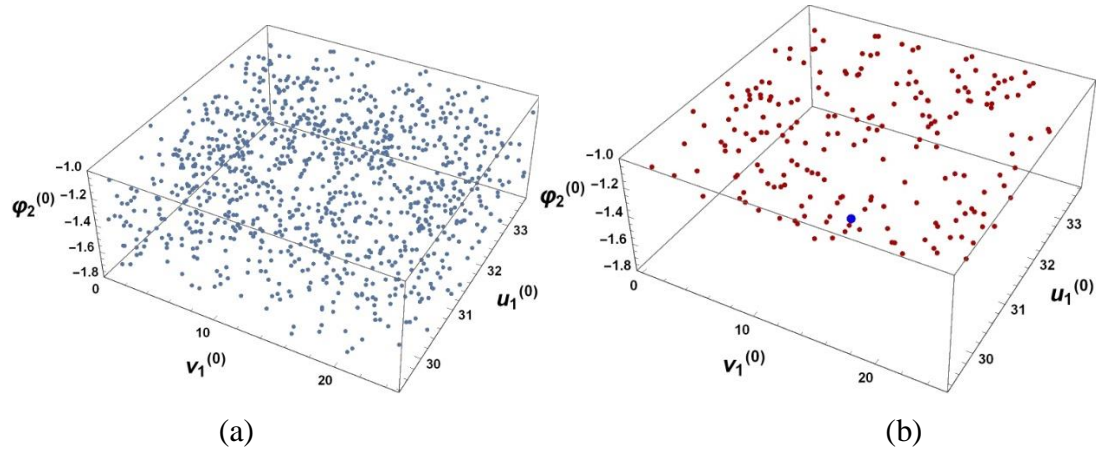


Figure 60. The outcomes of 1000 simulations using random starting points are depicted, where (a) displays the initial guess values and (b) exhibits the consequences of the conventional TCA model. In the image, a blue dot represents the accurate answer to which 800 points out of the 1000 converged.

Next, to fairly test the ability of the conventional TCA model, we have repeated exactly the same simulation process performed by Litvin et.al in [81] for aligned and misaligned helical gear engagement. The parametrization of the helical gear tooth surfaces in space, using the given parameters (u_i, v_i) , was expressed by applying a general involute equation.

$$\begin{aligned}
x_i &= u_i \cos \left(\cos^{-1} \left(\frac{r_b (\cos \theta_i + \theta_i \sin(\theta_i))}{u} \right) + \sin^{-1} \left(\frac{v_i \sin \beta}{r_b} \right) \right) + \delta_x , \\
y_i &= u_i \sin \left(\cos^{-1} \left(\frac{r_b (\cos \theta_i + \theta_i \sin(\theta_i))}{u} \right) + \sin^{-1} \left(\frac{v_i \sin \beta}{r_b} \right) \right) + \delta_y , \\
z_i &= v_i ,
\end{aligned} \quad (58)$$

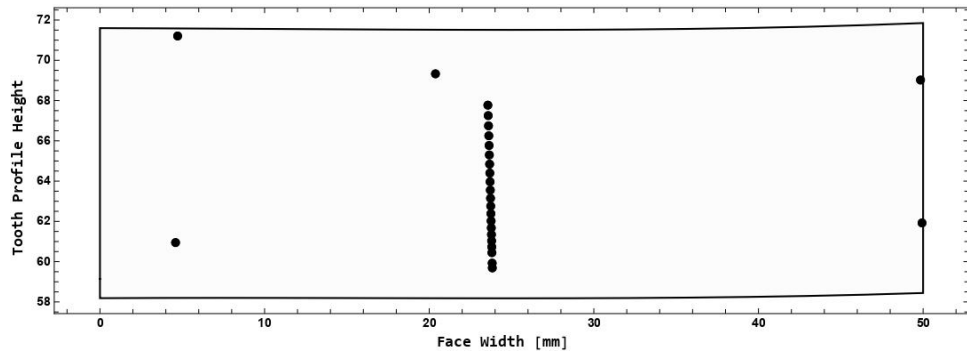
This expression includes the helix angle (β), the involuon angle (θ_i), and the tooth surface modification function ($\delta_{x,y}$). To objectively evaluate the TCA model, we have chosen the same parameters as in [81] for the pairs of helical gears and the crown size with misalignments, as shown in Table (8), which specifies the parameters of the contacting surfaces.

Table 9. Helical gears parameters

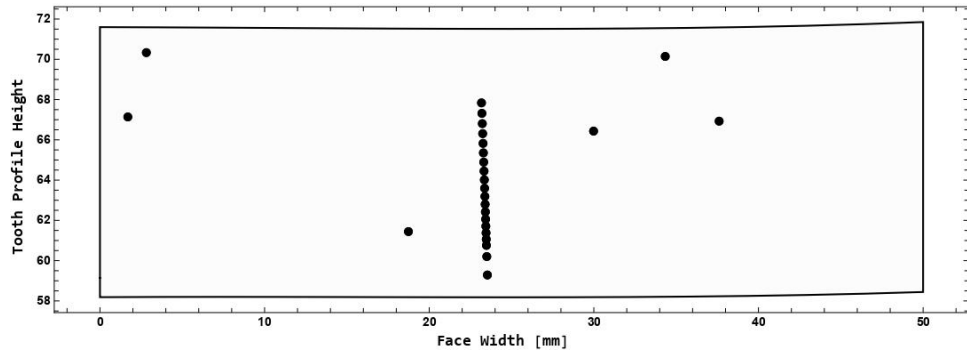
Parameters	Gear 1 and Gear 2	
Number of teeth	25	77
Module, mm	5	
Pressure angle, degree	27.5	
Helix angle, degree	20	20
Face width, mm	40	
Cross angle, degree	0	
Parabola parameter of profile crowning	1.4×10^{-3}	8×10^{-5}

To determine the contact path, the system of non-linear equations in Equations (26-32) can be solved numerically. However, the accuracy of this solution heavily depends on the selection of proper initial "guess values" due to the complexity of the contact equations. When the initial values are not selected appropriately, the numerical algorithm may result in an inaccurate solution with flawed contacts or insufficiently converged solutions, as illustrated in Figures (61-62). Incorrect results can be produced when the iterations return to the initial point or move the approximation farther from the required root. In Figure (61a) and (61b), the results of aligned helical teeth engagement and contacts in the presence of an alignment error $\Delta\lambda = -3$ arcmin are shown. In both cases, the value of $\varphi_2^{(0)}$ is close to the correct solution for 0.05 rad, but the starting values for the u_2^0 and v_2^0 parameters are randomly chosen. In Figures (62a-b), the same cases of contact path are shown, but now $\varphi_2^{(0)}$ is close to the correct solution for 0.05 rad, and the starting value is close to the actual contact for for $u_2^0 - u_2^{sol} = 4.89$ mm and

$v_2^0 - v_2^{sol} = 1.44$ mm. From Figures (61-62), it can be concluded that even with reasonable assumptions about the initial values, we cannot always rely on the results without human observation.

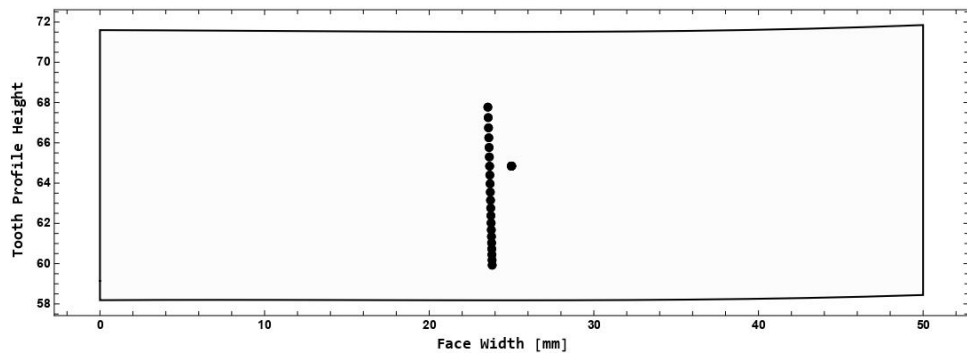


(a)



(b)

Figure 61. Path contact demonstration using arbitrarily selected starting values for the u_2^0 and v_2^0 parameters, but with a near approximation to the right solution for 0.05 rad for angle parameter φ_2^0 . (a) Path contact solution that is aligned; (b) misaligned result with an in-plane deviation of $\Delta\lambda = -3$ arcmin.



(a)

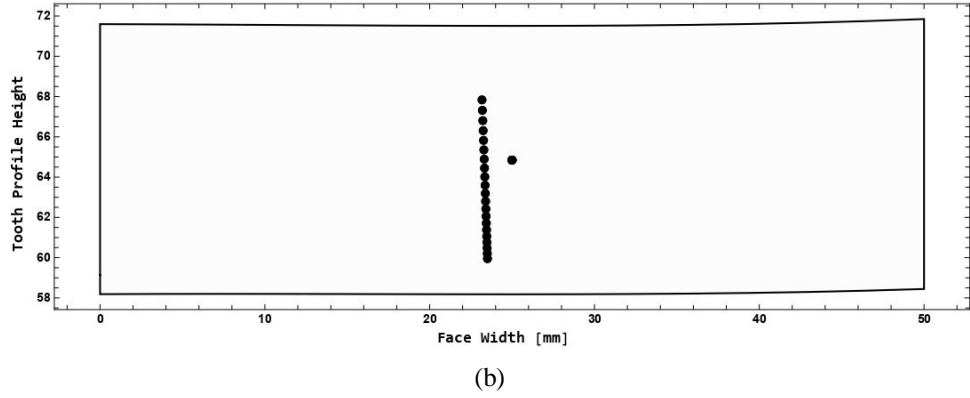


Figure 62. The path contact of helical gears where the initial value close to actual contact for $u_2^0 - u_2^{sol} = 4.89$ mm and $v_2^0 - v_2^{sol} = 1.44$ mm and $\varphi_2^{(0)}$ close to right solution for 0.05 rad. (a) The contact trace is aligned; (b) the contact is misaligned with an in-plane deviation of $\Delta\lambda = -3$ arcmin.

The pitch point contact position of parallel axes helical gears with $\Delta\lambda = -3$ arcmin in-plane misalignment in space was calculated using a set of 1000 randomly generated starting values for the $(u_1^{(0)}, v_1^{(0)}, \varphi_2^{(0)})$ -parameters, as shown in Figure (63a). However, none of the points were able to converge, as illustrated in the solution range displayed in Figure (63b).

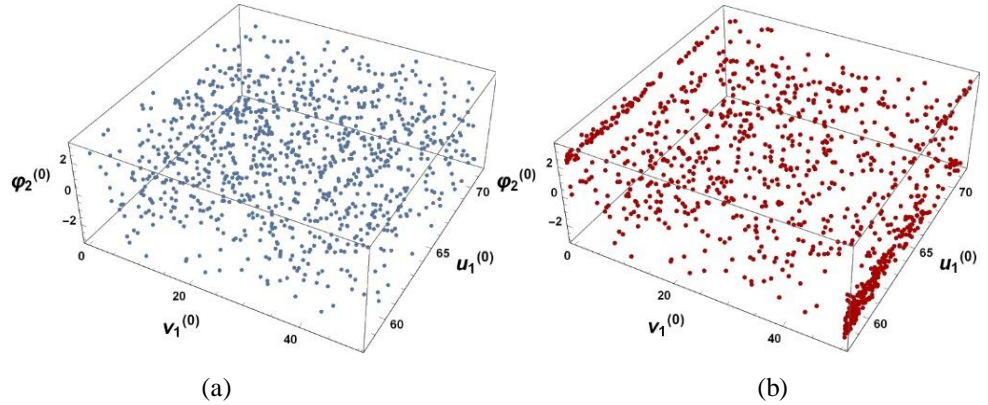
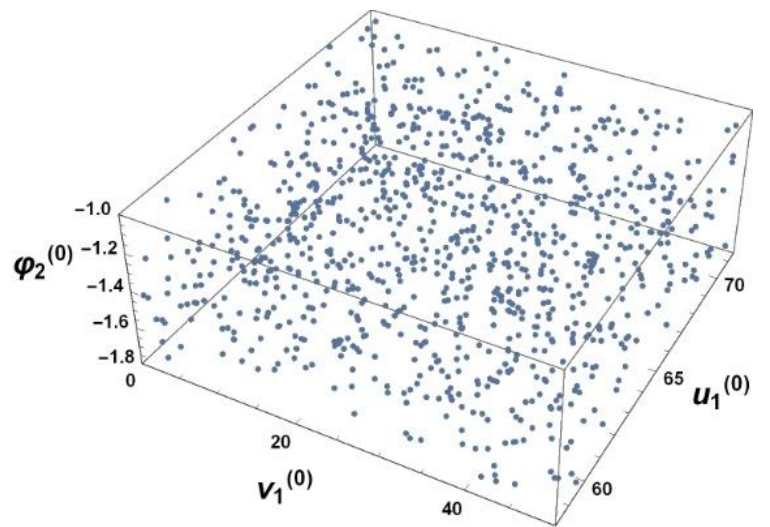


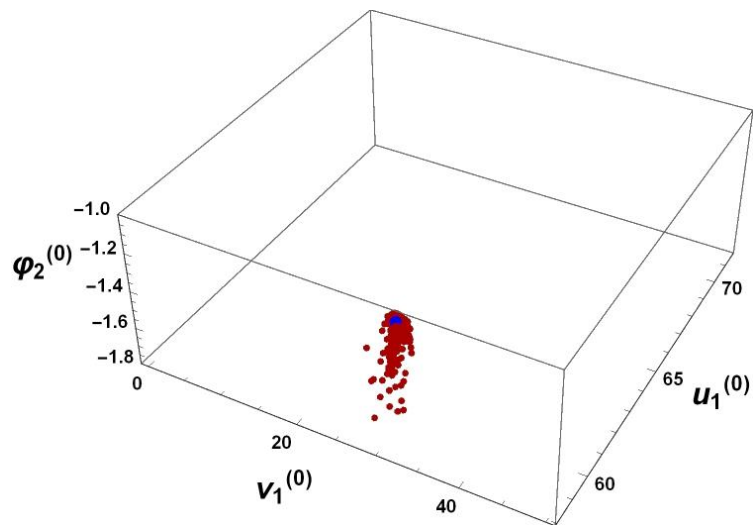
Figure 63. The simulation results were obtained by analyzing 1000 random points on the surface of helical gear teeth. The starting guess values are depicted in (a), while the results of Litvin's solution, in which almost no single point converged, are shown in (b).

The simulation procedure shown in Figure (63) was repeated in Figures (64-65), but with a reduced range of the randomly generated angular parameter $\varphi_2^{(0)}$, which was limited to -1.7 rad $< \varphi_2^{(0)} < -1.3$ rad. The upper limit was close to the solution by -1.3 rad $- \varphi_2^{sol} = -0.335$ rad and the lower limit was close to the solution by -1.7 rad $- \varphi_2^{sol} = -0.065$ rad, where the actual solution is $\varphi_2^{sol} = -1.635$ rad. The proportion of convergence was better than in Figure (63), but still only 13-15%. Additionally, as depicted in Figures (64b-65b), some

points approached the correct solution, but did not reach it. As previously mentioned, the traditional TCA model-based system of nonlinear equations can produce several converged solutions, but some of them may not lead to the actual point of contact. The number of Newton-Raphson iterations was increased to determine whether the failed converged points would eventually reach the precise root. However, the analysis demonstrated that the results remained consistent, indicating that this model can produce inaccurate outcomes.



(a)



(b)

Figure 64. The results of simulating 1000 random points on the surface of an aligned helical gear tooth contact where: (a) initial guess values; (b) Litvin's solution, where only 13.5% of the 1000 points converged to the correct answer (blue dot).

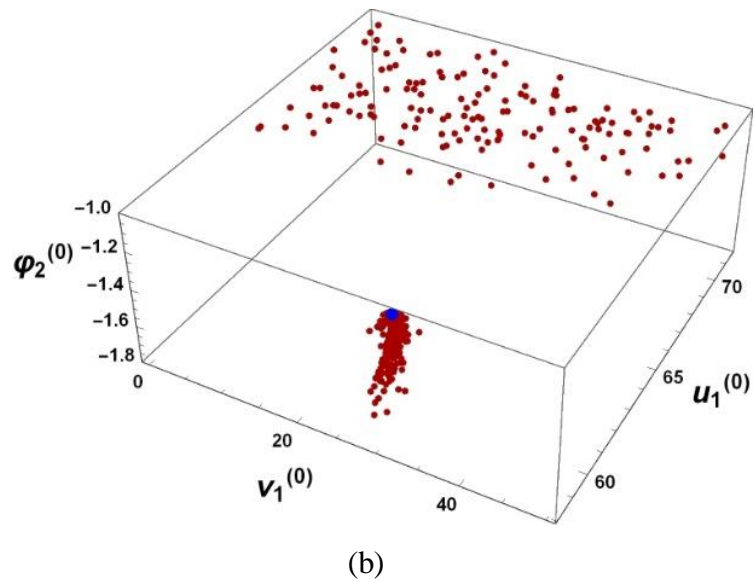
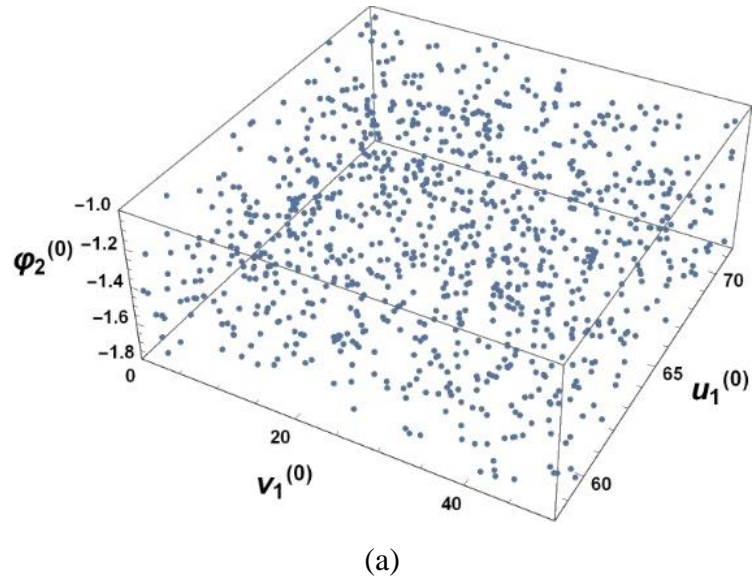
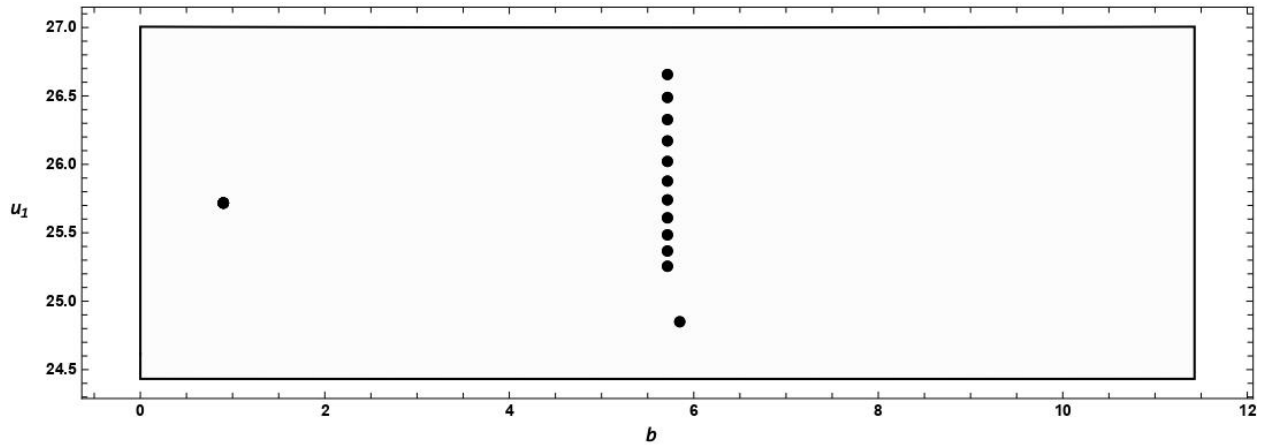


Figure 65. The simulation results were obtained by analyzing 1000 random points on the surface of misaligned helical gear teeth. The starting guess values are depicted in (a), while the results of Litvin's solution, where only 14.2% of the 1000 points converged to the correct solution (blue dot), are shown in (b).

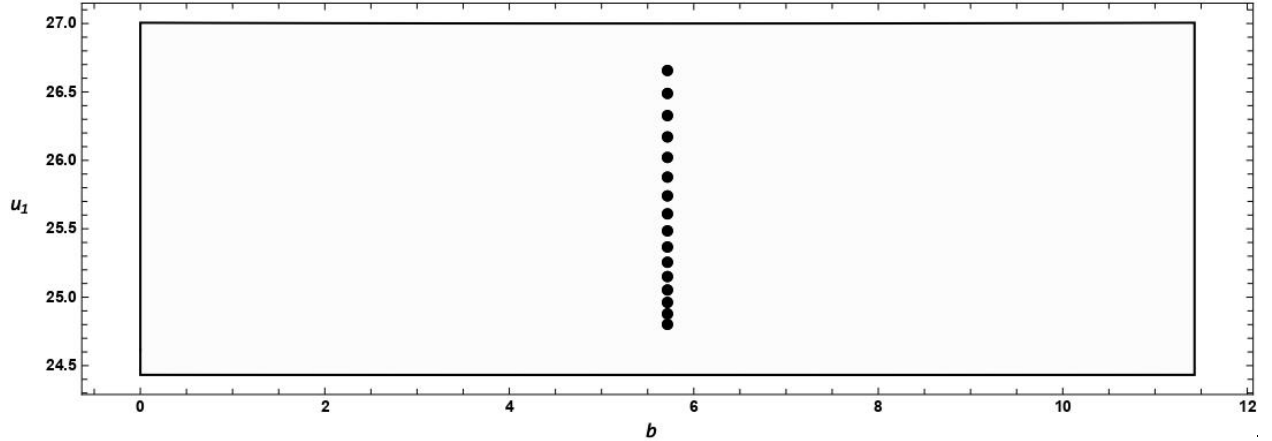
6.2 Comparison of conventional and new TCA method for spur gears

The set of nonlinear equations proposed by Litvin et al. [1] can be used to determine the path of contacts, but the success of the numerical solution heavily relies on the selection of

suitable initial guess values due to the complicated nature of the contact equations. Inappropriate initial values can lead to incorrect results, as shown in Fig (66a), where the numerical algorithm may produce faulty contacts or fail to converge to the correct solution. Incorrect outcomes refer to points where the iterations either return to the starting point or lead to an approximation that is different from the required root. However, the new model is able to produce dependable results with no divergence, as depicted in Fig (66b).



(a) Conventional TCA model



(b) Novel TCA model

Figure 66. The path of contacts on the spur gear tooth surface, where (a) some locations failed to converge due to inappropriate guess values for the parameter ϕ_2 , despite the fact that the selected guess values were within 0.2 rad of the correct response for the real pitch point contact solution.

In this section's preceding and subsequent modeling process, the gear parameters included: $N_1 = 52$ and $N_2 = 72$, module $m = 1$, pressure angle $\alpha = 20^\circ$, and face width $b =$

11.42. Both the module and tooth width have been non-dimensionalized. The gear pair is illustrated in Figure (67). To achieve point contact between the tooth surfaces, a parabolic alteration with longitudinal crowning coefficient $a_1 = 0.002857$ was implemented on the first gear.

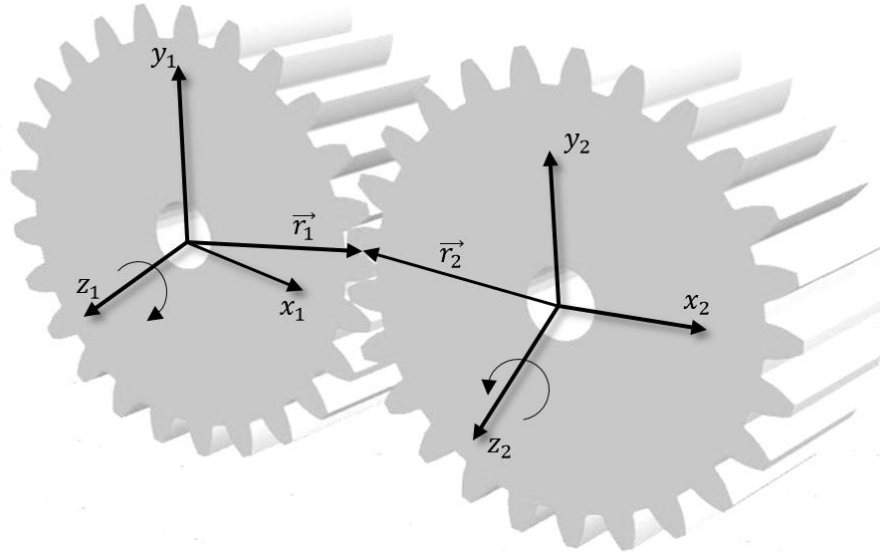


Figure 67. The schematic representation of a spur gear pair.

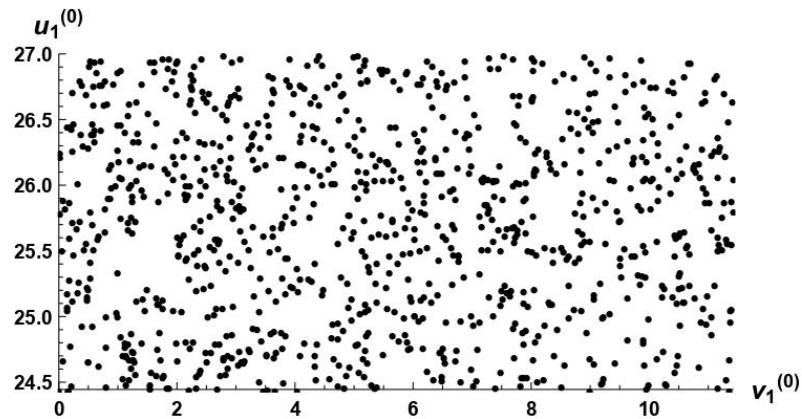
Table 10. Convergence outcomes of two algorithms

Model	Percent of convergence of 5000 guess starting points	Mean iteration steps per converging point	Total time of convergence of 5000 points ^(a)
Conventional TCA	27.32%	5.53	839.62 sec
Proposed novel TCA	99.98%	4	232.09 sec

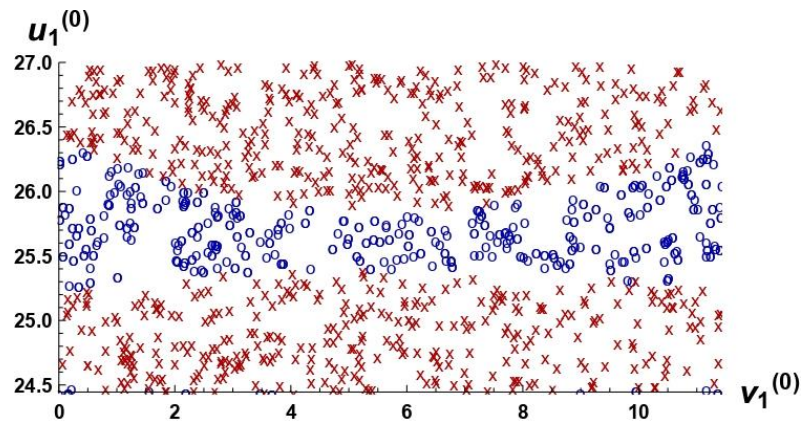
(a) Failed convergence points were swapped out for new random points until the convergence rate reached 100%.

Table (9) presents the results of the convergence of two methods, obtained using an equal number of randomly generated 5000 starting points on the uv -plane, in order to ensure a fair comparison of the two models. The table shows that the conventional method resulted in only about 27% of the initial points converging, while the proposed model successfully converged practically all initial points, indicating high reliability and robustness to initial value selection. It should be noted that the proposed model had only a few non-convergent points,

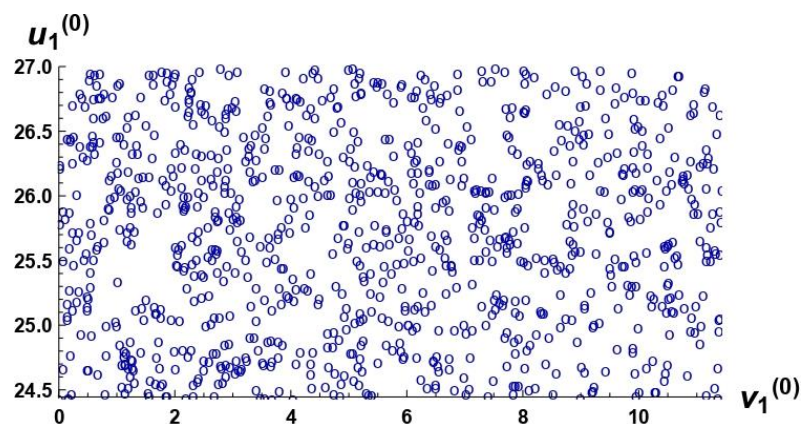
which were located along the edge of the tooth surface. In addition, the table clearly indicates that the conventional TCA solution required almost twice the number of iterations and overall convergence time for the 5000 points compared to the proposed model.



(a)



(b)



(c)

Figure 68. Converged and non-converged values are shown on the guess cloud on the uv -plane with 1000 randomly selected points, where (a) the imposed initial guess values (domain), (b) the results of the conventional TCA solution (range) with some correct contact solution, and (c) the proposed new solution (range) with fully converged results. The blue dots denote converged points, while the red crosses denote non-converged points or points that converged erroneously.

Compared to the conventional approach [1], the new TCA solution requires fewer equations and uses explicit calculation. The effectiveness of the new solution is demonstrated through a simulation where 1000 random starting values are used with the Newton-Raphson method, and it shows numerical convergence and insensitivity to the initial value chosen. Figure (68) displays the convergence outcomes of the two models, with Figure (68a) showing the domain of the 1000 initial random points produced for each technique. The solution results are displayed in Figures (68b) and (68c), where the conventional model only has approximately 25% of points that converge around the actual contact solution, while the new model produces 100% convergent results.

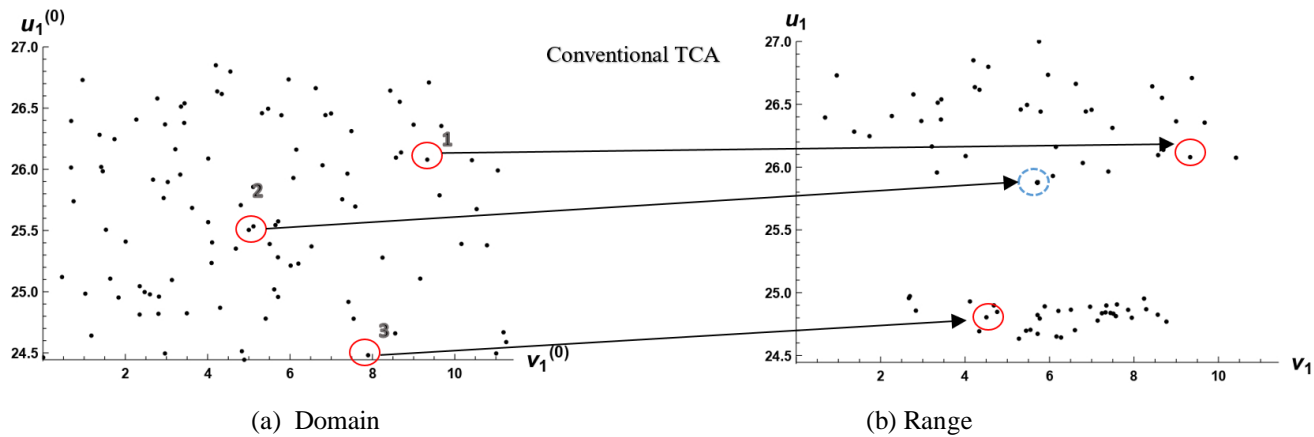


Figure 69. Convergence outcomes of conventional TCA model, where (a) random variables (domain), and (b) its result of Litvin's non-linear equations (range).

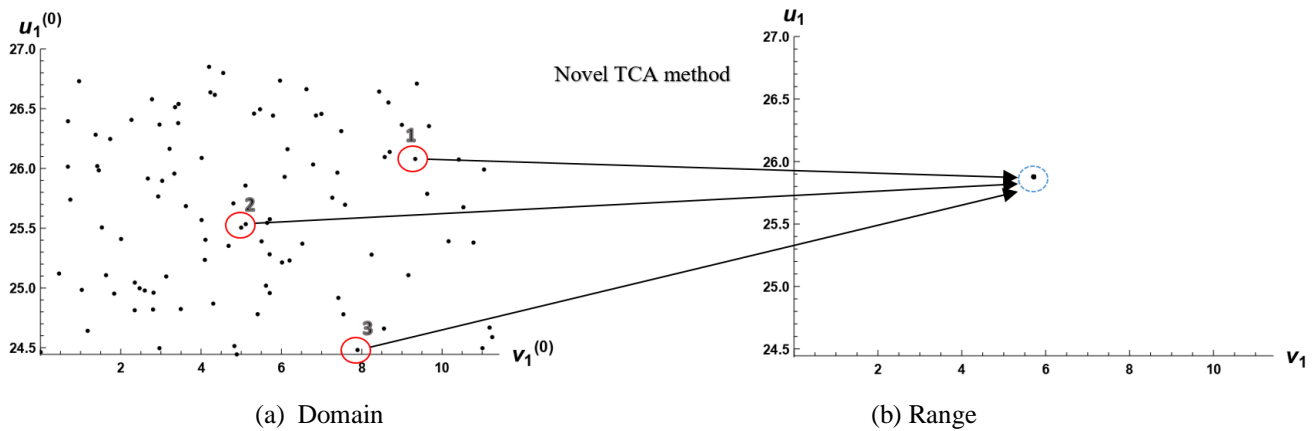


Figure 70. Convergence outcomes of novel TCA model, where (a) random variables (domain), and (b) its result of Litvin's non-linear equations (range).

Figures (69) and (70) display the solutions obtained from both models using the same initial values. The results reveal that for the conventional TCA approach, point "1" failed to converge and remained at its original location, while point "3" converged but with the incorrect outcome. On the other hand, point "2" converged correctly. However, for the new nonlinear equations with two unknowns, all points converged accurately. In the conventional TCA technique, the selection of the initial value significantly impacts the convergence, and it is essential to establish the angular position of the meshing surface to locate the point of convergence [2]. In contrast, the new model resolves this issue by precisely calculating u_2, v_2, ϕ_2 using the new parameterization and explicit geometric relations mentioned earlier. Additionally, reducing the number of free variables in the new model improves the likelihood of convergence, reduces the iteration steps, and speeds up computation time.

6.3 Comparison of conventional and novel TCA methods for straight bevel gear

In this section, the comparison analysis was performed for straight bevel gears, and it was shown that the non-linear equation system for TCA (tooth contact analysis) represented by Equations (26-32) can be solved numerically to determine the path of contacts or transmission errors. However, due to the complexity of the contact equations, the accuracy of the numerical solution is highly dependent on selecting appropriate initial "guess values." If the initial values are not chosen correctly, the numerical algorithm may produce inaccurate contacts or fail to converge, as illustrated in Figure (71).

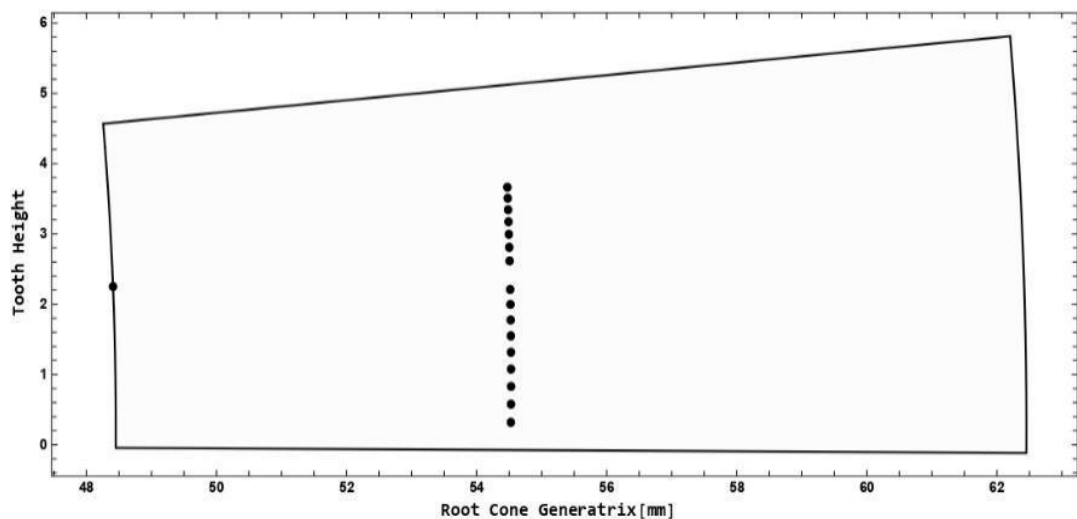


Figure 71. Even though the chosen guess value was within 92% of the correct answer, the route of contacts on the straight bevel gear tooth surface where one point failed to converge due to an inappropriate guess value of the parameter ϕ_2 .

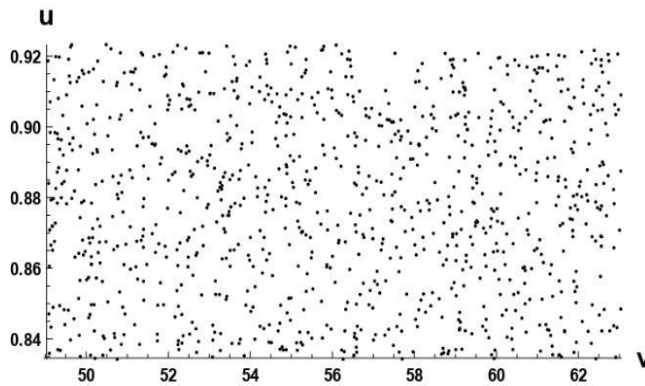
Table 3. Comparison of convergence result of two models.

Solution description	Average iteration steps per converging point	Total time of convergence of 1000 points^(a)	Percentage of convergence of 1000 random starting points^(b)
Conventional Litvin's solution	6.42	68.31 sec	29.4%
Proposed new solution	4	39.58 sec	100%

(a) Until the convergence reached 100%, failed convergence points were switched out for new random ones.

(b) Convergence rate from one loop as a percentage

Table (10) displays the convergence results for both methods. To ensure a fair comparison between the two models, 1000 random starting points were generated at the (u_1, v_1) -plane and applied to each solution method. The table shows that only about 30% of the initial points applied to Litvin's solution converged, while all starting points converged successfully in the proposed novel model. Furthermore, the total convergence time for 1000 points in Litvin's solution is almost twice as long as that of the proposed model.



(a)

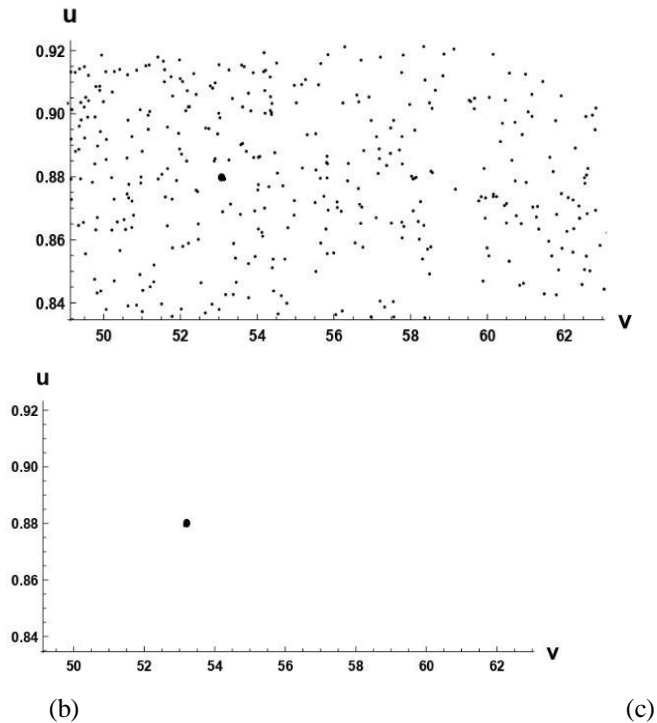


Figure 72. Results of convergence of a cloud of 1000 randomly chosen guesses, where (a) the applied initial guess values (domain), (b) the results of Litvin's solution (range) with some concentration around the correct contact point, and (c) the proposed new solution (range) with fully converged results at the single correct point.

Figure (72) depicts the convergence results of the two models. Figure (72a) displays the domain of 1000 randomly generated initial values applied to each method. Figures (72b) and (72c) show the solution results (range), where Litvin's model generates only approximate results with some concentration around the genuine contact point. On the other hand, the novel model provides an exact solution with 100% convergence.

6.4 Comparison of two TCA methods for spiral bevel gear

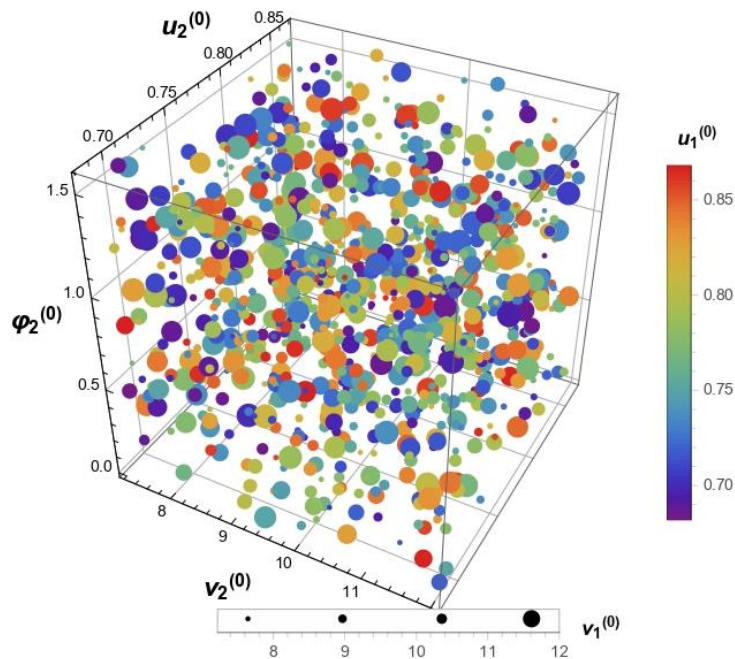
To consider the capabilities of the conventional and proposed TCA model, a comparative analysis was performed for spiral bevel gears. Table (11) demonstrates that the results of simulation process where the new model has several advantages. Firstly, it requires fewer iterations and less time to converge compared to the conventional model. Secondly, it is more accurate with a lower average absolute error. The results of 1000 simulations with different initial values show that the new model has a higher probability of convergence, while the conventional model only has a 36% success rate. This indicates that the conventional model is

more sensitive to the input starting values. To run the iterative calculation process for the conventional TCA model, five random variables must be applied for its five unknown free parameters.

Table 12. Computational results of two methods

	Average steps per iteration toward convergence	Average convergence time	Probability of convergence	Mean absolute errors
Conventional model	43	0.0633 sec	35.8%	10^{-3}
Proposed new model	21	0.0409 sec	100%	10^{-10}

Figure (73a) displays the 1000 generated random variables for each parameter, with the position of the bubble indicating the applied variable for the u_2 , v_2 and φ_2 parameters, and the color and size of the bubble indicating the applied variable for the u_1 and v_1 parameters. Figure (73b) shows the convergence result of the conventional TCA model, where all successfully converged points will be located in the same position in the (u_2, v_2, φ_2) -space with the same color and size.



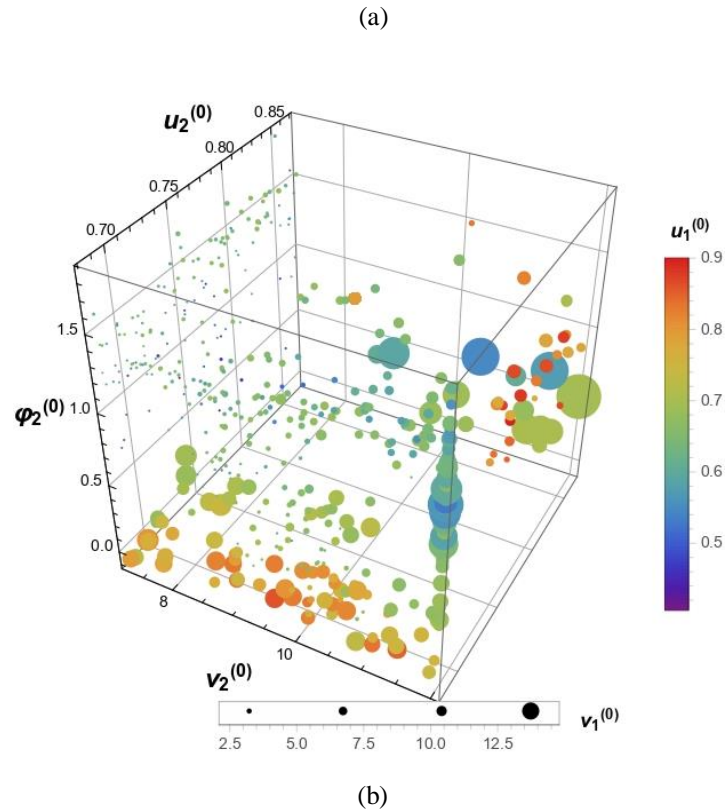


Figure 73. Convergence result of conventional TCA model where: (a) generated two dimensional 1000 random variables; (b) solution with 36% of convergence in five dimensional parametric space.

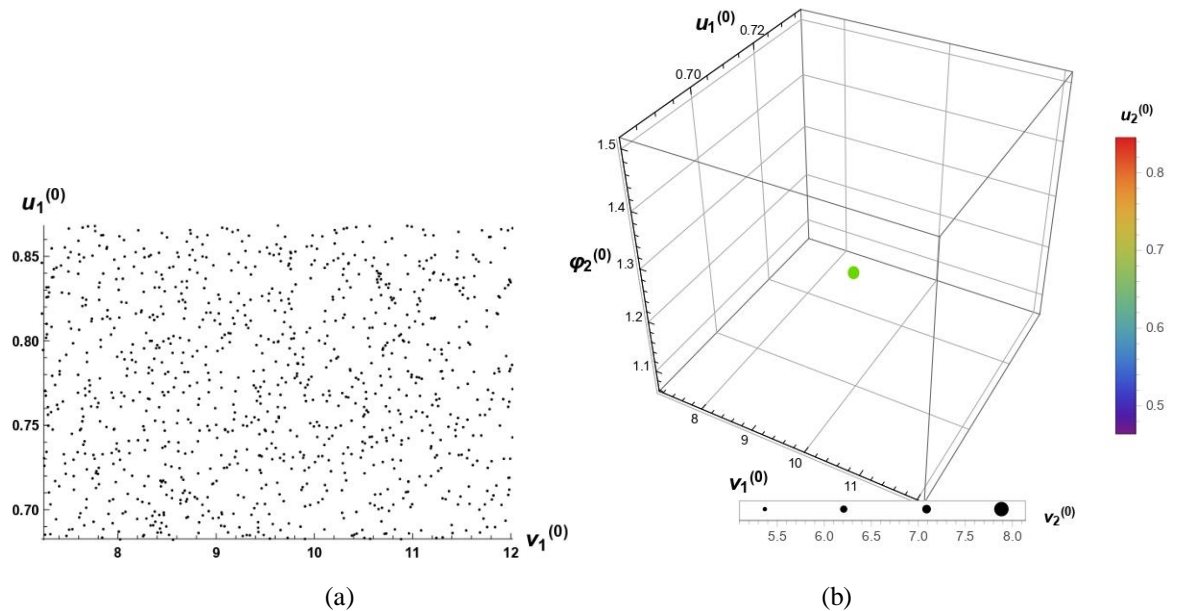
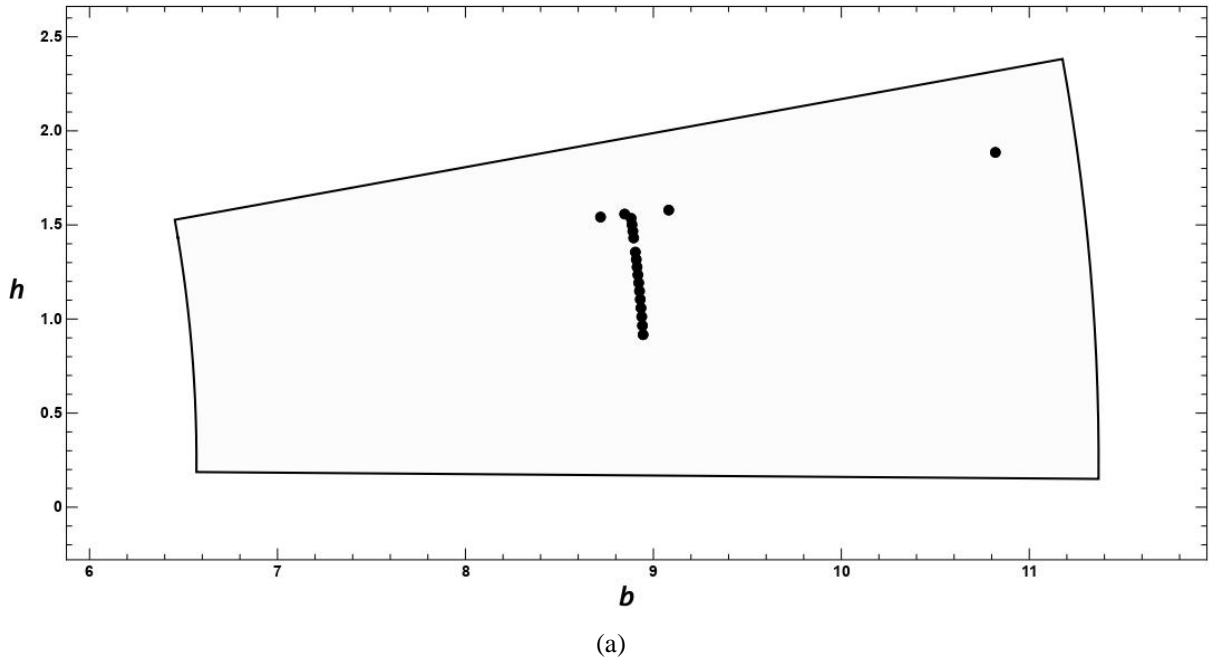


Figure 74. Convergence result of new TCA model where: (a) generated two dimensional 1000 random variables; (b) solution with 100% of convergence in five dimensional parametric space.

The proposed model has a significant advantage over the conventional model in that it

only has two unknown free parameters. This means that to start the iterative process and calculate the contact position of the engagement tooth, only two variables need to be applied, and the other parameters can be calculated by back substitution to Eqs. (33-43). Figure (74a) illustrates the 1000 generated random variables in two dimensional (u_1, v_1) space, and Figure (74b) shows the results of the new TCA algorithm. All 1000 generated variables for each parameter u_1 and v_1 lead to convergence, and thus, on a five-parameter plot ($u_1, v_1, u_2, v_2, \varphi_2$), all points have the same position, color, and size. Figures (75) and (76) compare the paths of the contact solution performed by the two TCA methods. In the conventional model, an inaccurate choice of initial values can lead to an erroneous contact position, where the iterations process either leads exactly to the starting point or takes the approximation away from the desired root. However, in the proposed model, due to the updated computational process, this problem does not arise.



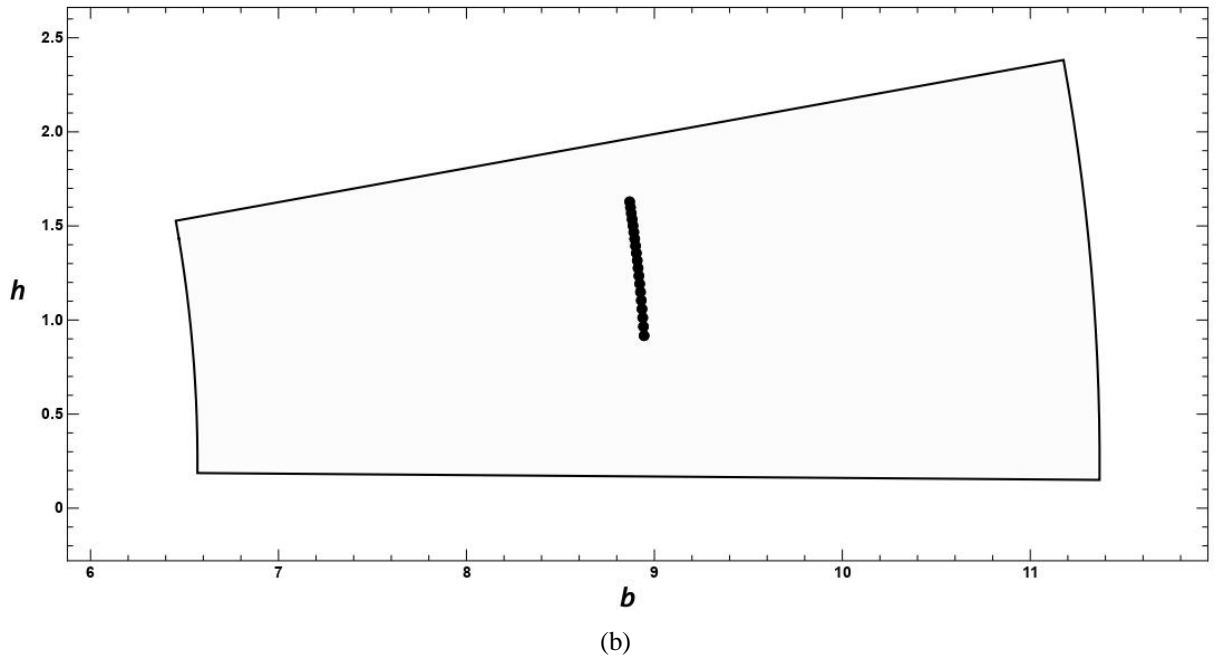


Figure 75. Path contact solution of two methods, where (a) conventional and (b) proposed model.

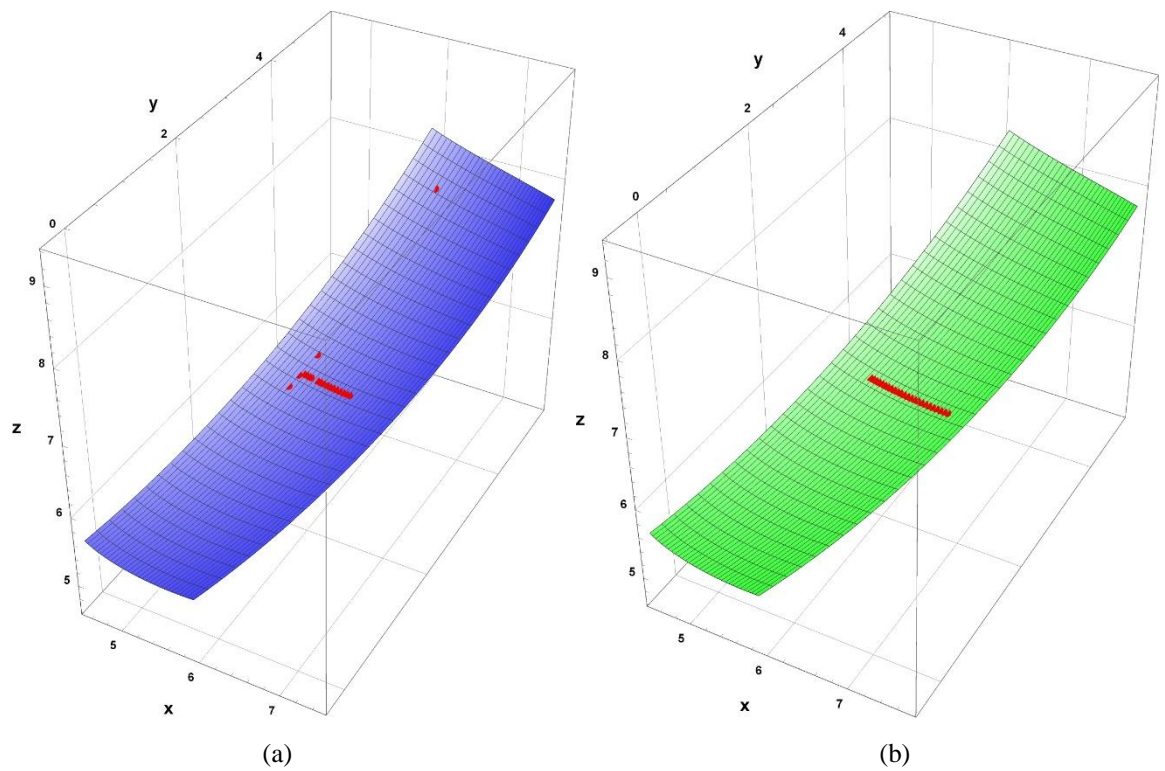


Figure 76. The path contact solution for (a) conventional and (b) proposed model in space.

Chapter 6. Conclusions

6.1 In the end

The PhD dissertation presents a novel Tooth Contact Analysis (TCA) method for evaluating the contact of gears in transmission systems. The proposed method is designed to overcome the issue of convergence in the conventional TCA algorithm proposed by Litvin et al. [1-3], which requires careful selection of initial values for the iterative process. By transforming the same contact conditions as in the conventional model, the new TCA method reduces the five conventional nonlinear tooth contact equations with five free parameters to a system of two nonlinear equations with only two unknown parameters, resulting in a more robust, explicit, and fast converging algorithm.

The proposed method is implemented in the Wolfram Mathematica computational environment to analyze the contact characteristics of various types of gears, including the impact of tooth surface to various misalignments and tooth surface modifications. The study also investigates the effects of three types of longitudinal crowning and tip/root profile relief of tooth on gear meshing. The proposed model is compared with the conventional TCA method for various gear systems in terms of accuracy, computational efficiency, and convergence probability, where the findings demonstrate the superiority of the new TCA method. Furthermore, the efficiency and accuracy of the proposed TCA model enables the determination of acceptable values for tooth modifications and the identification of the most suitable design approach for different types of gears in a timely manner, thereby demonstrating its significant potential for enhancing the technology and quality of gears in various fields.

The study utilized the developed model to analyze the impact of different in-plane and out-of-plane angular misalignment on crowned spur and helical gears. The evaluation was based on parameters such as the path of contact, maximum contact pressure, and transmission error (TE). To assess the sensitivity, three different types of lead crowning were employed, namely parabolic, circular, and logarithmic modifications. These modifications were expressed mathematically in terms of the planar coordinates of the tooth surface of both spur and helical gears. Metrics were developed using the TE function and contact pressure to compare the performance of each crown design. The study identified the optimal design based on these metrics. Also, the investigation highlights the importance of considering different crown designs

and their impact on gear performance in the presence of angular misalignment. The simulation results indicate that out-of-plane misalignment causes a more significant increase in TE and deviation of contact path from the tooth surface center than in-plane misalignment. For spur gears, the logarithmic crown produced smaller negative effects on the TE function than traditional crowning type as parabolic for both misalignment types, although the improvement in contact path was not substantial. The differences in results between modifications were smaller for in-plane misalignment than out-of-plane misalignment. In the case of helical gears, circular crowning produced a smaller shift in the path of contact for in-plane misalignment, while parabolic crowning showed better results for out-of-plane misalignment. The logarithmic crowning consistently gave smaller values for TE in all cases. However, for large misalignment angles, the difference between traditional modifications and logarithmic crowning was significant. The shift of the contact path from the tooth center during gear meshing was almost an order of magnitude larger for helical gears than spur gears. The logarithmic profile was found to be effective for extreme misalignments due to its increased curvature at the edges, while the circular and parabolic crowning profiles presented singularities at the tooth edge. The maximum contact pressure varied with different crown profiles, with logarithmic crowning generally resulting in higher pressure for both spur and helical gears.

The study suggests that in the case of straight and spiral bevel gears, tip relief crowning has a greater effect on transmission error function than lead modification. It also indicates that it is impossible to achieve a continuous transmission function without tip relief modification, and that longitudinal modification is necessary to avoid edge contact. Therefore, the study recommends the use of double crowning with appropriate amounts of modification for the bevel tooth surfaces in the presence of any type of misalignment to avoid tooth edge contact and smooth transmission to avoid shock loads and noise. It was also founded that a certain value of profile crowning can help avoid edge contact or intermittent transmission at the deviation of centre distance, but the same amount of modification can lead to undesirable results at another misalignment type like axial displacement. The method of changing the contact trajectory by altering the quantity of crowning was illustrated in comparison to the results without additional crowning. The study further compares three types of crowning used to modify the tooth surface in the longitudinal direction and suggests that the differences between them are not significant.

The conventional TCA method has been subjected to critical analysis in terms of the convergence and accuracy of its numerical iterative calculation process. The analysis revealed that the method is sensitive to the initial guess values, particularly the starting value of the angular position, which results in around 30% convergence for most gear systems, including

spur, helical, and bevel gears. These convergence problems are attributed to the complexity of the non-linear equations and the presence of several roots for the unknown parameters. As a result, the conventional TCA method can lead to divergence, infinite looping, or random loss of convergence. Although an automatic guess value determination approach was proposed to mitigate this problem [2,3], it is computationally expensive and impractical. On the other hand, the proposed method demonstrates its superiority in terms of the probability of convergence, where almost in all cases achieved 100% convergence. Moreover, the proposed method stands out for its speed and accuracy of calculations. Therefore, the conventional TCA method's convergence and accuracy issues indicate a need for improved approaches like the proposed method to overcome these challenges. Overall, the proposed method has the potential to contribute to the development of more efficient and reliable gear systems for various industrial applications, such as aerospace, automotive, and power transmission.

6.2 Further research

The proposed method can also serve as a starting point for further research in the field of gear design and optimization. For example, future studies could explore the effects of different gear materials, crowning, and loading conditions on the performance of zero bevel gears. Furthermore, the proposed method could be extended to other types of gears, such as worm or cycloidal gears, to investigate their contact characteristics and performance under different operating conditions.

This method would offer a more comprehensive understanding of the contact pattern and tooth stresses in the zero bevel, cycloidal and worm gears. Overall, this research plan would contribute to advancing the understanding of the performance and durability of gears and could potentially lead to improved design and manufacturing practices. In addition, numerical simulations can complement experimental findings that can be obtained from the “8-axis Rotary Test Bed”, providing a more comprehensive understanding of tooth contact behavior. The “8-axis Rotary Test Bed” is a testbed with a CNC router machine where we can place gearboxes to experimentally simulate tooth contact under various conditions, shown in Figure (78). The simulated results can be used in conjunction to validate the accuracy of the method and determine how different factors, such as tooth geometry, load and lubrication, influence tooth contact behavior. This will assist in forecasting kinematic, dynamic, and failure modes, as well

as optimizing tooth profile modification to minimize harmful noise and vibration and regulate transmission error. The high-stiffness “8-axis Rotary Test Bed” enables gear contacts and dynamic behaviors to be replicated in-the-loop, simulating realistic deterministic and quasi-chaotic operating conditions, including misalignments, shock loads, and rattling.

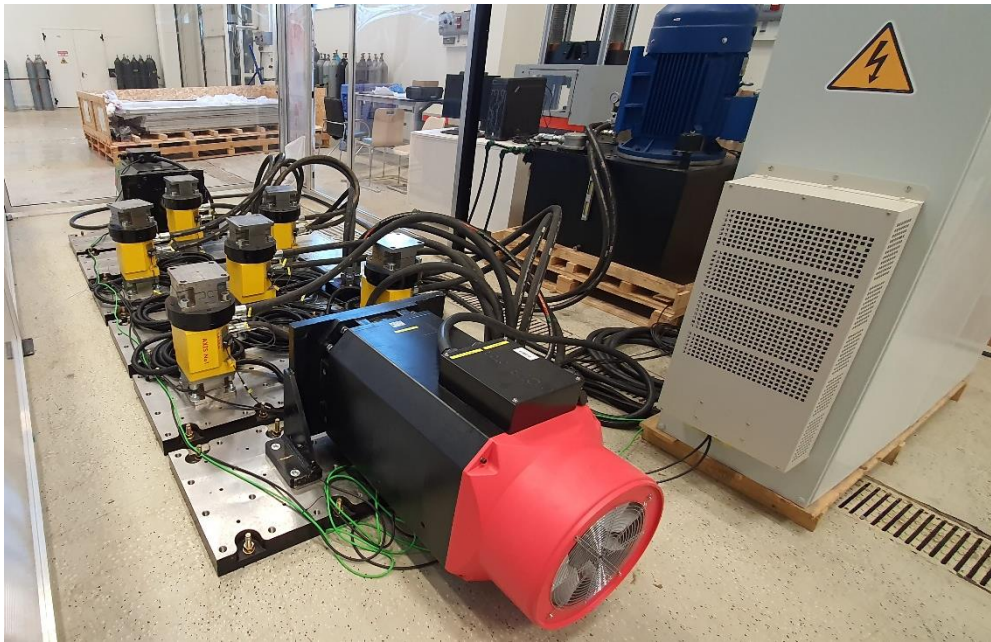


Figure 78. The 8-axis Rotary Test Bed with a CNC router machine.

References

1. Litvin, F. L., & Fuentes, A. (2004). *Gear geometry and applied theory*. Cambridge University Press.
2. Litvin, F. L., Sheveleva, G. I., Vecchiato, D., Gonzalez-Perez, I., & Fuentes, A. (2005). Modified approach for tooth contact analysis of gear drives and automatic determination of guess values. *Computer Methods in Applied Mechanics and Engineering*, 194(27-29), 2927–2946. <https://doi.org/10.1016/j.cma.2004.07.031>
3. Litvin, F. L., Vecchiato, D., Fuentes, A., & Gonzalez-Perez, I. (2004). Automatic determination of guess values for simulation of meshing of gear drives. *Computer Methods in Applied Mechanics and Engineering*, 193(33-35), 3745–3758. <https://doi.org/10.1016/j.cma.2004.02.005>
4. Buckingham, E. (1988). *Analytical Mechanics of Gears*. Dover Publications.
5. Litvin, F. L., & Kim, D. H. (1997). Computerized design, generation and simulation of meshing of modified involute spur gears with localized bearing contact and reduced level of transmission errors. *Journal of Mechanical Design*, 119(1), 96–100. <https://doi.org/10.1115/1.2828795>
6. Gabiccini, M., Bracci, A., & Battaglia, E. (2011). On the estimation of continuous mappings from cradle-style to 6-axis machines for face-milled hypoid gear generation. *Mechanism and Machine Theory*, 46(10), 1492–1506. <https://doi.org/10.1016/j.mechmachtheory.2011.05.003>
7. Litvin, F. L., Fuentes, A., Gonzalez-Perez, I., Carvenali, L., Kawasaki, K., & Handschuh, R. F. (2003). Modified involute helical gears: Computerized design, simulation of meshing and stress analysis. *Computer Methods in Applied Mechanics and Engineering*, 192(33-34), 3619–3655. [https://doi.org/10.1016/s0045-7825\(03\)00367-0](https://doi.org/10.1016/s0045-7825(03)00367-0)
8. Dudley, D. W., & Townsend, D. P. (1992). *Dudley's Gear Handbook*. McGraw-Hill.
9. Dudley, D. W. (2002). *Handbook of practical gear design*. CRC Press.
10. Spitas, C., & Spitas, V. (2008). Direct analytical solution of a modified form of the meshing equations in two dimensions for non-conjugate gear contact. *Applied Mathematical Modelling*, 32, 2162–2171. <https://doi.org/10.1016/j.apm.2007.07.007>.

11. Lee, Y.-H., & Fong, Z.-H. (2019). A mathematical model for grinding a stick blade profile to cut hypoid gears. *Journal of Mechanical Design*, 142(5).
<https://doi.org/10.1115/1.4045245>
12. Zhang, Y., & Fang, Z. (1999). Analysis of tooth contact and load distribution of helical gears with crossed axes. *Mechanism and Machine Theory*, 34(1), 41–57.
[https://doi.org/10.1016/s0094-114x\(98\)00006-8](https://doi.org/10.1016/s0094-114x(98)00006-8)
13. Yu, W., & Mechefske, C. K. (2016). Analytical modeling of Spur Gear Corner Contact effects. *Mechanism and Machine Theory*, 96, 146–164.
<https://doi.org/10.1016/j.mechmachtheory.2015.10.001>
14. Chen, Z., Zhang, J., Zhai, W., Wang, Y., & Liu, J. (2017). Improved analytical methods for calculation of gear tooth fillet-foundation stiffness with tooth root crack. *Engineering Failure Analysis*, 82, 72–81. <https://doi.org/10.1016/j.engfailanal.2017.08.028>
15. Wang, C. (2021). Study on 3-D modification for reducing vibration of helical gear based on TCA Technology, LTCA technology and system dynamics. *Mechanical Systems and Signal Processing*, 146, 106991. <https://doi.org/10.1016/j.ymsp.2020.106991>
16. Moya, J. L., Machado, A. S., Goytisoló, R. A., & Becerra, A. M. (2009). The finite element method in the design process of Spur Gears. *Volume 4: Design and Manufacturing*. <https://doi.org/10.1115/imece2009-10174>
17. Amabili, M., & Rivola, A. (1997). Dynamic analysis of spur gear pairs: Steady-state response and stability of the SDOF model with time-varying meshing damping. *Mechanical Systems and Signal Processing*, 11(3), 375–390.
<https://doi.org/10.1006/mssp.1996.0072>
18. Amani, A., Spitas, V., & Spitas, C. (2015). Influence of centre distance deviation on the interference of a spur gear pair. *International Journal of Powertrains*, 4(4), 315.
<https://doi.org/10.1504/ijpt.2015.073785>
19. Liu, Y., Zhao, Y., Liu, M., & Sun, X. (2019). Parameterized high-precision finite element modelling method of 3D helical gears with contact zone refinement. *Shock and Vibration*, 2019, 1–17. <https://doi.org/10.1155/2019/5809164>
20. Wu, Y. J., Wang, J. J., & Han, Q. K. (2011). Static/dynamic contact finite element analysis for tooth profile modification of helical gears. *Applied Mechanics and Materials*, 86, 384–388. <https://doi.org/10.4028/www.scientific.net/amm.86.384>
21. AGMA (1976). AGMA 170.01: Design Guide for Vehicle Spur and Helical Gears. AGMA Standard. Chicago, IL, USA.

22. Litvin, F. L., & Lu, J. (1993). Computerized simulation of generation, meshing and contact of double circular-arc helical gears. *Mathematical and Computer Modelling*, 18, 31-47. [https://doi.org/10.1016/0895-7177\(93\)90131-H](https://doi.org/10.1016/0895-7177(93)90131-H).
23. Klingelnberg, J. (2016). Fields of application for bevel gears. *Bevel Gear*. <https://doi.org/10.1007/97836624389301>
24. Padmanabhan, S., Raman, V. S., Asokan, P., Arunachalam, S., & Page, T. (2011). Design optimisation of Bevel Gear Pair. *International Journal of Design Engineering*, 4(4), 364. <https://doi.org/10.1504/ijde.2011.048133>
25. Litvin, F. L., Fuentes, A., & Hayasaka, K. (2006). Design, manufacture, stress analysis, and experimental tests of low-noise high endurance spiral bevel gears. *Mechanism and Machine Theory*, 41(1), 83–118. <https://doi.org/10.1016/j.mechmachtheory.2005.03.001>
26. Spievak, L. E., Wawrzynek, P. A., Ingrassia, A. R., & Lewicki, D. G. (2001). Simulating fatigue crack growth in spiral bevel gears. *Engineering Fracture Mechanics*, 68(1), 53–76. [https://doi.org/10.1016/s0013-7944\(00\)00089-8](https://doi.org/10.1016/s0013-7944(00)00089-8)
27. Zolfaghari, A., Goharimanesh, M., & Akbari, A. A. (2017). Optimum design of straight bevel gears pair using evolutionary algorithms. *Journal of the Brazilian Society of Mechanical Sciences and Engineering*, 39(6), 2121–2129. <https://doi.org/10.1007/s40430-017-0733-9>
28. Chen, M., Xiong, X., & Zhuang, W. (2020). Design and simulation of meshing performance of modified straight bevel gears. *Metals*, 11(1), 33. <https://doi.org/10.3390/met11010033>
29. Kolivand, M., Ligata, H., Steyer, G., Benedict, D. K., & Chen, J. (2015). Actual tooth contact analysis of straight bevel gears. *Journal of Mechanical Design*, 137(9). <https://doi.org/10.1115/1.4031025>
30. Fan, S., Zou, J., & Shi, M. (2014). Parametric surface and properties defined on Parallelogrammic Domain. *Journal of Computational Design and Engineering*, 1(1), 27–36. <https://doi.org/10.7315/jcde.2014.003>
31. Simon, V. V. (2009). Loaded tooth contact analysis and stresses in spiral bevel gears. In Proceedings of the ASME 2009 International Design Engineering Technical Conferences & Computers and Information in Engineering Conference, San Diego, CA, USA, August 30-September 2, 2009 (Vol. 6). <https://doi.org/10.1115/detc2009-86164>
32. Ding, H., & Tang, J. (2020). Machine-tool settings driven high-order topology optimization to grinding tooth flank by considering loaded tooth contact pattern for spiral

- bevel gears. *International Journal of Mechanical Sciences*, 172, 105397.
<https://doi.org/10.1016/j.ijmecsci.2019.105397>
33. Peng, S., Ding, H., & Tang, J. (2019). Accurate numerical computation of loaded tooth surface contact pressure and stress distributions for spiral bevel gears by considering time-varying meshing characteristics. *Advanced Engineering Software*, 135, 102683.
<https://doi.org/10.1016/j.advengsoft.2019.05.005>
34. Hu, Z., & Mao, K. (2017). An investigation of misalignment effects on the performance of acetal gears. *Tribology International*, 116, 394–402.
<https://doi.org/10.1016/j.triboint.2017.07.029>
35. Amani, A., Spitas, V., & Spitas, C. (2015). Influence of centre distance deviation on the interference of a spur gear pair. *International Journal of Powertrains*, 4(4), 315.
<https://doi.org/10.1504/ijpt.2015.073785>
36. Kumar, P.; Hirani, H.; Kumar Agrawal, A. Effect of gear misalignment on contact area: Theoretical and experimental studies. *Measurement* **2019**, 132, 359–368.
<https://doi.org/10.1016/j.measurement.2018.09.070>
37. Ye, S.-Y., & Tsai, S.-J. (2016). A computerized method for loaded tooth contact analysis of high-contact-ratio spur gears with or without flank modification considering tip corner contact and shaft misalignment. *Mechanism and Machine Theory*, 97, 190–214.
<https://doi.org/10.1016/j.mechmachtheory.2015.11.008>
38. Simon, V. V. (2009). Design and manufacture of spiral bevel gears with reduced transmission errors. *Journal of Mechanical Design*, 131(4).
<https://doi.org/10.1115/1.3087540>
39. Ding, H., Tang, J., Zhong, J., Wan, G., & Zhou, Z. (2016). Simulation and optimization of Computer Numerical Control-milling model for machining a spiral bevel gear with new tooth flank. *Proceedings of the Institution of Mechanical Engineers, Part B: Journal of Engineering Manufacture*, 230(10), 1897–1909.
<https://doi.org/10.1177/0954405416640171>
40. Cui, T., Li, Y., Zan, C., & Chen, Y. (2022). Dynamic Modeling and analysis of Nonlinear Compound Planetary System. *Machines*, 10(1), 31.
<https://doi.org/10.3390/machines10010031>
41. Xiao, Z., Chen, F., & Zhang, K. (2021). Analysis of dynamic characteristics of the multistage planetary gear transmission system with Friction Force. *Shock and Vibration*, 2021, 1–10. <https://doi.org/10.1155/2021/8812640>

42. Mao, K. (2007). Gear tooth contact analysis and its application in the reduction of fatigue wear. *Wear*, 262, 1281–1288. <https://doi.org/10.1016/j.wear.2006.06.019>
43. Sigg, H. (1965). Profile and Longitudinal Corrections on Involute Gears; No. 6. AGMA Standard, 109. Chicago, IL, USA.
44. Niemann, G., & Winter, H. (1983). *Maschinenelemente: Band I, II, III*. Springer. Berlin/Heidelberg, Germany.
45. Spitas, C., Spitas, V., & Rajabalinejad, M. (2013). Dynamical Simulation and Calculation of the Load Factor of Spur Gears with Indexing Errors and Profile Modifications for Optimal Gear Design. In *Power Transmissions* (pp. 183–196). Springer. https://doi.org/10.1007/978-94-007-6558-0_13
46. Li, S. (2012). Contact Stress and Root Stress Analyses of Thin-Rimmed Spur Gears with Inclined Webs. *Journal of Mechanical Design*, 134(5), 051001. <https://doi.org/10.1115/1.4006324>
47. Spitas, C., & Spitas, V. (2006). Calculation of overloads induced by indexing errors in spur gearboxes using multi-degree-of-freedom dynamical simulation. *Proceedings of the Institution of Mechanical Engineers, Part K: Journal of Multi-Body Dynamics*, 220, 273–282. <https://doi.org/10.1243/1464419JMBD67>.
48. Gonzalez-Perez, I., Fuentes, A., Litvin, F. L., Hayasaka, K., & Yukishima, K. (2007). Application and investigation of modified helical gears with several types of geometry. *Volume 7: 10th International Power Transmission and Gearing Conference*. <https://doi.org/10.1115/detc2007-34027>
49. Hsi Lin, H., Oswald, F. B., & Townsend, D. P. (1994). Dynamic loading of spur gears with linear or parabolic tooth profile modifications. *Mechanics & Machinery Theory*, 29, 1115-1129. [https://doi.org/10.1016/0094-114X\(94\)90003-5](https://doi.org/10.1016/0094-114X(94)90003-5).
50. Gurumani, R., & Shanmugam, S. (2011). Modeling and contact analysis of crowned spur gear teeth. *Engineering Mechanics*, 18, 65-78.
51. Litvin, F. L., Zhang, J., & Handschuh, R. F. (1988). Crowned spur gears: Methods for generation and tooth contact analysis—Part I: Basic concepts, generation of the pinion tooth surface by a plane. *Journal of Mechanical Design, Transactions of the ASME*, 110(4), 337-342. <https://doi.org/10.1115/1.3267467>
52. Zhen, W. T., & Wu, K. J. (1997). *Mechanical theory* (pp. 222-228). Higher Education Press: Beijing, China.
53. Bergseth, E., & Björklund, S. (2010). Logarithmical crowning for spur gears. *Journal of Mechanical Engineering*, 56, 239-244.

54. Lundberg, G. (1939). Elastic contact between two semi-infinite bodies. *Forschung im Ingenieurwesen*, 5, 201-211.
55. Guo, Y., Lei, X., & Wang, Y. (2020). Research progress of logarithmic crown of bearing roller. In *E3S Web of Conferences* (Vol. 179, p. 01017).
<https://doi.org/10.1051/e3sconf/202017901017>
56. Johns, P. M., & Gohar, R. (1981). Roller bearings under radial and eccentric loads. *Tribology International*, 14, 131-136. [https://doi.org/10.1016/0301-679X\(81\)90058-X](https://doi.org/10.1016/0301-679X(81)90058-X)
57. Ma, J., Xu, W., & Liu, S. (1997). Engineering design of logarithmic roller. *Bearing*, 6, 25.
58. Fujiwara, H., Kobayashi, T., Kawase, T., & Yamauchi, K. (2010). Optimized logarithmic roller crowning design of cylindrical roller bearings and its experimental demonstration. *Tribology Transactions*, 53, 909-916. <https://doi.org/10.1080/10402004.2010.510619>.
59. Fujiwara, H., & Kawase, T. (2006). Logarithmic profile of rollers in roller bearing and optimization of the profile. *Transactions of the Japan Society of Mechanical Engineers Part C*, 72, 3022-3029. <https://doi.org/10.1299/kikaic.72.3022>
60. Harianto, J., & Houser, D. R. (2007). A methodology for obtaining optimum gear tooth micro-topographies for noise and stress minimization over a broad operating torque range. *Volume 7: 10th International Power Transmission and Gearing Conference*.
<https://doi.org/10.1115/detc2007-34655>
61. Litvin, F. L., Gonzalez-Perez, I., Fuentes, A., Vecchiato, D., Hansen, B. D., & Binney, D. (2005). Design, generation and stress analysis of face-gear drive with Helical Pinion. *Computer Methods in Applied Mechanics and Engineering*, 194(36-38), 3870–3901.
<https://doi.org/10.1016/j.cma.2004.09.006>
62. Litvin, F. L., Lian, Q., & Kapelevich, A. L. (2000). Asymmetric modified spur gear drives: Reduction of noise, localization of contact, simulation of meshing and stress analysis. *Computer Methods in Applied Mechanics and Engineering*, 188(1-3), 363–390.
[https://doi.org/10.1016/s0045-7825\(99\)00161-9](https://doi.org/10.1016/s0045-7825(99)00161-9)
63. Litvin, F. L., Peng, P. H., Lagutin, S. A., Townsend, D. P., & Sep, T. M. (2001). Helical and spur gear drive with double crowned pinion tooth surfaces and conjugated gear tooth surfaces. U.S. Patent No. US6205879B1.
64. Litvin, F. L., Fuentes, A., Zanzi, C., Pontiggia, M., & Handschuh, R. F. (2002). Face-gear drive with spur involute pinion: Geometry, generation by a worm, stress analysis. *Computer Methods in Applied Mechanics and Engineering*, 191(25-26), 2785–2813.
[https://doi.org/10.1016/s0045-7825\(02\)00215-3](https://doi.org/10.1016/s0045-7825(02)00215-3)

65. Litvin, F. L., Gonzalez-Perez, I., Fuentes, A., Hayasaka, K., & Yukishima, K. (2005). Topology of modified surfaces of involute helical gears with line contact developed for improvement of bearing contact, reduction of transmission errors, and stress analysis. *Mathematical and Computer Modelling*, 42(9-10), 1063-1078.
<https://doi.org/10.1016/j.mcm.2004.10.028>
66. Bracci, A., Gabiccini, M., Artoni, A., & Guiggiani, M. (2009). Geometric contact pattern estimation for gear drives. *Computer Methods in Applied Mechanics and Engineering*, 198(17-20), 1563–1571. <https://doi.org/10.1016/j.cma.2009.01.009>
67. Lin, C.-H., & Fong, Z.-H. (2015). Numerical tooth contact analysis of a bevel gear set by using measured tooth geometry data. *Mechanics & Machinery Theory*, 84, 1–24.
<https://doi.org/10.1016/j.mechmachtheory.2014.09.010>.
68. Spitas, C., & Spitas, V. (2011). Fast unconditionally stable 2-D analysis of non-conjugate gear contacts using an explicit formulation of the meshing equations. *Mechanics & Machinery Theory*, 46, 869–879. <https://doi.org/10.1016/j.mechmachtheory.2011.02.010>
69. Wang, S., Zhou, Y., Chu, C.-H., & Tang, J. (2022). Novel kinematic and geometric views for improving tooth contact analysis of spatial gears. *Journal of Computational Design and Engineering*, 9(3), 1076–1096. <https://doi.org/10.1093/jcde/qwac041>
70. Ding, H., & Tang, J. (2020). Machine-tool settings driven high-order topology optimization to grinding tooth flank by considering loaded tooth contact pattern for spiral bevel gears. *International Journal of Mechanical Sciences*, 172, 105397.
<https://doi.org/10.1016/j.ijmecsci.2019.105397>
71. Johnson, K. L. (1985). *Contact Mechanics*. Cambridge University Press.
<https://doi.org/10.1017/CBO9781139171731>
72. Ling, F. F., Lai, W. M., & Lucca, D. A. (2002). *Fundamentals of surface mechanics: With applications*. Springer.
73. Brekhovskikh, L. M., & Goncharov, V. (n.d.). *Mechanics of Continua and wave dynamics*.
74. Muvdi, B. B., & Elhouar, S. (2016). *Mechanics of materials: With applications in Excel*. CRC Press.
75. Sandström, J. (2012). Evaluation of tangential stress in hertzian rolling contact. *Fatigue & Fracture of Engineering Materials & Structures*, 35(12), 1088–1094.
<https://doi.org/10.1111/j.1460-2695.2012.01696.x>
76. Zhang, K., Wei, Z., & Chen, Y. (2021). Contact analysis of measured surfaces based on modified interacting and coalescing Hertzian asperities (ICHA) model with oblique

- contact asperities. *Advances in Mechanical Engineering*, 13(7), 168781402110330. <https://doi.org/10.1177/16878140211033090>
77. Bodzás, S. (2015). Computer aided geomemtric modelling of cylindrical worm gear drive having arched profile. *Analecta Technica Szegedinensia*, 9(1), 1–6. <https://doi.org/10.14232/analecta.2015.1.1-6>
78. Bodzás, S. (2019). Computer aided designing and modelling of spur gear pairs having normal and modified straight teeth. *International Review of Applied Sciences and Engineering*, 10(2), 157–163. <https://doi.org/10.1556/1848.2019.0019>
79. Jayakiran Reddy, E., & Pandu Rangadu, V. (2018). Development of knowledge based parametric CAD modeling system for SPUR GEAR: An approach. *Alexandria Engineering Journal*, 57(4), 3139–3149. <https://doi.org/10.1016/j.aej.2018.07.010>
80. Patil, S., Karuppanan, S., & Wahab, A. A. (2013). Contact pressure evaluation of a gear pair along the line of action using finite element analysis. *Applied Mechanics and Materials*, 393, 403–408. <https://doi.org/10.4028/www.scientific.net/amm.393.403>
81. Jammi, S. (2013). Gear tooth stresses from finite element analysis compared with AGMA standards. *Volume 5: 25th International Conference on Design Theory and Methodology; ASME 2013 Power Transmission and Gearing Conference*. <https://doi.org/10.1115/detc2013-12037>
82. Korn, G.A. and Korn, T.A. (1968) *Mathematicals Handbook for Scientists and Engineers*. S.l.: Mcgraw-Hill.
83. Barber, J. R. (2018). *Contact Mechanics*. Springer.
84. Artoni, A., Guiggiani, M., Kahraman, A., & Harianto, J. (2013). Robust optimization of cylindrical gear tooth surface modifications within ranges of torque and misalignments. *Journal of Mechanical Design*, 135(12). <https://doi.org/10.1115/1.4025196>
85. Huangfu, Y., Chen, K., Ma, H., Li, X., Han, H., & Zhao, Z. (2020). Meshing and dynamic characteristics analysis of spalled gear systems: A theoretical and experimental study. *Mechanical Systems and Signal Processing*, 139, 106640. <https://doi.org/10.1016/j.ymsp.2020.106640>
86. Munro, R. G., Morrish, L., & Palmer, D. (1999). Gear transmission error outside the normal path of contact due to corner and top contact. *Proceedings of the Institution of Mechanical Engineers, Part C: Journal of Mechanical Engineering Science*, 213(4), 389–400. <https://doi.org/10.1243/0954406991522347>
87. Thirumurugan, R., & C, C. C. (2020). Study on the quality and tooth root load carrying capacity of the high contact ratio asymmetrical gear tooth machined using WCEDM

- process. *Materials and Manufacturing Processes*, 35(12), 1352–1361.
<https://doi.org/10.1080/10426914.2020.1772489>
88. Zhang, Q., Xu, Z., & Lyu, S. (2011). A study on tooth modification for spur gear for articulated hauler. *Volume 8: 11th International Power Transmission and Gearing Conference; 13th International Conference on Advanced Vehicle and Tire Technologies*.
<https://doi.org/10.1115/detc2011-47295>
89. Cooley, C. G., Parker, R. G., & Vijayakar, S. M. (2011). A frequency domain finite element approach for three-dimensional gear dynamics. *Journal of Vibration and Acoustics*, 133(4). <https://doi.org/10.1115/1.4003399>
90. Han, J., Liang, L., Zhang, H., & Zhao, Y. (2021). Dynamics modeling and experimental investigation of gear mechanism with coupled small clearances. *Entropy*, 23(7), 834.
<https://doi.org/10.3390/e23070834>
91. Yang, Y., Xu, M., Du, Y., Zhao, P., & Dai, Y. (2018). Dynamic analysis of nonlinear time-varying spur gear system subjected to multi-frequency excitation. *Journal of Vibration and Control*, 25(6), 1210–1226. <https://doi.org/10.1177/1077546318814951>
92. Chen, M., Xiong, X., & Zhuang, W. (2020a). Design and simulation of meshing performance of modified straight bevel gears. *Metals*, 11(1), 33.
<https://doi.org/10.3390/met11010033>
93. Bodzás, S. (2019). Tooth contact analysis of straight bevel gears in the function of the modification of number of teeth of the driving gear. *Australian Journal of Mechanical Engineering*, 20(1), 24–30. <https://doi.org/10.1080/14484846.2019.1654964>
94. He, D., Ding, H., & Tang, J. (2018). A new analytical identification approach to the tooth contact points considering misalignments for spiral bevel or hypoid gears. *Mechanism and Machine Theory*, 121, 785. <https://doi.org/10.1016/j.mechmachtheory.2017.12.003>
95. Gonzalez-Perez, I., & Fuentes-Aznar, A. (2019). Conjugated action and methods for crowning in face-hobbed spiral bevel and hypoid gear drives through the spirac system. *Mechanism and Machine Theory*, 139, 109–130.
<https://doi.org/10.1016/j.mechmachtheory.2019.04.011>
96. Peng, S.D., Ding, H., & Tang, J.Y. (2019). Accurate numerical computation of loaded tooth surface contact pressure and stress distributions for spiral bevel gears by considering time-varying meshing characteristics. *Advances in Engineering Software*, 135, 15. <https://doi.org/10.1016/j.advengsoft.2019.05.005>

97. Hu, Z.H., Ding, H., Peng, S.D., Tang, Y., & Tang, J.Y. (2019). Numerical determination to loaded tooth contact performances in consideration of misalignment for the spiral bevel gears. *International Journal of Mechanical Sciences*, 151, 343-355.
<https://doi.org/10.1016/j.ijmecsci.2018.11.014>
98. Zhou, Y.S., Peng, S.D., Liu, X.R., Liu, S.J., & Tang, J.Y. (2019). A novel method to generate the tooth surface model of face-milled generated spiral bevel gears. *International Journal of Advanced Manufacturing Technology*, 102, 1205-1214.
<https://doi.org/10.1007/s00170-018-2951-4>